Improving the Energy Efficiency and Reliability of Wireless Sensor Networks Using Coding Techniques

by

Georgios Angelopoulos

B.S., University of Patras, Greece (2009)
S.M., Massachusetts Institute of Technology (2011)

Submitted to the Department of Electrical Engineering and Computer Science
in partial fulfillment of the requirements for the degree of

Doctor of Philosophy

at the

MASSACHUSETTS INSTITUTE OF TECHNOLOGY

February 2016

Signature redacted

Author .....
Department of Electrical Engineering and Computer Science
January 15, 2016

Signature redacted

Certified by .....
Muriel Médard
Cecil H. Green Professor of Electrical Engineering and Computer Science
Thesis Supervisor

Signature redacted

Certified by .....
Anantha P. Chandrakasan
Vannevar Bush Professor of Electrical Engineering
Thesis Supervisor

Signature redacted

Accepted by .....
Leslie A. Kolodziejski
Chair, Department Committee on Graduate Students

Improving the Energy Efficiency and Reliability of Wireless Sensor Networks Using Coding Techniques

by

Georgios Angelopoulos

Submitted to the Department of Electrical Engineering and Computer Science
on January 15, 2016, in partial fulfillment of the
requirements for the degree of
Doctor of Philosophy

Abstract

Wireless sensor networks (WSNs) are rapidly being adopted in a wide range of applications, from continuous health monitoring to automated industrial infrastructures, and soon will have a major environmental, financial and societal impact. Some of the main technical challenges in designing and deploying WSNs are meeting their communications reliability and energy consumption requirements. In order to address these two challenges, this thesis proposes new coding schemes and communication protocols, a novel paradigm for information acquisition, and the design and implementation of specific circuits architectures.

The reliability and energy efficiency trade-offs of splitting the inserted redundancy in multiple layers of the network stack are investigated through analysis and over-the-air experiments. Not only appropriate and efficient coding schemes for each layer are examined, but their interaction and synergistic functioning are explored. The energy benefits of each approach are quantified by designing a low-power custom transmitter using a 65nm TSMC process, integrating the first hardware implementation of a multi-rate forward error correction (FEC) and random linear network coding (RLNC) accelerator.

In addition, a physical layer (PHY) independent partial packet reception (PPR) scheme is proposed for asymmetric networks, i.e. WSNs with a star topology, called packetized rateless algebraic consistency (PRAC). PRAC reduces the number of retransmissions by harnessing information contained in partial packets. Experiments with off-the-shelf transceivers validate our analysis results on the data reliability and energy consumption benefits of the proposed scheme.

Apart from communicating information, acquiring the signals of interest can account for a significant fraction of the power consumption of a sensor node. For this reason, the thesis proposes a nonuniform sampling scheme in order to exploit the inherent compressibility and sparse structure of typical signals encountered in many WSNs. Simulations results with real datasets and an energy comparison against the state-of-the-art sampling schemes demonstrate its rate and energy efficiency advantages.

Finally, the thesis studies the joint fundamental performance bounds of acquiring and transmitting sparse signals through noisy channels. An integrated source representation-to-transmission scheme, called AdaptCast, is proposed and, using rate distortion analysis, its asymptotically optimal performance is proved. Based on simulation results in the context of a health monitoring application, AdaptCast's performance benefits are demonstrated against other coding schemes and PHY architectures in terms of the provided data reliability and reconstruction distortion.

Thesis Supervisor: Muriel Médard
Title: Cecil H. Green Professor of Electrical Engineering and Computer Science

Thesis Supervisor: Anantha P. Chandrakasan
Title: Vannevar Bush Professor of Electrical Engineering

Dedicated to the memory
of my mother, Maria.

Acknowledgments

Throughout my life, I consider myself to have been lucky, and my PhD experience isn't an exception. I've had the great fortune to work under the supervision of two wonderful mentors: Prof. Muriel Médard and Anantha P. Chandrakasan. I can't possibly imagine a more supportive and cross-disciplinary pair of advisors! Muriel and Anantha, I feel very privileged to have access to your technical intuition and wisdom, and very honored to be part of your groups. Thanks a lot for your efforts to convey to me the required skills, mindset and character in order to become a professional researcher. I highly appreciate the guidance, intellectual freedom and moral support I've had throughout the years. Words fall short to accurately describe my gratitude to you.

Next, I would like to thank my external thesis committee member, Prof. Andrea Goldsmith. Andrea, thanks a lot for your time, feedback and comments on my thesis. I feel very fortunate to have collaborated with you and your research group. Taking advantage of this opportunity, I would also like to thank you for your amazing book on wireless communications, which was probably one of the foremost reasons on getting me hooked on this engineering field and teaching me all the fundamental ideas which enabled me to write this thesis!

Among the (many) people I am indebted to, I would like to thank my collaborators. It has been a true blessing to work with Prof. Dina Katabi, Prof. Vivek K Goyal, Arun Paidimarri, Shirley Shi, Soheil Feizi, Colleen Josephson and some MIT undergraduate/M.Eng. students. Thanks for encouraging me to jointly explore obscure engineering problems and always being willing to teach me topics that I wasn't aware of along the way of my graduate studies. I am also grateful to my inspiring collaborators during my summer internships, Srinath Hosur, Anuj Batra, Ariton Xhafa, Jin-Meng Ho, Alice Wang and Gangadhar Burra. In addition, I would like to thank all the RLE and MTL support team, and especially Margaret, Megan and Michael, for their amazing assistance and their behind-the-scenes work.

I would like to acknowledge all the sources and agencies that funded my research,

including the MIT Paris Kanelakis Fellowship, George and Marie Vergottis Fellowship, SRC, VT iDirect and NSF. Special thanks to Avago and TSMC for the chip fabrication and Texas Instruments for equipment donation and support.

Special thanks are due to all current and graduated Network Coding and Reliable Communications (NCRC) and Energy Efficient Circuits and Systems (EECS) group members. It is fair to say that you guys have been the best part of this multi-year journey! I consider myself extremely fortunate to have had such wonderful office-mates/friends. I will never forget our white-board/wall/glass chats, conversations over lunches or coffee breaks, late-hour discussions about random topics and in-lab soccer games! I can hardly imagine a more pleasant environment to work in on a daily basis. To Ahmad, Arman, Arun, Flavio, Jason, Mat, Omid, Phil, Salman, Shirley, Soheil, Sunghyun, Sungjae, Ulric and Weifei, thanks a lot for your unconditional friendliness and support.

I would also like to thank all my friends in Boston for being a wonderful companion outside the lab. Your refreshing energy contributed a lot to the completion of this thesis, but, most importantly, the interaction with you taught me how to become a better person in general. To my friends back in Greece (and Spain!), thanks a lot for your constant moral support and encouragement; although thousands of miles away, you have been emotionally very very close. Special thanks to my girlfriend, Konstantina! Konstantina, I can hardly imagine myself successfully completing this thesis without your support. Thanks a lot for your advice, patience and love; you have tremendously helped me to overcome not only technical problems related to this thesis but also numerous crucial life challenges.

Last but not least, I would like to thank my parents and sister for being my very first teachers in life and for supporting me throughout all my career. Encouragement for completion of this thesis is just the tip of your never-ending guidance and love. Thank you for providing me everything that was required in order to reach the point of writing this thesis and constantly helping me to improve myself personally.

Contents

List of Figures

List of Tables

Chapter 1

Introduction

1.1 Wireless Sensor Networks

The continuous scaling of electronics over the last two decades has enabled the ubiquitous use of wireless communication systems in many aspects of the human life. Nowadays, several wireless devices correspond to every person, and this number is expected to grow fast within the next years [1]. The increasing number of devices combined with the exponential growth in the amount of communicated information impose several challenges in the design of efficient, scalable and robust wireless networks. Personal smartphone is an example of a device which had major impact on our lives recently, by transforming the way we communicate and perceive our surrounding world. This couldn't have been accomplished if it wasn't the seamless and nearly instant access to a wealth of services enabled by high speed communication links and efficient processing units. This constant and rapid evolution of wireless communication systems is responsible for the significantly higher spectral efficiency and data rates, while consuming less energy resources.

Similarly to personal communication using smartphones, wireless sensor networks (WSNs) are emerging as a promising network architecture. A WSN is a network of spatially distributed devices (or *sensor nodes*) that capture, process, display and

transmit information contained in specific signals of interest, while being able to receive information in order to actuate and interact with their surrounding environment. The range of applications of WSNs is already very wide and it continues to expand with increasing rate. The ultimate goal of WSNs is to provide reliable means of communications to every machine, device and object in the world so that they can receive and send information from and to points of interest, potentially thousands of miles away. According to recent market reports and predictions, it is expected that more than 50 billion sensor nodes will be interconnected by 2020, creating a market of more than $15B [2]. Some of the recent terms used to describe modern WSNs are *Internet of Things* (IoT) or *Internet of Everything* (IoE). These terms reflect the potential and scale of this technology in the near future, with significant financial, societal and environmental impact, enabling new services and applications, as shown in Fig. 1-1.

For instance, WSNs enable data-driven patient management and improved healthcare effectiveness by continuously capturing and transmitting vital health signals through miniaturized or implanted devices. These data could allow for patients to have shorter hospital stays with reduced cost and improved care. Smarter home monitoring systems upgrade quality of life in the elderly and people with special needs. In addition, captured data improve the decisions made by physicians and could result in less or more effective medicine administration. The importance of this specific application has resulted in the establishment of a separate term for WSNs tailored to its requirements, called body area networks (BANs).

Smart buildings is an other application of WSNs, in which an intelligent network of electronic devices monitor and control different services, in order to achieve better energy efficiency and improved experience for occupants. Automatic control of the lighting in a building based on the current occupancy pattern or adjusting the HVAC according to predictive meteorological data, are some examples of WSNs used in this space. Wireless nodes can also be used to continuously monitor the structural

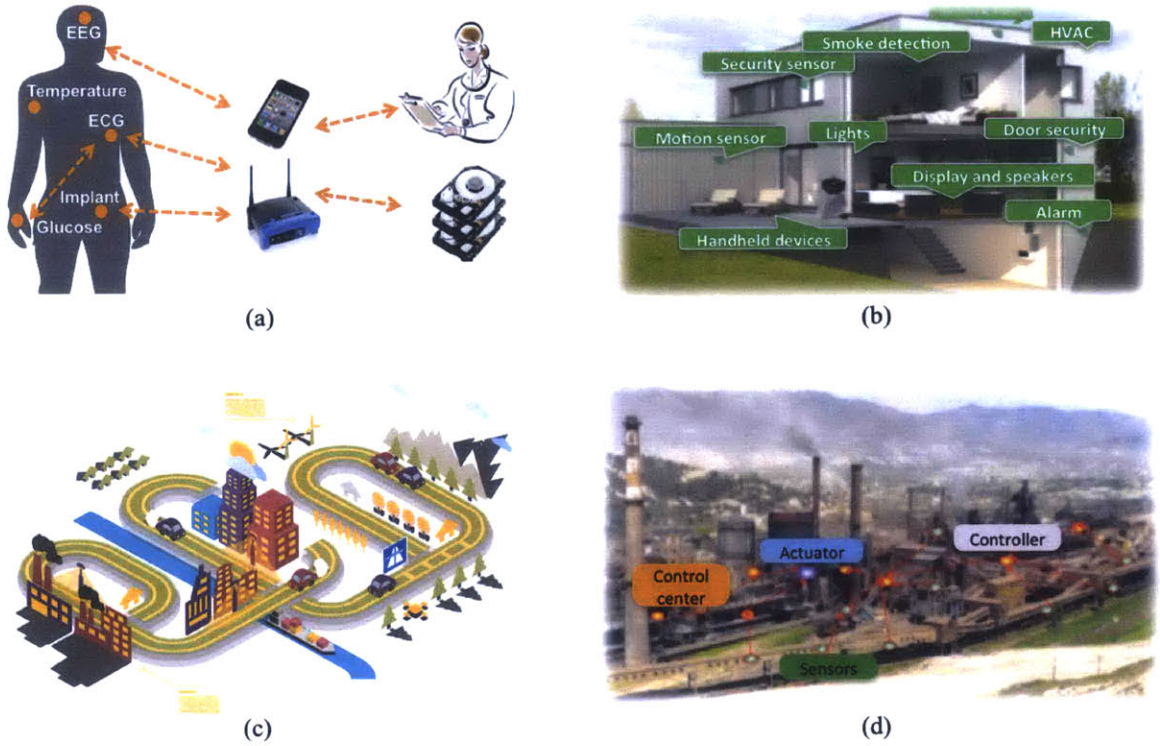

Figure 1-1: Examples of WSN applications with significant environmental, societal and financial benefits. (a) Continuous health monitoring, (b) Smart buildings, (c) Smart cities, and (d) Industrial infrastructures.

condition of the building or easily provide wireless capabilities to devices that didn't have them.

In principle, WSNs are not limited in the coverage area or number of connected devices. Resource allocation in smart cities can be optimized by monitoring thousands of objects generating data and efficiently scheduling services. In smart industrial infrastructures, WSNs add connectivity to manufacturing processes, resulting in increased productivity, real-time inventory monitoring and reduced costs. This allows remote machines to communicate among themselves, optimizing the production pipeline and avoiding potential accidents.

Most of the techniques investigated in this thesis are applicable to any wireless communication system but, because of the major importance, huge opportunity and

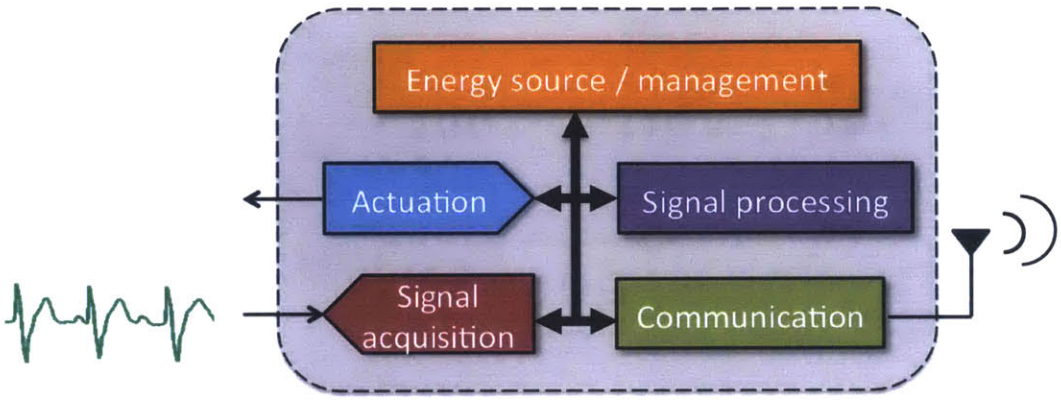

Figure 1-2: Block diagram of a typical sensor node.

recent interest in WSNs, they are presented and evaluated in the context of improving the effectiveness and efficiency of WSNs.

1.2 Challenges and Motivation

Although different WSN applications exhibit diverse requirements in terms of energy, throughput, latency, etc., the vast majority of them captures analog signals and aims to transmit them to one or more nodes with little distortion while maintaining low power consumption. Very strict constraints are associated with the energy consumption of sensor nodes because they are typically powered by energy harvesting sources or small batteries whose replacement cost is usually considered prohibitively high. In addition, the end-to-end communication performance of WSNs is typically challenged by the significantly stronger nearby interfering sources and the harsh environment they usually operate in. Thus, ensuring on-time and reliable delivery of information as well as extended operation times is quite challenging. To make matters worse, easy deployment and seamless configuration regardless of the application or the environment are usually expected.

The block diagram of a typical sensor node is shown in Fig. 1-2. All blocks are crucial for achieving the desired operation of the node and significant amount of re-

search, in both the academia and industry, is conducted in order to optimize each individual block. In this thesis, we mainly focus on the challenges associated with the signal acquisition and communication blocks. In more detail, the thesis addresses the challenges of efficiently capturing and representing signals, as well as reliably communicating them to the designated destinations. This is achieved by devising information acquisition schemes, transmission codes and communication protocols, as well as designing and implementing efficient systems and circuits. The main contributions of the thesis on improving the reliability and energy efficiency of WSNs are listed in the following section.

1.3 Thesis Organization and Contributions

The considered approach in this thesis for improving the reliability and energy efficiency of WSNs spans the circuits, signal processing and wireless communications fields. The main contributions are summarized in the following subsections and in Table 6.1.

1.3.1 Joint Channel and Network Coding

The thesis proposes a communication scheme which improves data reliability and energy efficiency in WSNs with star-like topologies, usually called asymmetric WSNs. Random linear network coding (RLNC) [3] is explored and its synergy with forward error correction (FEC) codes at the physical layer (PHY) are investigated. The hostile wireless environment that sensor nodes usually operate in, with significant interference from nearby networks, motivate us to propose a joint channel and network coding (JCNC) scheme. We demonstrate its performance benefits through simulations and experimental results. The co-optimization of the algorithm performance and low power implementation of the considered schemes are also explored.

In order to quantify the energy consumption of RLNC, FEC and JCNC schemes,

we design a custom system-on-chip (SoC), which integrates on-chip a low-power 2.4 GHz transmitter and an accelerator implementing a multi-rate convolutional code and RLNC, consuming 580μW while transmitting packet data with a rate of 1Mbps. According to measurement results performed in typical office environments, RLNC of code rate 4/8 can provide an effective SNR improvement, or coding gain, of about 3.4dB at a PER of 10^{-2}, outperforming the FEC code of the same code rate. In addition, we demonstrate that the coding gains of RLNC and FEC are approximately additive when they simultaneously operate as a JCNC, without requiring any coordination among them.

1.3.2 Harnessing Partial Packets

The thesis proposes a partial packet recovery (PPR) scheme, called Packetized Rateless Algebraic Consistency (PRAC). PRAC exploits intra and inter-packet consistency to identify and recover erroneous packet segments, without recourse to cross-layer or detailed feedback information. PRAC allows, but does not rely upon, the use of any FEC code, requires no feedback other than a notification of completion and, in the absence of partial packets, incurs no overhead. We demonstrate that exploiting information from partial packets reduces the number of retransmissions, resulting in throughput and energy benefits.

Our software implementation and experimental results in a 7-node indoor testbed using off-the-shelf wireless boards equipped with CC2500 radio transceivers reveal that PRAC offers an average throughput gain of 35% compared to a baseline ARQ scheme discarding partial packets and 13% compared to an ideal genie-aided HARQ (iHARQ) scheme. Considering only links with high PERs, PRAC significantly enhances their robustness and its maximum throughput gain is 148% and 34% compared against the baseline and iHARQ schemes, respectively. Apart from the reliability benefits, PRAC offers significant energy savings as well. In order to quantify them we use an experimental setup with four sensors mounted on a human body, transmitting

information to a receiving node in a typical office environment. By precisely modeling the state transitions and energy consumption of sensors, we compare the efficiency of PRAC against a baseline ARQ protocol. Our results indicate that exploiting partial packets reduces on average the energy consumption of our sensors by 8-20%. The energy savings are pronounced in challenged channel conditions of high PER, where they can be up to 50%.

1.3.3 Adaptive Nonuniform Sampling

Apart from communicating data in WSNs, capturing the signals of interests usually consumes a significant amount of resources. For this reason, the rate and energy efficiency of an adaptive nonuniform sampling scheme, called Time-Stampless Adaptive Nonuniform Sampling (TANS), are investigated. A new TANS method is proposed, called TANS with finite sampling rates (TFR). Performance of TFR is compared against two other TANS methods, as well as against state-of-the-art sampling techniques, in terms of their rate and energy performance in the context of a health monitoring application. The results of a practical implementation architecture of TFR demonstrate that TANS provides significant improvements in terms of both the rate-distortion performance and energy consumption compared against the state-of-the-art methods.

1.3.4 Acquisition, Transmission and Reconstruction of Sparse Signals

The thesis introduces AdaptCast, an integrated signal representation-to-transmission scheme for WSNs that efficiently represents collected data and increases their robustness against channel errors across a wide range of SNR values in a rateless fashion. AdaptCast leverages sparsity inherent in the majority of physical signals in order to parsimoniously represent them without relying on a specific signal model. The pro-

posed scheme does not suffer from the sudden degradation in the trade-off between distortion and SNR of rated FEC schemes due to its direct, relative bit importance preserving modulation mapping.

Through rate-distortion analysis, we prove the asymptotic optimality of the proposed scheme in terms of achieved distortion in the high SNR regime. AdaptCast's application-independent operation is demonstrated by using several typical signals captured in WSNs, such as an ECG signal and IR images. Based on our analysis and simulation results, considering the trade-off between distortion and channel quality, AdaptCast performs close in a point-to-point scenario to an idealized layered transmission scheme with instantaneous channel state information (CSI) and offers significant benefits in fading environments against schemes without CSI.

1.4 Summary

WSNs have great potential to positively influence several aspects of human life and revolutionize whole industry sectors. This thesis proposes coding schemes and circuit architectures to address the data reliability and energy efficiency challenges in WSNs. Although all thesis chapters are interrelated, an effort has been performed to make them self-contained for readers interested in specific topics.

Chapter 2

Joint Channel and Network Coding: Hardware Design and Performance Evaluation

Random linear network coding (RLNC) is an emerging coding technique that can provide several advantages in wireless networks, such as throughput gains, increased data robustness and better utilization of network resources. In this chapter, we examine its energy efficiency and error recovery performance in the context of asymmetric wireless sensor networks (WSNs). In addition, we present the first custom VLSI implementation of RLNC, integrated with an ultra low-power 2.4GHz transmitter. The chip is fabricated in a 65nm CMOS process and consumes 580pJ/bit for processing and transmitting information at 1Mbps. The digital part of the chip, consisting of an on-chip memory, a multi-rate convolutional encoder and a RLNC accelerator with configurable redundancy, consumes 15μW, operating at 0.4V. According to our over-the-air experiments, RLNC can provide an effective SNR improvement of 5.6dB when combined with FEC rate 1/2, and 3.4dB without FEC, at a PER equal to 10^{-2}.

2.1 Motivation

Wireless sensor networks (WSNs) have been an emerging technology with a continuously expanding range of applications, including real-time health monitoring, smart buildings of reduced energy footprint and automated industrial infrastructures. Among the different topologies of WSNs, asymmetric networks organized in a 'star' topology represent the vast majority of WSNs and are the focus of this chapter. In these networks, low power and energy constrained sensor nodes are directly communicating with nearby collection hubs which are typically more powerful and serve the role of the network coordinator, or gateway, connecting the local network to the rest of the Internet.

Optimizing the communications efficiency of battery operated or energy harvesting asymmetric WSNs, sometimes at the expense of additional complexity at the receiving hubs, is of major importance in order to ensure extended operation times. The harsh environments these networks typically operate in, with frequent channel quality variations and external interference from nearby networks of several order of magnitude higher transmission power, i.e. WLANs and cellular networks, imposes severe challenges in ensuring the required data reliability and desired efficiency.

Several schemes have been proposed to achieve reliable and efficient communication over unreliable channels in asymmetric WSNs. Physical layer (PHY) forward error correction (FEC) schemes insert redundancy in the transmitted information by transforming an uncoded message of k bits into a coded packet of n bits. Thus, FEC schemes increase the probability of successful recovery of the channel-corrupted message at the receiver at the expense of bandwidth efficiency [4]. The efficiency benefits of these schemes have been studied in numerous works, including [5, 6, 7]. An alternative approach for improved communications reliability is the use of packet-level erasure codes, inserting redundancy across packets [8]. Performance advantages of using packet-level erasure codes in terms of delay, reliability and energy efficiency are analyzed in [9, 10, 11].

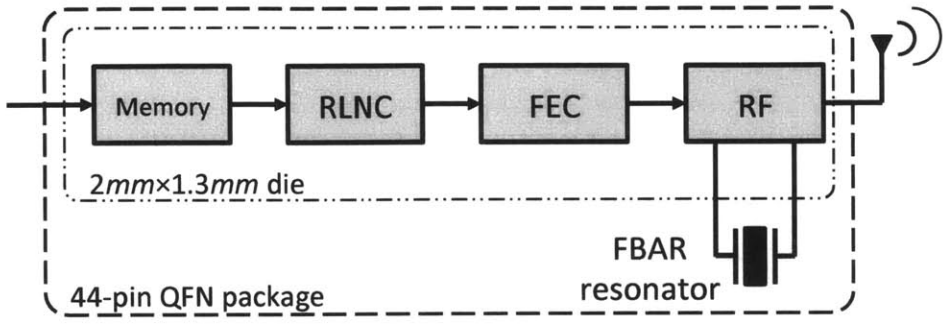

Figure 2-1: Block diagram of the proposed 2.4GHz transmitter for asymmetric WSNs.

In this chapter, we consider the use of random linear network coding (RLNC) [3] and we explore its energy efficiency and reliability benefits in asymmetric WSNs. RLNC is a relatively new coding paradigm which encourages intermediate nodes within a network to code and mix information, and lets the final destinations decode the mixtures. A vast literature exists in theoretically characterizing the performance of RLNC in WSNs, reporting significant benefits [12, 13, 14]. The analysis presented in this chapter investigates the benefits of RLNC in asymmetric WSNs and its interplay with PHY FEC schemes, as well as the design of a low power transmitter for these resource constrained applications and over-the-air experimental results.

In more detail, we present the energy benefits of RLNC in asymmetric WSNs under specific scenarios of operation. In addition, we propose a low power architecture for a 2.4GHz transmitter operating at 1Mbps, with variable output power and custom accelerators for FEC and RLNC schemes, using a TSMC 65nm process. The chip consumes 580μW while transmitting at -10dBm and, to the best of our knowledge, it is the first reported implementation of a transmitter with custom multi-rate accelerators for FEC and RLNC in the literature. The fabricated chip is co-packaged with film bulk acoustic wave resonators (FBAR), generating the carrier frequency in a PLL-less manner, similarly to [15]. The block diagram of the proposed transmitter architecture is shown in Fig. 2-1.

The main contributions of this chapter are summarized below:

- Investigation of the power savings benefits of RLNC in asymmetric WSNs.
- Design of the first reported custom hardware implementation of RLNC and co-optimization of the code performance with the computational complexity.
- Integration of the RLNC engine with a low power 2.4GHz transmitter, supporting different FEC and RLNC rates.
- Experimental measurements on the reliability and energy efficiency of the designed transmitter in typical indoor environments, communicating with commercial receivers.

The rest of the chapter is structured as follows. In Section 2.2, a brief overview of RLNC is provided and its energy savings are quantified in a few representative scenarios. In Section 2.3, the system architecture is presented and the operation of every major block is explained, while in Section 2.4 the low power design of the RLNC accelerator is presented. Section 2.5 provides the measurement results of the proposed design and Section 5.6 concludes the chapter.

2.2 Background and Related Work

In this section, background information on the RLNC scheme is provided, its encoding and decoding processes are described, and its energy savings in asymmetric WSNs are quantified.

2.2.1 Random Linear Network Coding

Network coding [16, 17] is a new coding technique which has received significant attention in the Wireless Communications research community due to its advantages in a wide range of applications. From a data reliability perspective, network coding can be considered a cross-packet rateless coding method, similar to LT and Raptor

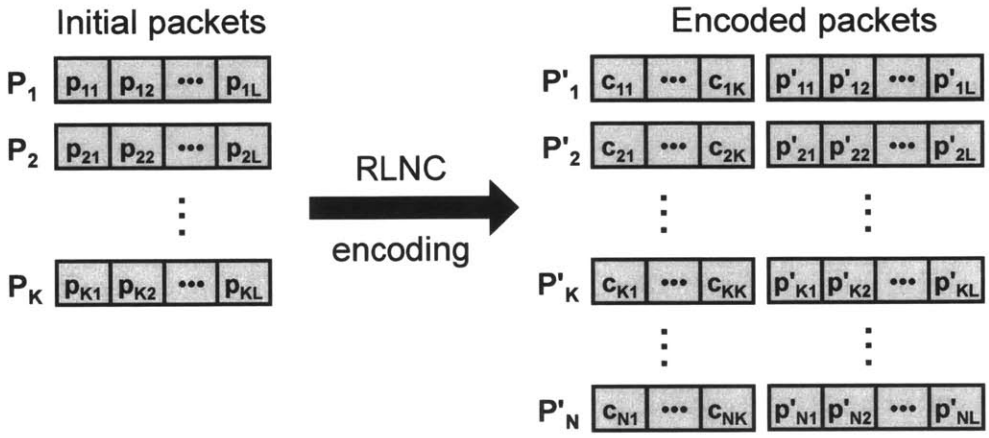

Figure 2-2: Encoding process of RLNC. K initial packets are mapped to N coded packets. Each of the coded packets is a linear combination of the initial packets, weighted according to a set of randomly selected coefficients.

codes [18] but, in general, its use extends to many broader scenarios which go beyond the scope of this chapter. The mixing of packets can be performed with several techniques which determine the specific type of network coding. According to random linear network coding (RLNC) [3], encoded packets are produced as linear combinations of the initial packets, weighted according to randomly selected coefficients.

Assume that K packets have to be transmitted $(P_1, P_2, ..., P_K)$ from a sensor node to a receiving coordinator, each of them containing L symbols of data, i.e. $P_1 = \{p_{11}, p_{12}, ..., p_{1L}\}$, as shown in Fig. 2-2. Let every symbol contain q bits; thus, every packet for transmission is assumed to be Lq bits long. Assuming K/N is the coding rate, the encoding process of RLNC transforms the K packets and creates N coded packets $(P_1^{'}, P_2^{'}, ..., P_N^{'})$ of equal length, where $N \geq K$. A coded packet $P_i^{'} = \{p_{11}^{'}, ..., p_{1L}^{'}\}$ is produced by randomly selecting a set of K coefficients $(C_i = \{c_{i1}, c_{i2}, ..., c_{iK}\})$, each of them being q bits long, and creating a linear combination of the initial packets, according to

$$p_{il}^{'} = \sum_{j=1}^{K} p_{jl} \times c_{ij}, \tag{2.1}$$

where $1 \leq l \leq L$ and $1 \leq i \leq N$. Using matrix notation, the encoding process is described by

$$P' = C \times P, \tag{2.2}$$

where P is the matrix of initial packets, C the matrix composed of the sets of coefficients and P' the matrix of coded packets. The set of coefficients associated with a coded packet is usually appended to its header.

The encoding process of RLNC can be considered as the creation and transmission of N linear equations of K unknowns. Thus, at the destination's side, receiving any K out of the N transmitted packets is sufficient to recover the initial packets. The decoding process consists of the opposite process of inverting the coefficients matrix (C) and multiplying it by the coded packets,

$$P = C^{-1} \times P'. \tag{2.3}$$

RLNC encoding and decoding processes, described by Eq. (2.2) and (2.3), are performed over finite fields. A finite field of size 2^q, usually represented as GF(2^q) in honor of Evariste Galois, is a set of 2^q elements, with the operations $+$ and $\times$, often called addition and multiplication, satisfying certain properties. One of these properties is that the field is closed under the two operations, meaning that when an operation is applied to some elements, the result will also be an element of this field. This property guarantees that the result of any operation has the same length as the initial operands. Thus, the encoded packets will be of the same length as the initial ones. The details of finite field operations and their implementation are covered in Section 2.4.

2.2.2 RLNC in WSNs

Several researchers have analyzed and demonstrated the potential benefits of RLNC in WSNs. For instance, authors of [19] presented a protocol design which

uses RLNC to encode transmitted information and achieves a significant reduction in the required time the receiver of a sensor node has to be listening. Considering a small network of a few sensors and assuming transmission energy per packet to be equal to reception energy per packet, simulation results reveal that the total energy consumption of sensors is reduced by 30% [20]. In [13], RLNC increases data reliability in dynamic scenarios of WSNs by 50% and, according to experimental results [11], RLNC masks inefficiencies of the physical layer and offers a 2.7dB coding gain. In addition, use of RLNC can simplify other part of the protocol stack, such as data encryption. According to [21], encryption of the coefficients only instead of the whole packet payload can ensure the same level of security while reducing the encryption energy consumption by approximately 10×. According to [22], 40% less data traffic is required to be communicated when firmware is updated in WSNs by the use of RLNC, while [23] leverages the same coding scheme to extend the duty cycle of low power WSNs.

2.2.3 Implementation of RLNC

Because of its advantages in both wireless and wireline networks, RLNC has attracted a lot of interest and its implementation has been considered by many researchers. Multi-core CPUs and GPUs have been used to accelerate its encoding and decoding processes, achieving throughput in the order of hundreds of MB/s [24, 25, 26]. Implementation of RLNC on FPGA platforms has been considered in [27]. In addition, MCUs and embedded processors have been used as implementation platforms for RLNC, exploring its energy requirements in portable applications [28, 29].

The strict energy consumption constraints associated with asymmetric WSNs require a very detailed description of the energy overhead of RLNC. In the following sections, we present a custom, low power implementation of RLNC encoder and its integration in a complete 2.4GHz transmitter architecture targeting asymmetric

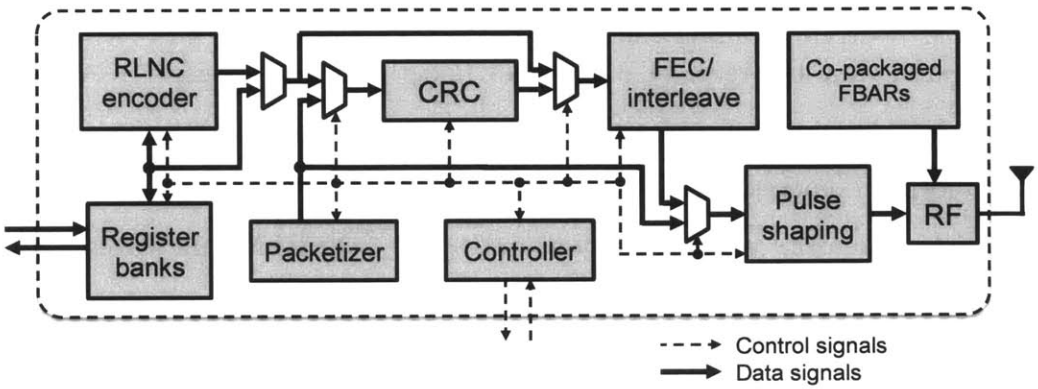

Figure 2-3: Block diagram of the 2.4GHz transmitter, targeting asymmetric WSNs. The system supports multiple FEC and RLNC coding rates while using a FIFO-less architecture.

WSNs.

2.3 System Architecture

In this section, an overview of the designed system is provided, along with details on its architecture and its main processing blocks.

2.3.1 Architecture Description

The architecture of the proposed system is shown in Fig. 2-3. The system is designed to transmit information at a constant rate of 1Mbps in short-range distances of up to 6 meters. Because of the channel quality variations and path losses in typical WSN environments, the system is designed to offer different levels of redundancy in the transmitted data in order to meet the desired BERs. The RLNC and FEC/Interleaver engines support different coding rates and the RF block adjusts its output transmission power through pre-configuration by external control signals or adjusted on the fly.

Incoming data from a sensor's AFE are temporarily stored on on-chip register banks and, when sufficient information is accumulated, the encoding and transmis-

sion processes are triggered. First, the RLNC block processes the stored data, and after the formation of an appropriate packet structure, the FEC/Interleaver block encodes the data before their transmission by the RF block. Apart from the RLNC encoder which is described in more detail in Section 2.4, the main building blocks of the transmitter are the following:

Register banks: The system is designed to receive information at different rates and duty cycles, independent from the later stages of processing and transmission. Thus, an on-chip memory is included in the design in order to decouple information acquisition and transmission. Because of the low power requirements and the near-threshold operation of the system, the memory is based on registers in order to avoid the low voltage performance challenges of SRAMs [30]. The total size of the memory is 2Kb and is organized in four segments, each one corresponding to the payload of a packet for transmission.

Packetizer: Every transmitted packet contains, apart from its payload, required information for its correct reception, synchronization and parsing. For instance, special bit sequences of preambles are appended at the beginning of the packet and sequence numbers for identification are contained in packets' header. This extra information, along with protocol related data, are properly added by the packetizer in an efficient manner.

CRC: An error detection parity check is added on the transmitted information, enabling the receiver to identify if the captured and decoded packet is erroneous or not, before its propagation to the application layer. The system attaches a 16bit checksum to every packet, calculated through a shift register line according to the polynomial: $x^{16} + x^{15} + x^2 + 1$.

FEC/Interleaver: A convolutional encoder of constraint length 4 is used to protect transmitted information against channel impairments, followed by a 32 bits interleaver to combat bursty transmission errors. The convolutional encoder supports four coding rates (1, 3/4, 1/2 and 1/3), each one used for different channel qualities. The

encoder is implemented by a shift register line, while the interleaver using 32registers, written and read in the opposite directions.

Controller: The operation of all blocks and data transfer among them are orchestrated by a main controller, implemented as a finite state machine. The controller is externally pre-configured and its settings include the RLNC/FEC coding rate, length of coded packets together and output transmission power.

FBAR oscillators: Because of the improved power trade-off and high-Q factor of micro-electro-mechanical (MEM) devices, we make use of FBAR oscillators, co-packaged with the fabricated die. This enables the carrier frequency generation without the use of a PLL, reducing the power consumption of the system.

RF: Information is transmitted using Frequency Shift Keying (FSK) modulation by tuning the center frequency of the high-Q FBAR-based local oscillator by switching the capacitor bank between two codes depending on the data [15]. For minimum bandwidth at 1Mbps, a frequency separation of 500kHz is used.

Pulse shaping: FSK modulation produces side-bands in the spectrum, but it is highly desirable to reduce this emission to improve interoperability in the busy 2.4GHz ISM band. Fig. 2-4 shows the implemented architecture for Gaussian pulse-shaped FSK (GFSK) with BT product = 0.3. Fixed coefficients are used to reduce the FIR filter to simple shift and add operations. The coefficients and the 5× oversampling speed are chosen as a trade-off between power and spectral efficiency through Matlab simulations. Fig. 2-5 shows the coefficients used, along with the error with respect to an ideal 5× oversampled filter. The sum of coefficients is designed as a power of 2 (512 in this case) so that the inputs to the FIR filter can be the required max and min capacitor bank settings. The lower bits of the FIR filter are dropped before driving the oscillator.

Low power design techniques are used in order to achieve minimum energy operation. Near-threshold voltage scaling is applied to the digital part of the system and low voltage operation on the RF. Through careful design, the chip is functional while

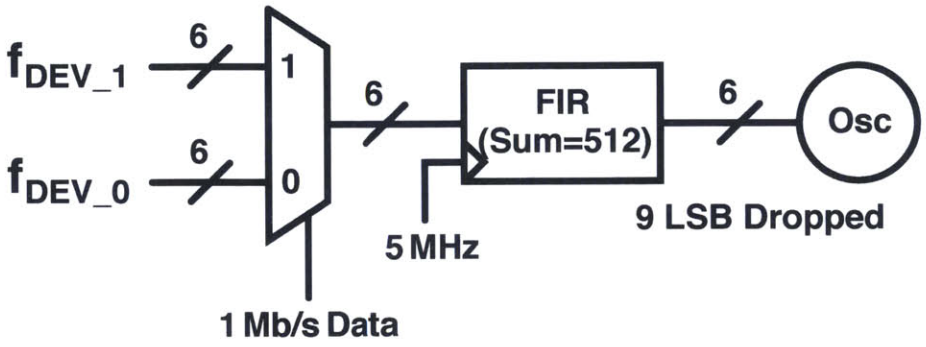

Figure 2-4: Architecture for the pulse shaping block.

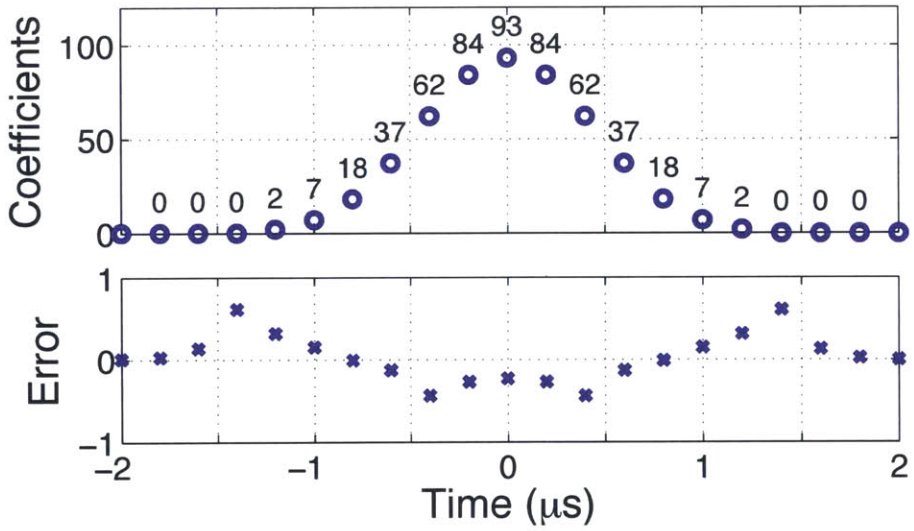

Figure 2-5: The impulse response of the Gaussian filter used and error from the ideal filter.

the digital supply voltage is scaled down to 0.35V, resulting in $> 10\times$ power savings. In addition, clock gating is used to reduce dynamic power and custom level-shifters are implemented to interface with other voltage domains, including the RF block and IO. On the architecture level, careful design and timing is performed in order to avoid use of FIFOs between the blocks, minimizing the active and leakage energy consumption.

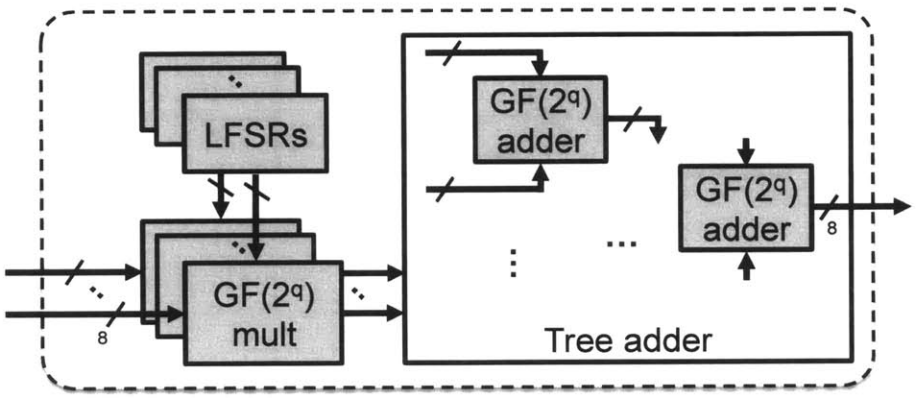

Figure 2-6: Block Diagram of the RLNC encoder. All operations are performed over GF(2^q).

2.4 RLNC Accelerator

The block diagram of the RLNC encoder, implementing Eq. (2.1), is shown in Fig. 2-6. It is a fully parallel implementation, calculating one symbol of a coded packet in every clock cycle. Stored data from the register banks are fetched and processed by the RLNC encoder. The incoming symbols are first multiplied with the coding coefficients and then added together to form the coded packet symbols. The pseudo-random coefficients are produced by linear feedback shift registers (LFSRs) which are initialized by appropriate values in order to ensure linear independence in the decoding process.

2.4.1 Finite Field Arithmetic

In general, finite fields play an important role in many communication systems and cryptographic schemes, such Reed-Solomon codes and AES encryption. Since digital computing machines use Boolean logic, the binary field GF(2)=$\{0, 1\}$, and its extension fields GF(2^q), are widely used, due to the direct map between their elements and the Boolean values. All operations of the RLNC block are performed over the GF(2^8). Elements of a finite field of size 2^q are considered and treated as vectors

$[a_{q-1}, \ldots, a_0]$ or polynomials of degree at most (q-1) with coefficients from GF(2)

$$GF(2^q) = \{A|A(x) = a_{q-1}x^{q-1} + \ldots + a_1x^1 + a_0\}, \tag{2.4}$$

where $a_i \in GF(2)$ and $0 \leq i \leq q-1$. Assume $A(x)$ and $B(x)$ are two GF(2^q) elements. Their sum is equivalent of the bit-wise XOR of their polynomial representation while their multiplication is a two step operation composed by typical polynomial multiplication followed by modulo reduction:

$$P(x) = A(x) \times B(x) = (A(x) \cdot B(x)) \bmod p(x), \tag{2.5}$$

where $p(x)$ is the primitive polynomial of the field.

2.4.2 Representation Basis

The representation basis of the elements of a field is of crucial importance, determining the efficiency and complexity of the implementation of different arithmetic operations. There are several field representation bases; the standard (or polynomial) and the normal basis are the most common ones. Although the normal basis facilitates the multiplication of two numbers, we choose for our implementation to work entirely on the standard basis in order to avoid conversion and the associated energy consumption when data are exchanged between the RLNC encoder and other hardware modules; standard basis represents numbers in the same way as fixed-point representation does [31].

2.4.3 Low-power GF(2^8) Adder and Multiplier

Targeting resource constrained WSN nodes, both the GF adder and multiplier are designed to consume the lowest power consumption. As shown in Fig. 2-6, a tree-based, balanced adder structure is used of multiple GF(2^8) adder cells of 8 XOR

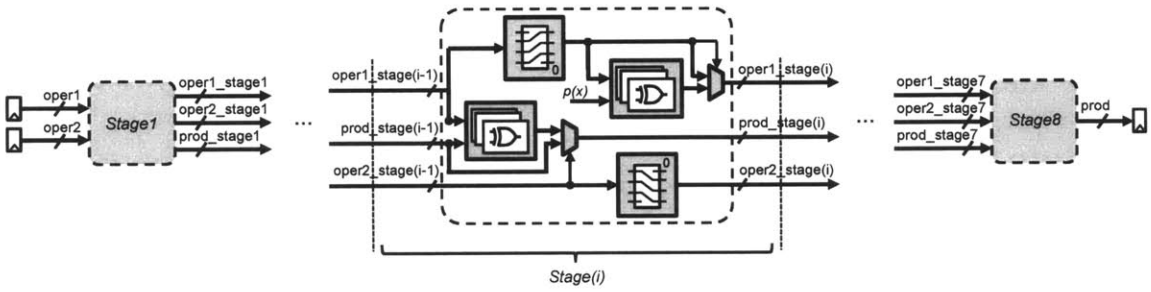

Figure 2-7: Block diagram of the bit-parallel GF(2^8) multiplier, showing its stages. The product of two numbers is calculated in one clock cycle.

gates each. Because multiplication is a more complex operation compared to addition, several works have proposed optimized algorithms and architectures [32, 33].

Our multiplier is a bit-parallel architecture of 8 stages using only XOR and shift operations in order to calculate the product. Implementation details of the i^{th} stage of the multiplier are shown in Fig. 2-7. The low data rate requirements of our system enable us to operate at a supply voltage near transistors' threshold and at low clock frequencies without the need for pipelining. The standard representation basis is used and the primitive polynomial is $p(x) = [1, 0, 0, 0, 1, 1, 1, 0, 1]$.

2.5 Performance measurements

In this section, the experimental setup is described, the power consumption of the chip is presented and the results of the performance comparison are discussed.

2.5.1 Experimental Setup

The experimental comparison of FEC and RLNC schemes, as well as their joint operation, is performed through careful and controlled experiments. The setup is shown in Fig. 3-9. The custom transmitter, representing a sensor node in a typical asymmetric WSN, is controlled by a Matlab program on a PC through an FPGA. A generic commercial transceiver (Texas Instruments CC2511 [34]) is used to receive

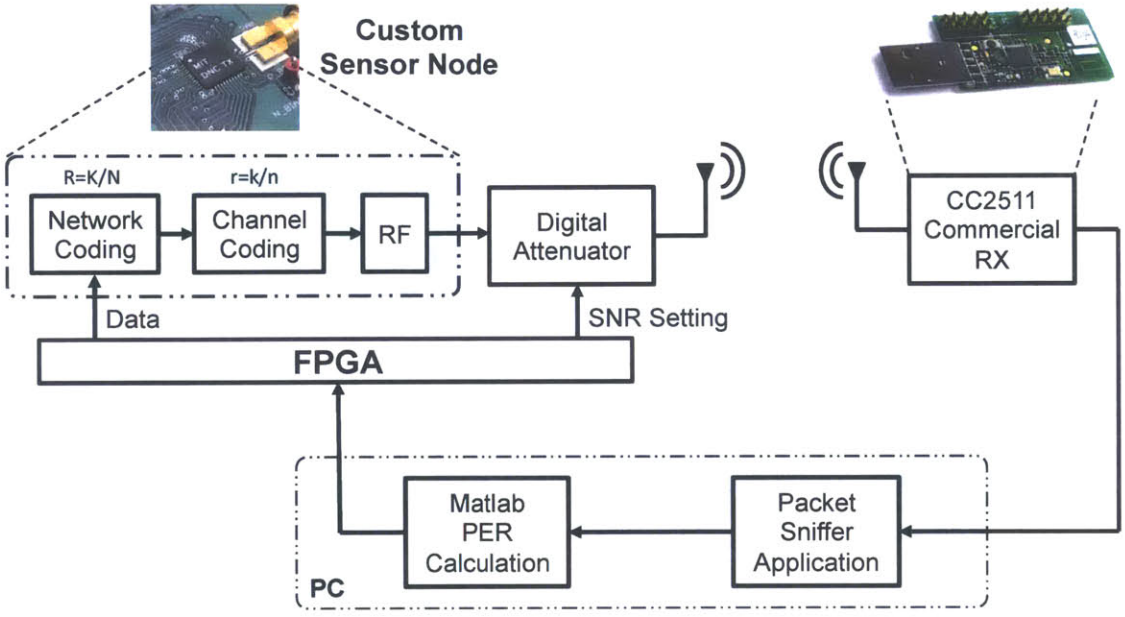

Figure 2-8: Block diagram of our experimental testing setup.

the data from the transmitter. A transmission data rate of 500 kbps is used for all our measurements, which is limited by the maximum supported data rate of the CC2511 receiver. FSK modulation is employed for data transmission and coherent demodulation is performed at the receiver; hard Viterbi decoding and an interleaver of 4 bytes length are also used. A PC-based packet sniffer software transfers the data from the CC2511 over a USB interface. This software then sends the received data over to the Matlab program which then computes the packet error rate.

The CC2511 chip provides the Received Signal Strength Indicator (RSSI), which is a good proxy for the SNR on the channel. In the rest of the chapter, RSSI and SNR values will be treated interchangeably. In order to perform detailed PER measurements and estimate coding gains, the SNR of the received signal needs to be changed. The intrinsic output power tuning on the transmitter is limited (about 7dB), and it is not possible to physically move the devices apart in a repeatably accurate manner. To overcome this issue, a digitally controlled RF attenuator is connected between the

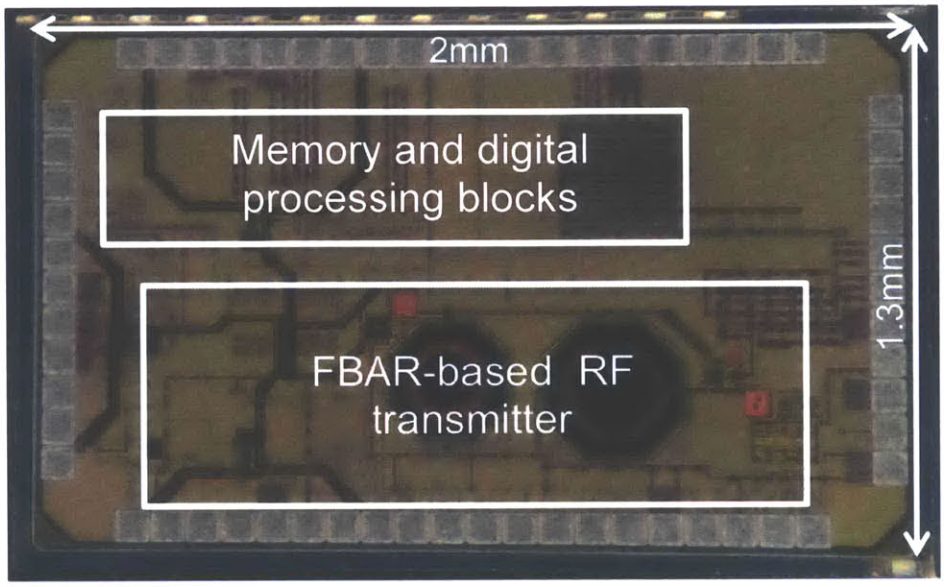

Figure 2-9: Chip die photo.

transmitter IC and the antenna. A 31dB dynamic range, with 1dB/step [35] provides a very repeatable method of sweeping the SNR of the channel. For each setting of the attenuator and code rate, 10^3 packets are transmitted, each of 48 bytes length.

2.5.2 Chip Power Consumption Measurements

The chip is implemented in 65nm CMOS. The 2mm$\times$ 1.3mm chip is co-packaged with an FBAR resonator in a 44-pin QFN package. The chip die photo is shown in Fig. 2-9. The digital part of the system consumes only 30μW for 1Mb/s data rate, when operating at 0.4V. The RF section consumes 550μW while transmitting with FSK modulation and -10dBm output power, achieving an energy efficiency of 550pJ/bit at 1Mb/s. The FIR filter for 1Mb/s GFSK consumes 15μW from a 1V supply, running off a 5MHz clock. Fig. 2-10 shows the spectra of 1Mb/s FSK and GFSK. The first side-lobe is reduced by 11dB and the second by 28dB. The much improved spectral efficiency occurs with only 15pJ/b overhead.

Table 2.1: Summary of chip measurements.

Technology	65nm
Datarate	1Mb/s
Modulation	FSK, GFSK
Digital blocks	
Supply (RLNC, FEC, etc)	0.4V
Supply (pulse shaping)	1V
Power	30μW
RF block	
Supply	0.7V
Power	550μW

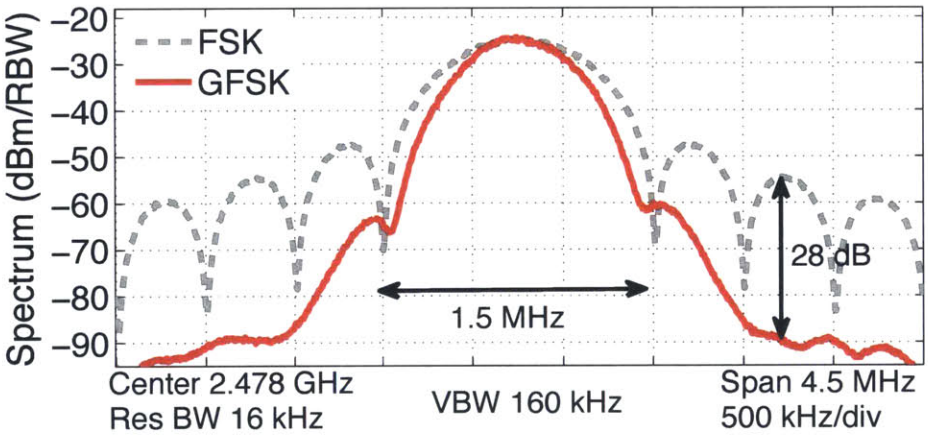

Figure 2-10: Spectra of 1Mbps FSK and GFSK.

2.5.3 Performance of FEC and RLNC Operating Separately

The error correction performance of the PHY-layer FEC code is shown in Fig. 2-11. The measured PERs for different code rates are plotted. A FEC of code rate 3/4 provides only a marginal improvement over uncoded data transmission, while FEC of code rate 1/2 provides approximately 2.25dB SNR improvement. Use of a FEC code

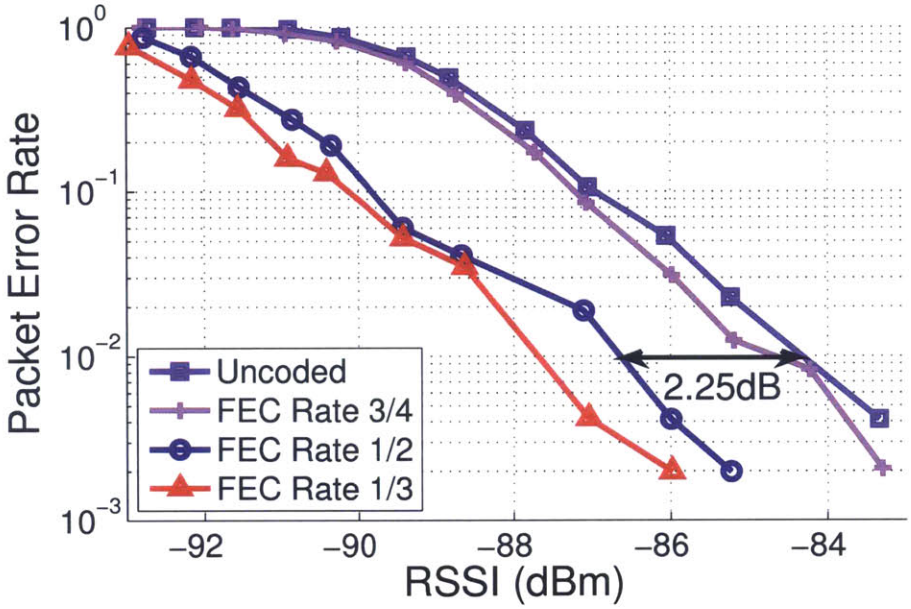

Figure 2-11: Measured packet error rate (PER) curves for a convolutional (FEC) code of rate = 3/4, 1/2 and 1/3 compared with uncoded packets' transmission.

with rate 1/3 offers only a small additional coding gain compared to the rate 1/2 code; as expected, increasing the redundancy of the FEC code provides diminishing returns in the coding gain.

Fig. 2-12 shows the performance of RLNC for several code rates, when no FEC code is used. At a PER of 10^{-2}, its effective SNR improvement is 2.5dB and 3.4dB for the 4/6 and 4/8 code rate, respectively. The PER curve of the FEC of rate 1/2 is also plotted in the same figure with dashed line. Comparing the PER curves of the two coding schemes in Figs. 2-11 and 2-12, a very important characteristic about their behavior becomes evident. Although the same amount of total information is transmitted for both PHY-layer FEC and RLNC of code rate 1/2, in the low RSSI regime, the FEC code performs better than RLNC but, for higher RSSI values, the roles are reversed. For instance, at PER of 10^{-2}, RLNC offers an additional coding gain of 1.1dB. This happens because the slope of the PER curves for RLNC is much steeper compared to that of the FEC curves.

The difference in the PER curves for the two coding schemes can also be explained

by examining the behavior of the wireless channel in typical indoor environments. For a AWGN channel with fixed and known SNR, FEC codes can be designed to communicate packets reliably, as long as their transmission rate is below the capacity of the channel. In that case, packet-level erasure codes are not necessary. On the other hand, for an erasure channel, in which packets are either received entirely correct or completely erased, a packet-level erasure code (such as RLNC) can be sufficient to provide the necessary reliability, making a physical layer code unnecessary. In practice, a realistic wireless indoor channel lays somewhere between these two extreme limits. Although noise is always present in the wireless medium causing random bit errors within a packet, its effects are more pronounced in the low SNR regime and these random errors are better corrected by a PHY-layer FEC code. However, for higher SNR values, interference from nearby networks operating at the same frequency band becomes the dominant limiting factor, creating packet collisions with large burst errors and making the channel behave like a block fading channel. In that case, RLNC performs better by introducing a longer dependency across packets, which can be translated to diversity gains.

2.5.4 Joint Performance of FEC and RLNC

The performance of the joint channel-network coding (JCNC) scheme is shown in Fig. 2-13. According to our measurement results, JCNC of effective rate 1/3 performs better than the FEC code of the same rate by approximately 1dB at PER of 10^{-2}. However, at the very low SNR regime, the FEC code has the best performance because, as explained earlier, use of RLNC requires successful reception of at least K packets for a block to be decoded. This graph confirms the harmonic synergy between FEC codes and RLNC in a joint coding scheme. As is shown, the coding gain of joint PHY-layer FEC and RLNC is 5.6dB for an effective code rate 1/4. Table 2.2 summarizes the effective SNR improvements for different PHY-layer FEC and RLNC code rates at two target PERs.

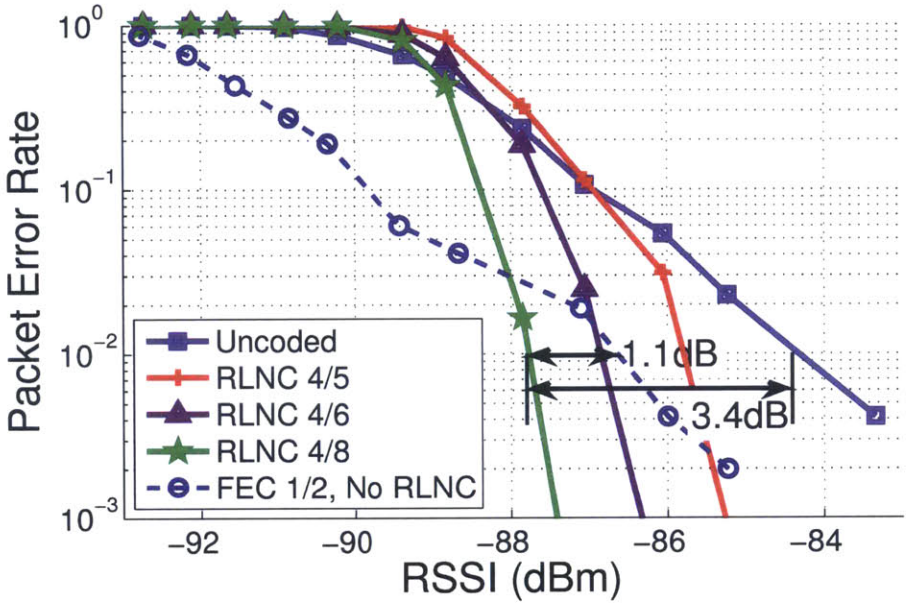

Figure 2-12: Measured packet error ate (PER) curves for RLNC of rate = 4/5, 4/6 and 4/8 compared with uncoded packets.

2.6 Summary

This work presents the first custom VLSI implementation of RLNC, integrated with a multi-rate convolutional FEC code and a low-power 2.4GHz transmitter, implemented in a 65nm CMOS process. RLNC is shown as a promising coding scheme which can enhance the reliability of transmitted data in resource constrained asymmetric WSNs. According to our measurement results, RLNC rate 4/8 offers 3.4dB coding gain compared to the uncoded case, and when combined with FEC rate 1/2, the coding gain is close to 5.6dB. The power consumption of the digital part of the chip, including the pulse shaping block, is 30pJ/bit at 1Mbps datarate, operating at 0.4V, whereas the RF block consumes 550pJ/bit, transmitting at −10dBm output power. More detail can be found in [36, 11].

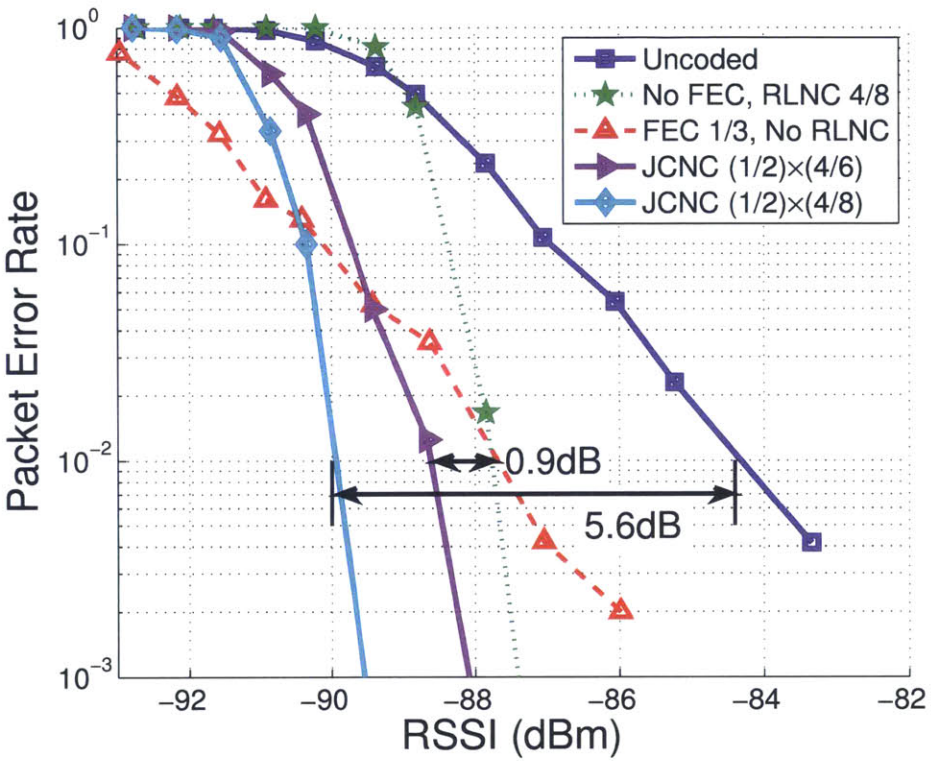

Figure 2-13: Measured packet error rate (PER) curves for the joint channel-network coding (JCNC) scheme.

Table 2.2: Effective SNR improvement for the JCNC scheme.

FEC Rate	RLNC Rate	SNR improvement	
		PER= 10^{-1}	PER=10^{-2}
1	1	-	-
1	4/5	0dB	1.5dB
1	4/6	0.625dB	2.5dB
1	4/8	1.5dB	3.4dB
1/2	1	2.5dB	2.25dB
1/2	4/5	2.25dB	4dB
1/2	4/6	2.75dB	4.25dB
1/2	4/8	3.5dB	5.6dB

Chapter 3

PRAC: Harnessing Partial Packets in Wireless Networks - Throughput and Energy Benefits

In light of the requirements for increased data reliability and higher energy efficiency in modern WSNs, this chapter proposes a partial packet recovery (PPR) scheme, called Packetized Rateless Algebraic Consistency (PRAC). PRAC exploits intra- and inter-packet consistency to identify and recover erroneous packet segments, *without* recourse to soft physical layer (PHY) or detailed feedback information. In the absence of cross-layer coordination or detailed feedback, the prevailing methods proposed in the literature have discarded packets with errors. PRAC uses a rateless linear packet code for data encoding and an iterative decoding process for data reconstruction. It allows, but does not rely upon, the use of any PHY forward error correction (FEC) code, requires no feedback other than a notification of completion and, in the absence of partial packets, incurs no overhead. In order to quantify PRAC's performance in terms of both throughput and energy efficiency, experiments are conducted using wireless off-the-shelf transceivers in two scenarios: a static, indoor testbed of seven nodes and a dynamic scenario of sensors being attached to a

person while doing typical body movements. Our implementation results reveal that PRAC offers an average throughput gain of 35% compared to a baseline automatic repeat request (ARQ) scheme discarding partial packets and 13% compared to an ideal genie-aided hybrid-ARQ (iHARQ) scheme. On high packet error rate (PER) links, throughput is improved by 148% and 34%, respectively. In addition, according to our experiments, PRAC reduces on average the total energy consumption of the transmitting nodes by 16%, while its energy savings benefits are increasing when links of high PER are considered.

3.1 Motivation

Wireless communication networks achieve reliable communication over unreliable channels using either physical layer (PHY) forward error correction (FEC) codes, automatic repeat request (ARQ) protocols, hybrid ARQ (HARQ) methods, cross-layer schemes or a combination of these techniques. PHY FEC schemes intelligently insert redundancy by transforming an uncoded message of k bits into a coded packet of n bits, increasing the probability of successful decoding of the channel-corrupted message at the receiver [37]. In general, data reliability increases with extra redundancy at the expense of bandwidth efficiency. Although PHY FEC codes significantly improve the data reliability, under certain conditions, they fail to ensure complete correctness in the decoded information. In order to prevent erroneous packets to be forwarded to higher layers of the protocol, error detection codes (e.g. cyclic redundancy checks-CRCs) are typically used, identifying packets with erroneous bits. In the rest of the chapter, packets which satisfy the error detection rule and can be propagated to higher layers are called *valid*, while packets which have been processed by the PHY and contain at least one erroneous bit are called *partial*. In a typical ARQ protocol, when a partial packet is detected, a retransmission is requested and all the information associated with the partial packet is discarded.

In communication channels with large signal-to-noise (SNR) variations, rate adaptation schemes are used to estimate the channel quality and adapt the modulation and coding scheme (MCS) accordingly [38]. In principle, exact knowledge of the channel state information combined with rate adaptation and infinitely long FEC codes can asymptotically guarantee reliable communication [39]. However, the highly varying nature of the wireless medium usually results in significant SNR dynamic ranges and makes quite challenging the task of channel tracking. Unlike ARQ protocols, HARQ schemes accumulate PHY soft information across multiple received copies of the same block, or its parity bits, and, by combining their redundancy, lower the effective coding rate to match the channel condition [40]. This approach usually results in higher throughput and improved energy efficiency at the expense of extra computational complexity. Similarly to HARQ schemes, partial packet recovery (PPR) schemes harness information contained in partial packets without discarding erroneous data blocks [41]. PPR schemes can be designed to be PHY independent [42] and offer more flexibility in their implementation, covering a wide range of communication networks, from high-speed WLANs to low-power wireless sensor networks (WSNs).

In this chapter, a new PPR technique is proposed, called Packetized Rateless Algebraic Consistency (PRAC), which leverages the information contained in partial packets in a PHY-independent manner and reduces the overall number of retransmissions. The main challenge in any PPR scheme is the identification of correct information within a partial packet. PHY soft information, multiple CRCs and/or pilot bits within a packet, detailed feedback information and additional redundancy enabling error estimation codes have been proposed as potential solutions. PRAC does not use any of these methods. Instead, transmitted data are encoded using a rateless linear cross-packet code and correct information is harnessed from partial packets making use of PRAC's algebraic consistency rule (ACR) check. ACR check exploits the property of linear (n, k) codes, according to it any k out of the n symbols are sufficient to decode the initial data and the other $(n - k)$ are linear combinations

of them. The recovery process is performed iteratively using an optimized search algorithm, ACR checks and CRC updates.

The main characteristics of the proposed scheme are the following:

- PHY soft information is not required to be exposed to higher layers, making the proposed algorithm easily deployed in current wireless networks[1].
- PRAC's encoding process incurs no transmission overhead for correctly received packets.
- PRAC requires minimal feedback information since it can operate with only a notification of completion.
- The computational requirements of PRAC's recovery algorithm can be easily adapted to the available resources, balancing the recovery performance with the algorithmic complexity.

We test and evaluate the performance of the proposed PPR mechanism in terms of both throughput and energy efficiency in typical indoor wireless network settings. Commercial boards with CC2500 and CC2511 radio modules are used [43, 34] in two sets of experiments. First, PRAC is tested over a 7-node indoor testbed investigating its reliability and throughput benefits. In addition, we use an experimental setup of four sensor nodes mounted on a human body and transmitting information to a nearby receiving hub, evaluating PRAC's energy efficiency. In both experiments, data traces are collected and processed off-line. PRAC's throughput performance is compared against a baseline ARQ protocol and an ideal genie-aided HARQ (iHARQ) scheme whose performance, in the absence of detailed feedback, is an upper bound on all cross-layer schemes. PRAC's average throughput improvement is 35% and 13% compared against the baseline and iHARQ, respectively, considering all links of the testbed. On high packet error rate (PER) links, throughput is improved by 148% and

[1]To the best of our knowledge, none commercial wireless card exposes cross-layer information, such as symbol-level PHY soft information, at the driver level.

34%, respectively. In terms of energy efficiency, PRAC achieves an average increase of 16%, while, in high PER links, savings can exceed 50%.

The rest of the chapter is structured as follows. Section 3.2 presents a summary of related techniques and an overview of the proposed scheme. Section 3.3 describes PRAC's encoding process while the decoding process is presented in Section 3.4. Section 3.5 provides details on the performance evaluation and experimental setups. Sections 3.6 and 3.7 present PRAC's measured throughput and energy benefits, respectively. Finally, Section 5.6 concludes the paper.

3.2 Background and Related Work

Achieving reliable communication over unreliable wireless links and exploiting correct information contained in partial packets in order to increase performance of wireless networks, including WSNs, have attracted extensive attention. In the following subsections, we present some of the main approaches.

3.2.1 FEC Codes and Rate Adaptation Techniques

One widely used approach for increasing reliability of wireless links and reducing the effect of channel-induced errors is the use of PHY FEC codes. The literature on this topic is vast and some of the codes are described in [37, 4]. Different channel conditions require different amounts of redundancy, since fixed code rate FEC schemes can operate well only within a specific SNR regime. Powerful low-rate FEC codes can deal with severe channel conditions, while high-rate codes are used under good channel conditions as being more throughput and energy efficient [5, 44].

Rate adaptation techniques are used in order to estimate the channel quality and adapt the modulation and coding rate accordingly [38, 45]. A trade-off exists between the amount of associated overhead (i.e. probing or channel state feedback) versus the accuracy of the measurements. In general, the incorporation of channel measure-

ment mechanisms increases system's complexity, and, in mobile environments, a rate adaptation mechanism might be inefficient to track changes of a wireless fast-varying channel [46]. For this reason, rateless codes which do not require a priori knowledge of the channel quality have been proposed. For instance, coding schemes described in [47] and [48] asymptotically achieve the capacity of the binary erasure channel (BEC) without knowledge of the erasure probability. More recently, [49] and [50] proposed practical rateless codes for AWGN and binary symmetric channels, respectively.

3.2.2 HARQ and PPR Schemes

HARQ schemes eliminate the inefficiency associated with ARQ protocols of completely discarding packets with some errors and requesting retransmissions. Instead, they incrementally adjust the effective code rate, dealing with the "all-or-nothing" behavior of fixed rate PHY FEC codes. For instance, the HARQ scheme analyzed in [40] accumulates PHY soft information corresponding to incoming and previously received partial packets, gradually increasing the probability of a successful reception by combining the corresponding information. According to another HARQ scheme [51], different coded versions of the received partial packet or extra amount of redundancy is transmitted, incrementally increasing the correcting ability of the scheme. Owing to their performance benefits, HARQ schemes have been adopted in several modern wireless communication systems, e.g. WiMax [52] and LTE-A [53], but, in general, they exhibit high computational complexity and limited flexibility, being almost prohibitive for WSNs.

Several PPR schemes have been proposed in the literature, operating at the data link or higher layers, independently or not of the PHY. Cross-layer PPR schemes, which operate in synergy with the PHY, typically annotate every decoded bit with a confidence hint, as shown in Fig. 3-1. This enables the link layer to identify which chunks of a packet have higher probability of being erroneous and request, through the use of additional feedback information, only those chunks, as in [41]. Similarly,

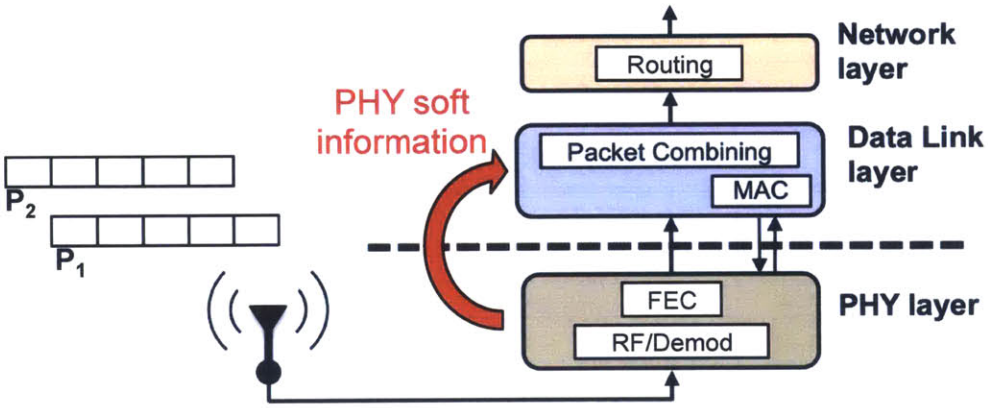

Figure 3-1: Simplistic block diagram of a protocol stack in a receiver using a cross-layer PPR scheme with propagation of PHY soft information to higher layers.

schemes proposed in [54] and [55] use PHY soft information from multiple receivers, leveraging spatial diversity.

PHY-independent PPR schemes typically identify correct segments by introducing some overhead within the transmitted packets, such as multiple CRCs per packet [56] or additional redundancy for error estimation codes [57]. Other schemes modify the feedback mechanism to include additional information in the acknowledgment frames [58] or use cross-packet coding methods based on erasure codes [42]. Table 3.1 summarizes some of the proposed approaches listing their main design features with respect to requiring access to PHY soft information, introducing fixed overhead for every transmitted packet and increasing the feedback information.

3.2.3 PRAC's System Architecture

PRAC sits between the data link and network layer. It is a PHY-independent scheme and does not violate the typical PHY and link layer interface of modern wireless systems. In addition, it can be transparent to higher layers; the only consideration is that packets are delivered to and from the the network layer in a batch mode, as it is explained in the next sections, right after a successful decoding. These two features enable PRAC's implementation either as a driver extension or a firmware patch, as

Table 3.1: Summary of partial packet reception schemes.

Scheme	PHY independent	Zero fixed overhead	Not increased feedback
PPR [41]	✗	✓	✗
SOFT [54]	✗	✗	✗
MIXIT [55]	✗	✓	✓
ZipTx [42]	✓	✓	✗
SPaC [59]	✓	✗	✓
Seda [56]	✓	✗	✗
Maranello [58]	✓	✓	✗
Unite [57]	✓	✗	✗
PRAC	✓	✓	✓

opposed to schemes requiring PHY soft information.

PRAC's encoding process introduces no fixed overhead to any transmitted packets and doesn't modify or increase the feedback information. More specifically, PRAC's core component is a cross-packet random linear rateless code, explained in Section 3.3, which enables its optimal operation without knowledge of the channel quality. Finally, the detection of correct and erroneous parts of partial packets is performed with a mechanism based on the cross-packet algebraic consistency rule (ACR) check, followed by an iterative correction algorithm, presented in Section 3.4.

3.3 PRAC at the Transmitting Node

At the transmitter side, packets arriving from the network layer to the data link layer are buffered and processed in batches before their transmission, since the encoding process is performed upon groups of packets. Let k be the number of packets

coded together. Following the typical nomenclature, k will be called generation size in the rest of the chapter. Several approaches, mainly based on erasure codes, can be used for packets encoding. This section analyzes the different trade-offs associated with some of them and describes PRAC's encoding process.

3.3.1 Packet Erasure Coding Schemes

PRAC introduces cross-packet dependency by using a random linear code and exploits some properties of the coded packets in order to detect and correct erroneous information [3]. The performance of random linear codes in terms of reliability and throughput-delay trade-off has been studied in [60] and [9]. The interaction of packet erasure codes with the PHY is analyzed in [61, 10, 11], suggesting that spreading the transmitted redundancy across and within packets significantly outperforms the case in which only one method is used, especially for wireless fading channels.

Although a fixed-rate code, such as a Reed Solomon *(n,k)* code, can be used to introduce the cross-packet dependency, the use of a rateless code may be preferable since it does not require knowledge of the channel characteristics in order to select the appropriate rate. Fountain codes, such as LT [47] and Raptor [48] codes, are excellent rateless code candidates with low encoding and decoding complexity requirements. However, these codes do not perform well with short block lengths and a coding overhead (ϵ) is associated with them. If k initial packets are encoded together, approximately $k(1+\epsilon)$ correct packets are required on average to be received for successful decoding. Although this overhead asymptotically approaches zero as $k \to \infty$ for appropriately designed degree distributions, in most practical scenarios, ϵ has a non-negligible value since latency requirements of data link or higher layers limit the number of packets (k) buffered and coded together. Thus, considering WSNs applications with small values of k (typically less than 10), coding overhead results in transmission of extra packets which negatively affects the achieved network performance. A family of codes with the desired characteristics of being rateless,

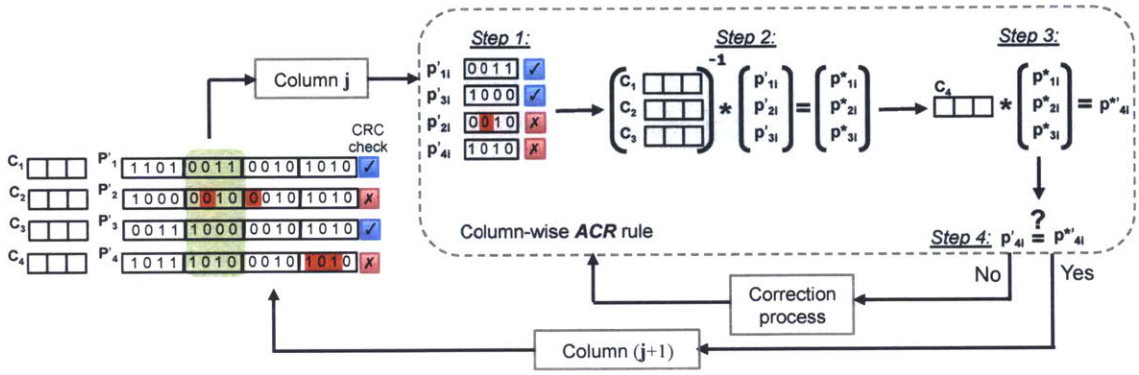

Figure 3-2: The four steps of the ACR check are shown, processing sequentially each of the columns of the received packets. If the condition of step 4 is true, the next column is examined; otherwise, the correction process is triggered.

performing well over small block lengths and having zero coding overhead are random linear codes. Although these codes do not provide similar encoding/decoding complexity guarantees as Fountain codes, they are selected as PRAC's core coding component.

3.3.2 PRAC's Encoding Process

Let P_i, where $i = 1, 2, .., k$, be the ith uncoded packet for transmission and p_{ij}, where $i = 1, 2, .., k$ and $j = 1, 2, .., l$, be the jth symbol of ith packet. In addition, let every symbol have q bits and be considered as an element from a finite field, $p_{ij} \in \mathbb{F}(2^q)$. We assume that all packets have the same length of ql bits; if not, zero padding is applied. Using matrix notation, the uncoded packets can be represented as a $k \times l$ matrix $\mathbf{P}$, whose entries are the symbols p_{ij}.

The encoding process transforms the k initial packets into k coded ones by the matrix multiplication, performed over finite field operations:

$$\mathbf{P'} = \mathbf{C} \times \mathbf{P}, \tag{3.1}$$

where $\mathbf{C}$ is a randomly generated matrix of coefficients c_{ij} over $\mathbb{F}(2^q)$, with $i, j =$

$1, 2, .., k$, $\mathbf{P}'$ is a matrix with the coded packets and $\times$ defines a matrix multiplication operation over finite fields. Thus, every coded packet is associated with a set of coefficients which can be conveyed with the packet transmission (e.g. in the header) or locally produced at the receiver by a random generator in sync with one at the transmitter. For the rest of the description, we assume that they are locally produced and error free. It can be seen that, when the channel is good, only k coded packets are transmitted, so PRAC incurs zero fixed overhead. If channel quality drops and additional packets are requested by the receiver, a new set of coefficients $\{c_i\}$, where $i = 1, 2, \cdots, k$, is generated. Using Eq. (3.1), a new coded packet can be created and transmitted by the PHY.

3.4 PRAC at the Receiving Node

Upon the reception of a new coded packet (P'_i), its CRC status is checked and it is properly buffered as valid or partial, along with the remaining packets of its batch. When the total number of received (valid and partial) packets exceeds the generation size (k), PRAC's recovery process is initiated. The correct and erroneous information within a packet are distinguished using an algebraic consistency rule (ACR) check, and the identified errors are corrected by an iterative process consisting of an optimized search algorithm and ACR checks.

3.4.1 Algebraic Consistency Rule Check

PRAC identifies correct information within partial packets by taking advantage of the algebraic consistency of the encoded packets. This process is performed column-wise over the matrix of received packets ($\mathbf{P}'$) in a sequential manner. The steps of ACR check for column j, assuming n packets have been received, including partial and valid ones, are the following ones:

Step 1 - Create a set of $(k+1)$ symbols which contains the symbols belonging to all

valid packets.

Step 2 - Pick randomly k symbols out of this set and multiply them by their inverted coefficients matrix to estimate the values of the uncoded symbols:

$$\begin{bmatrix} p^*_{1j} \\ \vdots \\ p^*_{kj} \end{bmatrix} = \begin{bmatrix} c_{11} & \dots & c_{1k} \\ \vdots & \ddots & \vdots \\ c_{k1} & \dots & c_{kk} \end{bmatrix}^{-1} \times \begin{bmatrix} p'_{1j} \\ \vdots \\ p'_{kj} \end{bmatrix}, \tag{3.2}$$

where " $*$ " denotes recovered symbol values.

Step 3 - Re-encode the estimated symbol values with the coefficients associated with the $(k+1)th$ packet:

$$p'^*_{(k+1)j} = \begin{bmatrix} c_{(k+1)1} \dots c_{(k+1)k} \end{bmatrix} \times \begin{bmatrix} p^*_{1j} \\ \vdots \\ p^*_{kj} \end{bmatrix} \tag{3.3}$$

and compare the result with its value.

Step 4 - If equality holds ($p'^*_{(k+1)j} = p'_{(k+1)j}$), the set of the $(k+1)$ symbols is consistent with high probability and the initial packet symbols of column j are the recovered symbols p^*_{ij} from Eq. (3.2). If not, PRAC's correction process is triggered.

An example of the steps of the decoding process for $k = 3$, $q = 4$, $l = 4$ and $x = 4$ are shown in Fig. 3-2.

3.4.2 Multiple rounds of ACR checks

When the result of the ACR rule for a column indicates consistency, there is also a probability for a false positive event (p_{fpe}), as with any other checking rule. Assuming that the effect of the channel on the received packets is uniform, the false positive event rate depends only on the value of field size (2^q) used. Thus, by increasing the field size, p_{fpe} can be set under any desired threshold. However, increase in the

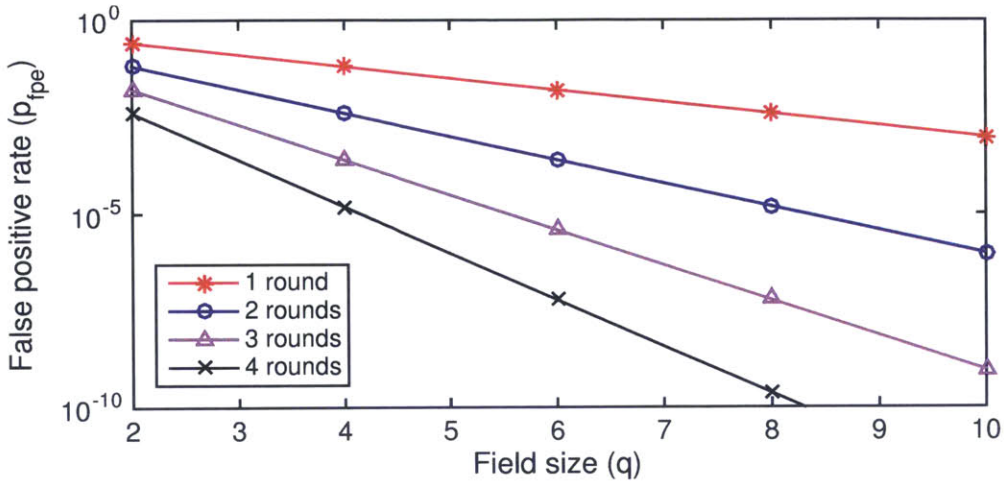

Figure 3-3: False positive event rate for different values of field size and number of ACR rounds.

field size, increases exponentially the complexity of PRAC's correction process. An alternative way to lower p_{fpe} is by executing multiple ACR rounds (step 1 to 4) for the same column with considering a different set of $(k+1)$ symbols each time.

If q is the length of each symbol and r is the number of consistency check rounds, the probability of a false positive event (p_{fpe}) of our check rule is:

$$p_{fpe} = (\frac{1}{2^q})^r. \tag{3.4}$$

This means that, by using a field size of eight and two ACR rounds for each column, p_{fpe} equals $1/2^{16}$, which is the same as the false negative event rate of 16-bit CRC rule. The desired value of p_{fpe} is an application specific choice and can be adjusted depending on the available computational resources and the desired algorithmic performance.

3.4.3 Correction Process

When ACR detects an erroneous column, PRAC's correction process is triggered to correct its erroneous symbols. This is an iterative process and each iteration

involves ACR checks, a search algorithm and CRC updates. The search algorithm attempts to identify the correct symbols until the ACR check associated with the specific column is satisfied. At the end of the correction process, the CRC status of the partial packets with corrected symbols is updated before the recovery algorithm processes the next column, gradually reducing the number of partial packets as the cross-column recovery scheme progresses.

Since no PHY soft information exists indicating potential erroneous bits, an exhaustive search algorithm is the optimal strategy in terms of recovering performance, whose complexity grows exponentially with the field and generation size. A reduced-complexity search algorithm is used in PRAC's correction process, examining first symbols with minimum Hamming distance from the received ones and setting a limit on the maximum number of trials. This provides a reduction on the average searching time and a trade-off between recovery performance and processing time, respectively.

3.5 Implementation and Performance Evaluation

PRAC is implemented as a software module and its performance is evaluated by processing stored data traces offline. Small values of field size reduce the probability of a column containing erroneous symbols and the search space of the correction process but increase ACR's false positive event probability. In terms of the generation size, increasing its value up to a certain point increases the channel diversity gains but it also exponentially increases the correction process's search space. Finally, the number of ACR rounds lowers the false positive probability of the check rule but increases the required computations. In our experiments and performance comparison, a field size of eight is used, a generation size of five and two ACR rounds, keeping the overall computational load of the CPU used at minimal levels.

PRAC's encoding process has minimal computational requirements. The recovery process exhibits higher complexity but it can be adjusted depending on the desired

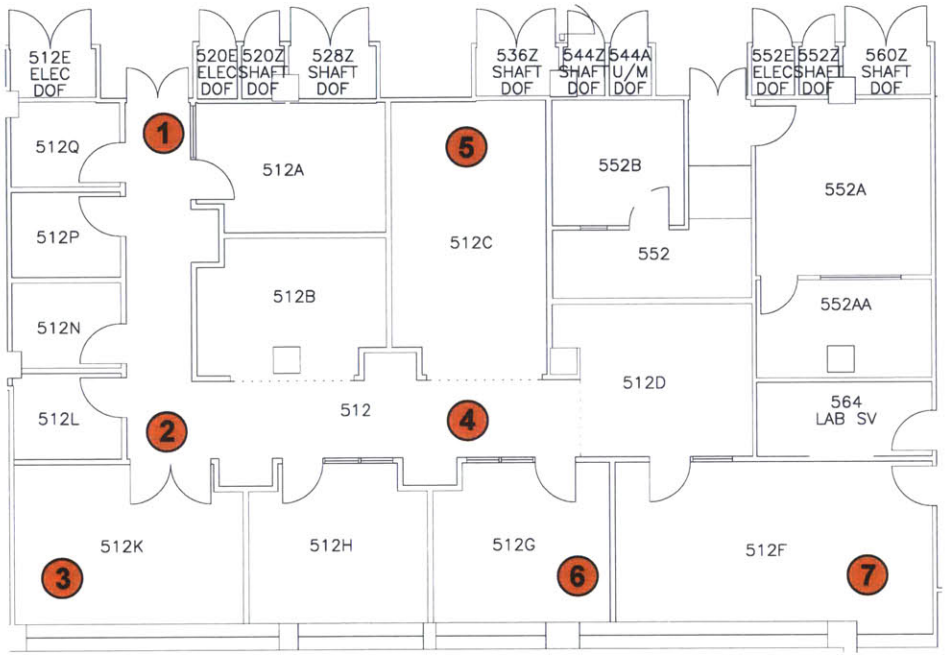

Figure 3-4: Floorplan of the indoor testbed.

performance. Its implementation in resource constrained devices can be challenging. However, due to its inherent parallelism, it can be efficiently mapped to a multi-threaded computing platform or an application specific circuit architecture, aspects which go beyond the scope of this chapter.

3.6 Throughput and Reliability Benefits

3.6.1 Experimental Setup

A static, indoor 7-node testbed is used, with fixed transmission rate links and deterministic routing, as shown in Fig. 3-4. Commercial boards [43] with CC2500 radio transceivers are used in the experiments, communicating in the 2.4GHz band, similar to the majority of current WSNs. The nodes are connected to a central PC, storing data traces and other link statistics, and operate in a centrally-controlled time division manner. Throughout all of our experiments, FSK modulation, 500Kbps transmission

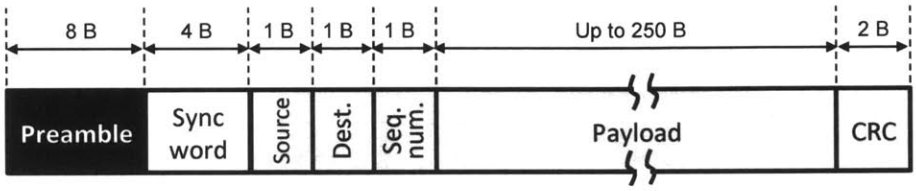

Figure 3-5: Packet format used in our experiments.

rate and +1dBm output transmission power (P_{TXout}) are used, unless otherwise specified. A rate 1/2 convolutional encoder, a Viterbi decoder and an interleaver are also used. The packet format contains: 8-byte preamble, 4-byte synchronization word, up to 250 bytes payload and 2-byte CRC check, as shown in Fig. 3-5. It should be emphasized here that, since PRAC is PHY-independent, any implementation platform can be used for evaluation without affecting its performance.

In the feedback mechanism 6-byte acknowledgment frames are used, transmitted upon the reception of a packet, indicating only its CRC status. No detailed feedback information about which segments of a packet are corrupted or how many errors exist in a packet is required. Data packets, including the retransmitted ones, have the same length. Although PRAC is a rateless code and feedback reduction techniques [62, 63] could be applied, we use the traditional per-packet acknowledgment throughout our experiments, for all recovery schemes tested, in order to decouple the benefits of harnessing partial packets from feedback suppression methods.

3.6.2 Channel Measurements

Our testbed consists of links with a wide range of link qualities; packet error rate (PER) varies from 0.1% to 68%, with an average value of 14%. Channel measurements are taken across several days and hours in a typical office environment without control over the external interference. PER accounts for both completely erased (not received at all) and partial packets. However, the benefit of any PPR scheme depends only on the percentage of partial packets since erased ones are not captured at all. Upper Fig. 3-6 shows the PER of three randomly selected links. The transmitter output power is

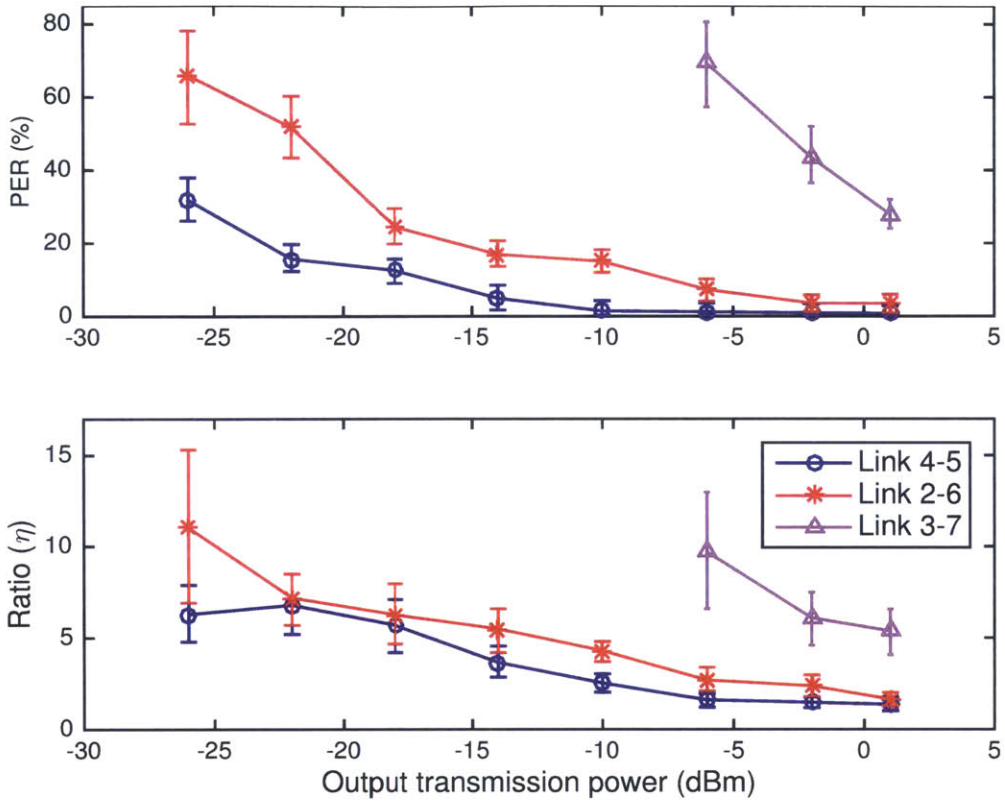

Figure 3-6: Packet error rate (upper figure) and ratio (η) of the number of partial over erased packets (lower packets) as a function of the output transmission power for three links in our testbed (link $i - j$ corresponds to link from node i to node j).

varied in order to emulate the behavior of links across the whole PER spectrum values. The ratio (η) of the number of partial over erased packets is plotted in the lower Fig. 3-6, in which it can be observed that the number of partial packets is significantly higher (on average 5.2× more) than the number of erased ones across the whole range of transmitter output power, or equivalently across links of any PER. This verifies the potential improvement in network's performance from a PPR mechanism.

3.6.3 Compared Schemes

PRAC's performance is compared against a baseline ARQ scheme, which discards partial packets, and a genie-aided ideal HARQ scheme, called iHARQ, which exploits partial packets by combining them with their retransmitted copies. A significant

difference between PRAC and iHARQ, which will be shown to have a major effect on performance, is that PRAC encodes and recovers a group of packets synergistically, while iHARQ processes and recovers individual packets. In more details, PRAC's performance is evaluated against:

- **Baseline ARQ scheme** - It is the combination of a convolutional code of rate 1/2 and an ARQ protocol. When a partial packet is detected, it is discarded and a new retransmission is requested. This approach is used in the majority of WSNs.

- **Genie-aided iHARQ** - This hypothetical scheme represents an ideal recovery mechanism with the ability to recover any received packet with at most one retransmission, if needed. In case a packet is detected as partial, it is buffered and a genie guarantees that, with its upcoming retransmitted copy, successful recovery will take place, even if the second retransmitted packet is partial as well. Obviously, this is an upper bound on the performance of combining schemes operating without detailed feedback.

3.6.4 Performance Evaluation Results

The performance evaluation of the aforementioned schemes is shown in upper Fig. 3-7. The achieved end-to-end throughput of 40 randomly picked source-destination pairs is plotted for each scheme. The baseline ARQ scheme performs well in links with low PERs but its performance degrades drastically in less robust links. This is explained by the "all-or-nothing" operation of FEC codes; they perform well up to a certain channel SNR and poorly beyond that. A rate adaption algorithm would limit the performance degradation but it is not included in any of the considered schemes.

The bottleneck in any wireless network comes from links of high PER, which usually limit the overall network performance. For instance, in our testbed, the baseline ARQ and iHARQ schemes fail to provide guarantees of robust connectivity across all

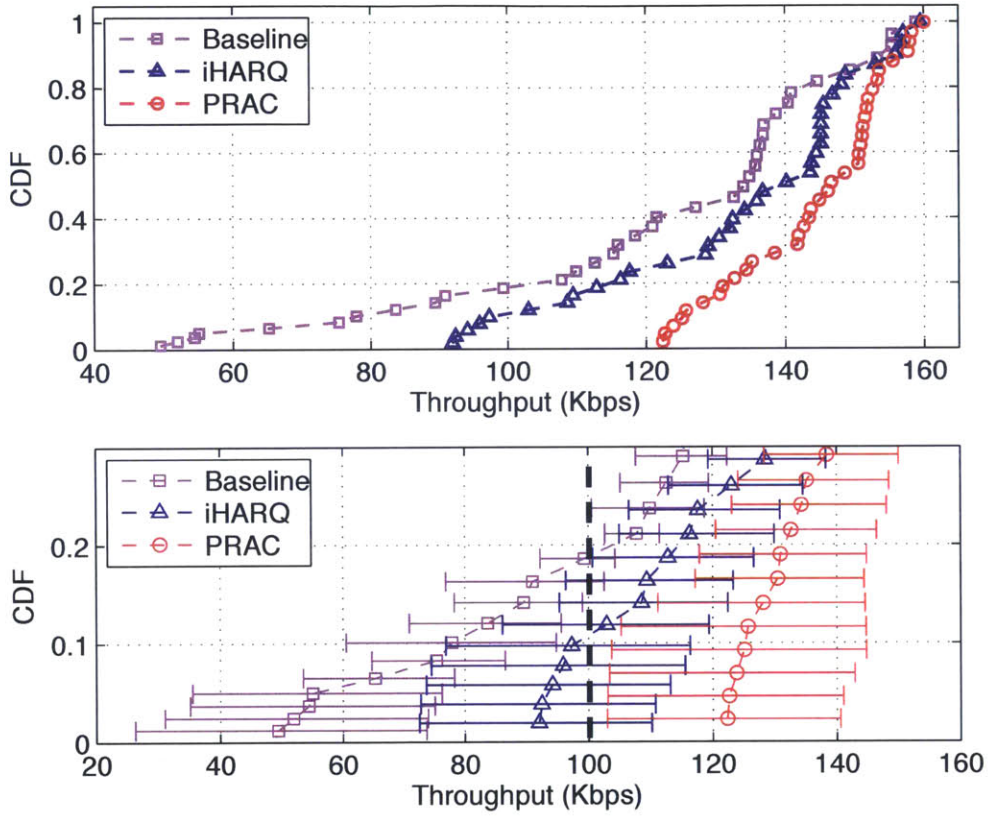

Figure 3-7: Performance comparison among the baseline ARQ scheme, iHARQ and PRAC, for 40 randomly picked source-destination pairs in our testbed (upper figure) and zoomed view including the error bars (lower figure).

nodes for an application of 100Kbps information rate, as shown in lower Fig. 3-7. The error bars reveal that only 65% and 77% of the links in our testbed will always support the required throughput threshold, for baseline and iHARQ schemes, respectively. However, PRAC significantly enhances the robustness of low quality links and, as shown from the error bars, guarantees that 100% of links meet the throughput requirement, enabling all nodes to reliably operate without communication outages.

Fig. 3-8 plots the average throughput of links in our testbed with PER $>$ 3%. The iHARQ scheme achieves an average throughput gain of 17% over the baseline ARQ scheme, while its maximum observed throughput improvement is 82%. PRAC outperforms on average the baseline by 35% and the iHARQ by 13%, while its maximum

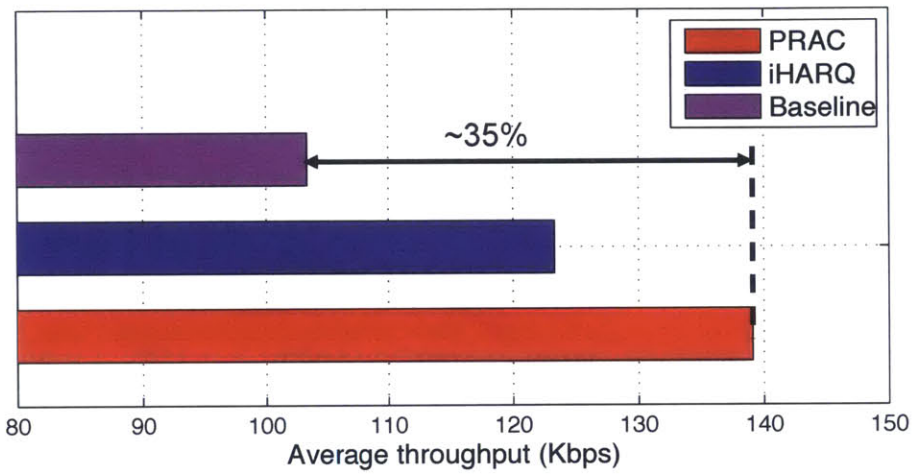

Figure 3-8: Average throughput performance of the baseline ARQ, iHARQ and PRAC schemes in links with PER > 3%.

observed throughput improvement in the network is 148%. Although PRAC does not require use of cross-layer information, it outperforms the genie-aided iHARQ. Similarly to other packet erasure codes, PRAC offers diversity benefits, especially in channels with deep fades and strong interference [10], such as in typical indoors channels experienced in our testbed. Since every received packet equally contributes towards the recovery of an entire group of packets, PRAC's performance can tolerate a few bad channel realizations, since they are amortized across the entire group. In contrast, iHARQ's performance considerably degrades in these challenged channel conditions due to the absence of diversity.

3.7 Energy Savings

3.7.1 Experimental Setup

Four transmitting sensor nodes attached to a human body are communicating with a receiving hub, mounted on a wall and connected to a PC storing the collected data traces and processing them offline. The on-body sensors are equipped with CC2511

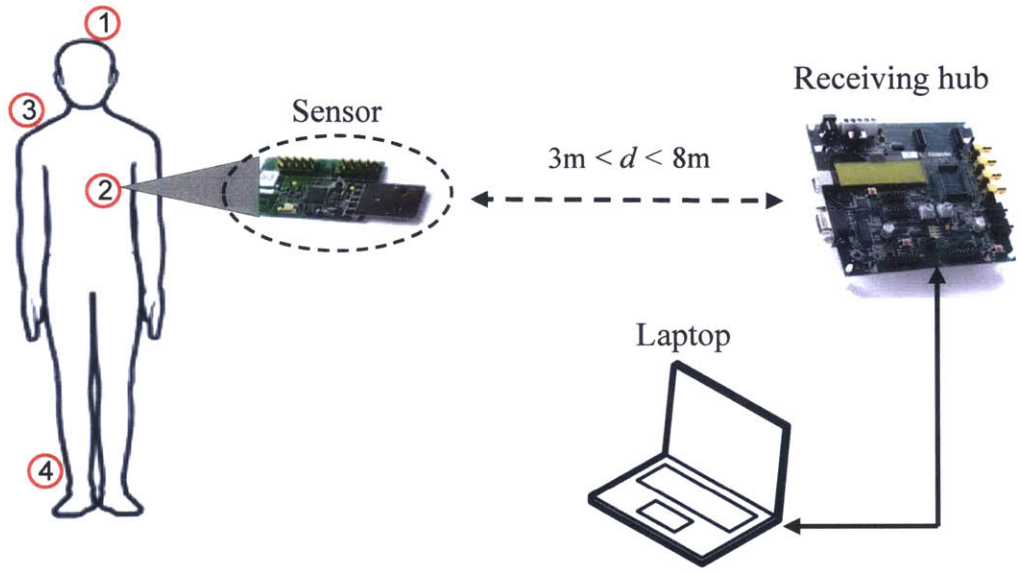

Figure 3-9: Experimental setup: four on-body sensors transmit information to a receiving hub while person is performing typical body movements. Collected data traces are stored in a laptop for further processing.

transceivers transmitting an ECG waveform stored in the on-board memory, and the receiving hub is a CC2500 development board [43]. The sensors are placed in four different body locations: *i)* top of scalp, *ii)* left chest, *iii)* back, and *iv)* right ankle. Scheduling among the sensors is performed by the hub, allocating time slots in each sensor, ensuring that no cross-sensor interference exists.

The output transmission power (P_{TXout}) of the sensors is adjusted from -25dBm to 1dBm. The transmission rate is fixed at 250kbps and communication is performed at the 2.4GHz ISM frequency band. Binary FSK modulation and coherent demodulation, a short interleaver, a convolutional rate 1/2 code and a hard Viterbi decoder are used at the PHY. The same packet format is used as the one shown in Fig. 3-5. Upon the reception of a packet by the hub, its CRC status is examined and it is buffered on the PC as valid or partial, depending on the result of the CRC check. The packet encoding described by Eq. (3.1) is performed by the microcontroller of the sensor, while PRAC's decoding process is implemented in software on the PC.

All experiments and measurements are performed in a typical indoors campus environment, with no control over the external interference. The distance between the sensors and the receiving hub varies in the 3-8m range as the person with the mounted sensors is performing typical tasks, including sitting in a chair and moving in the room.

3.7.2 Channel Measurements

Channel modeling and experimental measurements have been considered in several works, capturing the detailed characteristics of the wireless medium around the human body in indoors and outdoors environments [64]. In this thesis, we provide some experimental measurements of typical low power sensors communicating around the human body, not as an exhaustive modeling effort, but more as a characterization of the channel quality experienced during our measurements.

Fig. 3-10 plots the average PER for each P_{TXout} value in the four links of our experimental setup. As expected, the PER increases as P_{TXout} decreases. All four links exhibit approximately similar channel characteristics, with sensor 1 achieving the best average performance because of its position and the almost always available line-of-sight path to the receiver. Fig. 3-11 plots the variations on the channel quality due to channel impairments and body movements for one link of our experimental setup. Error bars for all links are not included for readability purposes.

3.7.3 Energy Modeling and Compared Approaches

In our analysis, we consider the energy consumption of the sensors only, without taking into account the energy of the receiving hub, assuming it is a less constrained device. This is a typical assumption in the majority of asymmetric networks, like many WSNs. For the energy consumption calculations, we assume that sensors are transitioning among four different states: transmission, reception, idling and sleep states. The power consumption associated with each state is shown in Table 3.2,

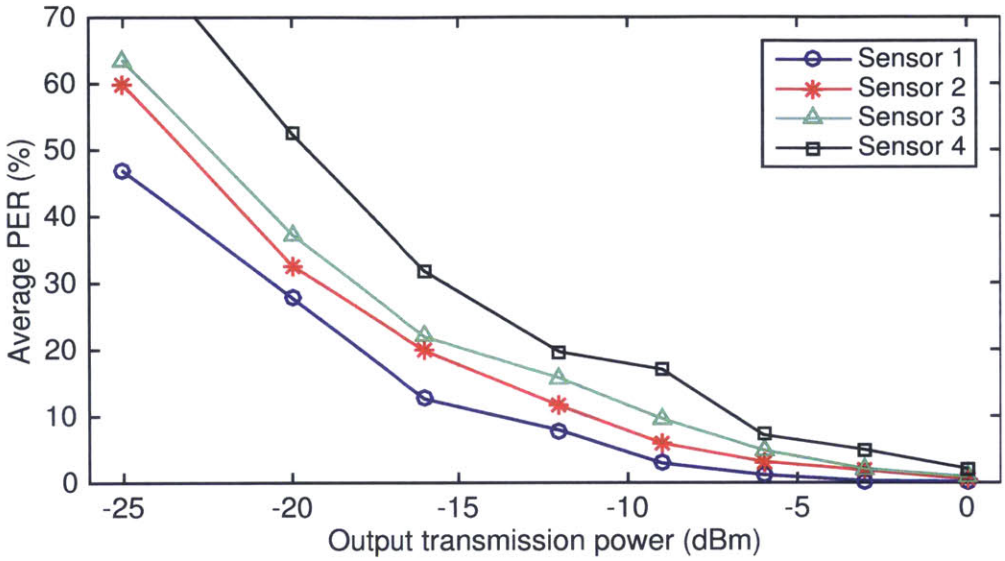

Figure 3-10: Average packet error rate with respect to output transmission power (P_{TXout}).

according to the data sheet of [65]. As expected, the power consumption during the transmission state depends on P_{TXout}. In the rest of our analysis, we assume that the power consumption during sleep states is approximately zero and sensors do not consume any energy.

The upper part of Fig. 3-12 shows the sequence of transmitted and received packets by a sensor, with timing details, which applies in both scenarios of using the baseline ARQ and PRAC scheme. Transmission of a packet is followed, after an interframe space interval (t_{sifs}), by an acknowledgment packet (ACK) sent by the hub, indicating its successful reception or not. The transition timings between the different states (t_1, t_2, t_3, t_4 and t_{sifs}) and the packet (ACK) transmission (reception) durations are summarized in Table 3.3 [43, 65]. In the lower part of Fig. 3-12 the power consumption of a sensor is shown over time. We assume that during the transition times, i.e. sleep to transmission mode, reception to idle mode, etc., the sensor has a constant power consumption.

The expected energy consumption of a sensor ($\bar{E}_{sen}$), given a transmission output

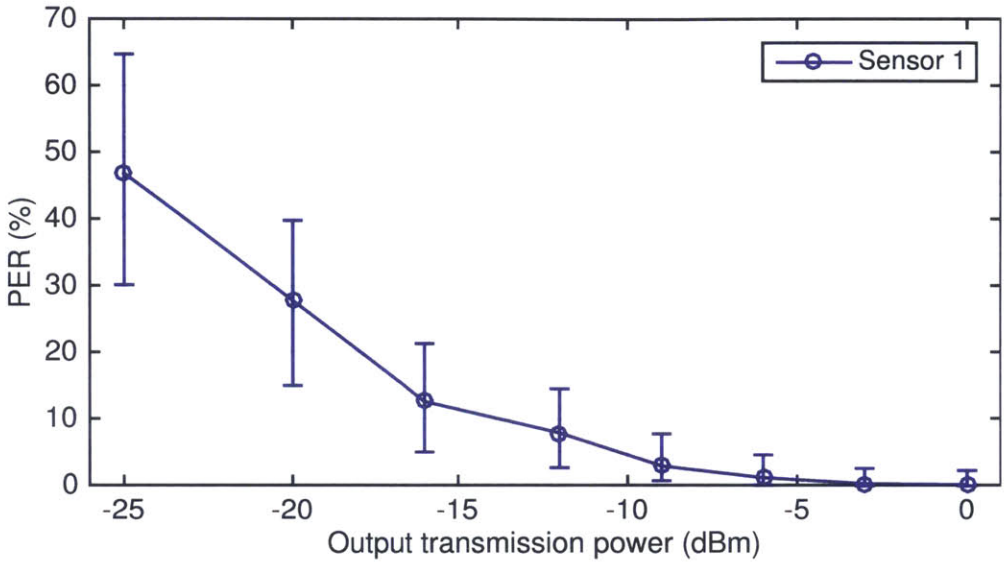

Figure 3-11: Channel quality variation of the link 'Sensor1-hub'; similar behavior is observed in the other links but not included for readability purposes.

power, in order to transmit N data packets to the hub is:

$$\bar{E}_{sen}(N)\Big|_{P_{TXout}} = \mathbb{E}[NE_{pack}]\Big|_{P_{TXout}} = \bar{N}E_{pack}\Big|_{P_{TXout}}, \tag{3.5}$$

where $\bar{N}$ is the expected number of transmitted packets and received ACKs, including the retransmitted ones, and E_{pack} is the energy of the sensor to transmit a packet at P_{TXout} and receive its ACK. $\bar{N}$ depends on the transmission parameters, e.g. P_{TXout}, experienced channel, receiver's sensitivity and the use of a PPR scheme or not. According to Fig. 3-12, E_{pack} is:

$$\begin{aligned} E_{pack} = {} & P_{TX}(t_1 + t_{pack} + t_2) + P_{ENC}t_{pack} \\ & + P_{IDLE}t_{sifs} + P_{RX}(t_3 + t_{ack} + t_4). \end{aligned} \tag{3.6}$$

Examining Eq. (3.5) and (3.6), $\bar{E}_{sen}$ depends linearly on P_{TX}; however, decreasing P_{TX} impairs packets' received signal quality, increasing the PER and consequently $\bar{N}$. Thus, a trade-off exists and careful optimization is required to ensure minimum

Table 3.2: Power consumption of a sensor node in different states.

State	Symbol	Value
Transmission	P_{TX}	$78mW$, $P_{TXout} = 0dBm$ $54.5mW$, $P_{TXout} = -6dBm$ $48mW$, $P_{TXout} = -12dBm$ $42mW$, $P_{TXout} = -20dBm$
Reception	P_{RX}	$63mW$
Idling	P_{IDLE}	$14.4mW$
Encoding	P_{ENC}	$\sim 0W$
Sleep	P_{SLEEP}	$\sim 0W$

Table 3.3: Timing notation and their values.

Symbol	Description	Value
t_1	transition time from SLEEP to TX mode	$0.9ms$
t_2	transition time from TX to IDLE mode	$1\mu s$
t_3	transition time from IDLE to RX mode	$0.3ms$
t_4	transition time from RX to SLEEP mode	$1\mu s$
t_{sifs}	interframe time interval	$0.4ms$
t_{frame}	transmission time of a packet	$4.45ms$
t_{ack}	reception time of an ack	$0.7ms$

energy consumption.

PRAC's recovery performance is compared against an idealized HARQ, representing an upper bound on the performance achieved by PPR schemes without detailed feedback in Section 3.6. In this section, PRAC is used in order to capture the potential

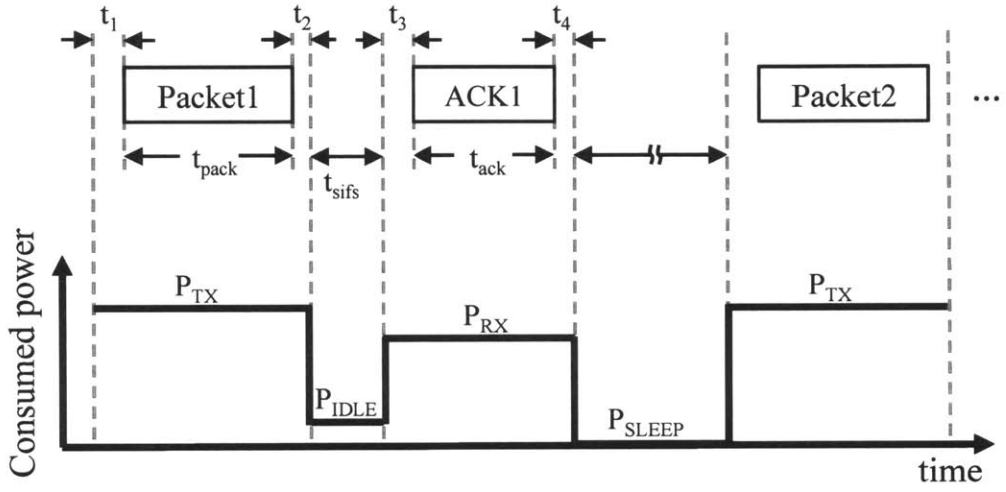

Figure 3-12: State transitions and power diagram for a sensor.

energy benefits of harnessing partial packets. Thus, its energy efficiency performance is compared against a baseline ARQ protocol which requests a retransmission upon the reception of a partial packet.

3.7.4 Performance Evaluation Results

Fig. 3-13 plots $\bar{E}_{sen}$, the total energy consumption for each of the four sensors, for both the baseline ARQ protocol and PRAC. In the high P_{TXout} regime, PER is low because of the adequate SNR value at the receiving hub. The high P_{TXout} regime corresponds to SNR values for received packets, reducing average PER. Using Eq. (3.5), it can be shown that the energy consumption is dominated by the E_{pack} factor and scales with it.

On the other hand, decreasing P_{TXout} below some value significantly impairs quality of transmission, increases PER and results in very frequent retransmission. The energy overhead associated with these retransmitted packets exceeds the energy savings through scaling P_{TXout} and dominates the total energy consumption. This behavior is depicted by the "u-shape" of all lines in Fig. 3-13.

The lower point in each line corresponds to the optimum P_{TXout} value for each

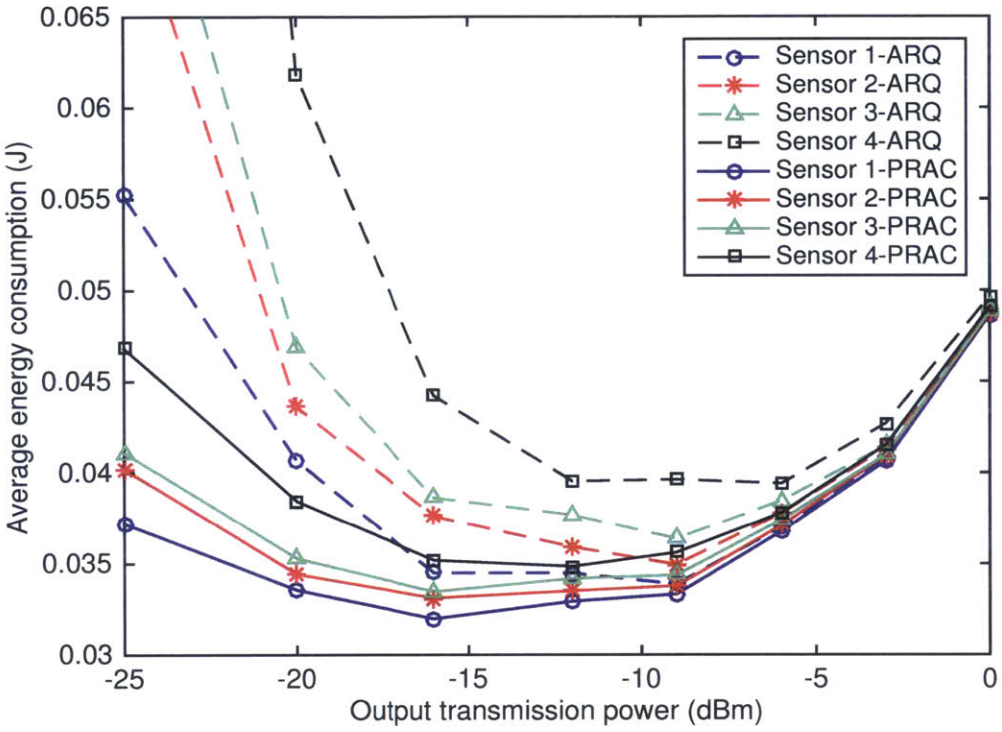

Figure 3-13: Total energy consumption of sensors for both using the baseline ARQ protocol and PRAC. In this experiment, we assume transmission of $N = 100$ packets to the hub.

sensor. In the absence of continuous power adaptation because of the additional required system complexity for channel tracking, PRAC lowers the energy penalty by not operating at the optimum energy point compared to the ARQ protocol. This is captured by the flatter "u-shape" of the lines. In addition, PRAC's recovery process decreases the required number of total transmitted packets and results in lower energy consumption. In Fig. 3-14, the average energy savings are plotted for each sensor with respect to P_{TXout}. As expected, the benefits are pronounced in the moderate to high PER regime (medium to low P_{TXout}) and can be up to 50% in challenged channel conditions. Averaging the energy savings of each sensor in our experimental setup across all values of P_{TXout} range, a 8-20% energy reduction is observed with PRAC.

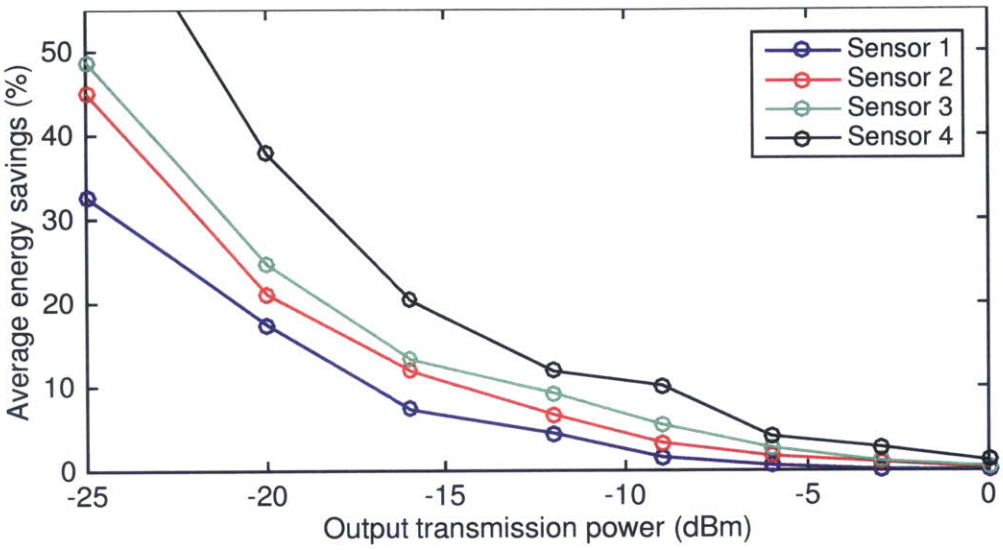

Figure 3-14: Average energy savings by harnessing partial packets.

3.8 Summary

The majority of current cWSNs operate in an "all-or-nothing" mode, discarding partial packets. Because of the useful information contained in these packets, several schemes have been proposed in the literature to harness partial packets by either making use of cross-layer information, introducing some overhead in transmitted packets or increasing the feedback information sent to the transmitter. In this chapter, a novel PPR scheme was presented, called Packetized Rateless Algebraic Consistency (PRAC). PRAC exploits the intra and inter-packet algebraic consistency of a group of packets, introduced by a rateless linear code and using an iterative decoding algorithm, identifies and corrects erroneous packet segments, significantly reducing the number of retransmissions. to harmoniously recover them through an iterative decoding algorithm. Being PHY independent, it does not require recourse to cross-layer information. In addition, no overhead occurs in the absence of partial packets and minimum feedback information is required.

Our implementation and experimental results in a 7-node indoor testbed of fixed rate links demonstrate an average throughput improvement of 35% compared to a

baseline ARQ scheme discarding partial packets, which can be up to 148% in challenged links. PRAC's performance is also compared against a genie-aided recovery scheme which represents the upper bound of performance for cross-layer schemes without detailed feedback, achieving an average throughput gain of 13% and 34% in high PER links. In terms of energy efficiency, PRAC achieves an average increase of 16%, while in high PER links, savings exceed 50% [66, 67].

Chapter 4

Backward Adaptation for Power Efficient Sampling

Apart from data communication, information acquisition usually consumes a significant factor of the total power consumption in typical WSNs. In this chapter, the rate and energy efficiency of a nonuniform sampling scheme, called time-stampless adaptive nonuniform sampling (TANS) is examined. A new method is proposed, called TANS with finite sampling rates (TFR), and compared against state-of-the-art methods. Practical implementation details of TFR are discussed. Our simulation results in the context of a health monitoring application demonstrate that TFR provides significant improvements in terms of both rate-distortion performance and energy consumption compared against other approaches.

4.1 Motivation

For bandlimited signals, the Nyquist sampling theorem provides an appropriate uniform sampling setup which leads to a signal reconstruction with zero error [68]. Although the Nyquist sampling theorem defines a sufficient condition on the sampling rate for bandlimited signals, it does not necessarily provide an efficient representation

because a signal may seem to have a lower bandwidth *locally* and thus sampling at the Nyquist rate seems to be a waste [69]. These extra samples not only increase the energy consumption of the sampling process, they also create some processing and transmission overheads. To avoid these energy and rate inefficiencies, sample redundancies can be removed using a compression method at the expense of increased computational costs.

An alternative to uniform sampling would be to take samples only when they are *innovative* for the relevant application. This leads to an adaptive nonuniform sampling scheme. For instance, a nonuniform sampling scheme based on level-crossing with iterative decoding is considered in [70], while reference [71] presents an approach based on level crossings with a filtering technique, which adapts the sampling rate and filter order by analyzing the input signal variations online. Two adaptive sampling schemes for bandlimited deterministic signals are also proposed in [69]. These schemes use definitions of local bandwidth, based on linear time-varying low pass filters [72] and time-warping of bandlimited signals [73]. Two main issues about these nonuniform sampling schemes make them difficult to be applied in practical applications: first, they are designed for specific signal models (i.e., they are not generic), and second, sampling times are required to be kept or transmitted in addition to sample values, in order to be used in the reconstruction process.

A relatively recent technique, called compressed sensing (CS) [74], has been used as a signal-agnostic acquisition method for highly sparse signals. In CS-based schemes, sampling is performed approximately at the information rate, rather than the Nyquist rate. Since CS has low encoding complexity, it has been adopted in several low power systems with the goal of reducing the power consumption [75, 76].

In this chapter, we consider a framework proposed in [77] to address the main limitations of previous sampling approaches. This new adaptive nonuniform sampling framework has two key characteristics: first, it continuously adapts the sampling rate according to the *local bandwidth* of the signal and consequently reduces the num-

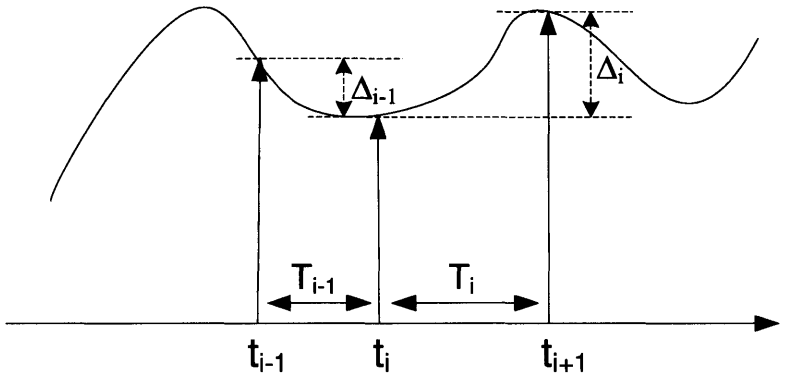

Figure 4-1: TANS setup.

ber of captured samples; second, unlike traditional nonuniform sampling procedures, sampling times do not need to be transmitted, since the receiver can recover them from the sample values themselves, thus avoiding the overhead of transmitting the sampling times which is required for traditional nonuniform sampling schemes. This sampling framework is called time-stampless adaptive nonuniform sampling (TANS).

A new TANS scheme is presented in this chapter, called TANS with finite sampling rates (TFR). We illustrate its energy efficiency in the context of transmitting an electrocardiography (ECG) signal from the MIT-BIH database [78]. By using detailed Verilog modeling of an ECG processor and transmitter, we show that TFR provides significant improvements in terms of energy consumption compared to the state-of-the-art.

4.2 Time-Stampless Adaptive Nonuniform Sampling

In this section, we review the TANS framework, proposed in [77]. Consider a continuous-time signal $X(t)$. Suppose the i-th sample is taken at time t_i. Define $T_i \triangleq t_{i+1} - t_i$ and $\Delta_i \triangleq X(t_{i+1}) - X(t_i)$, as shown in Fig. 4-1. We take the $(i+1)$st

sample after a time increment of

$$T_i \triangleq f(t_{i-m+1}, \ldots, t_{i-1}, t_i, X(t_{i-m+1}), \ldots, X(t_{i-1}), X(t_i)),$$

where f is called the sampling function, that allows us to reconstruct the time samples from the sample values themselves. Since the next sampling time step is a function of the m most recently taken samples, we say the order of the sampling function $f(\cdot)$ is m. The sampling function has to be known at both the sampling and reconstruction sides.

This sampling structure is nonuniform except in trivial cases, when the sampling function is a constant-valued function. The key characteristic of our approach is that, unlike traditional nonuniform sampling procedures, keeping sampling times (time-stamps) is not necessary in our framework because these times can be recovered by using the sampling function and previously taken samples. In the above example, we have $t_{i+1} = t_i + f(\bigcup_{j=i-m+1}^{i-1}\{T_j, \Delta_j\})$. Note that the first m sampling times should be kept to initialize the process. However, the effect of those initial samples is negligible, on average, when the number of samples increases.

In the above case, TANS is causal because the next sampling time depends on samples taken before that time. In general, it can be designed to be non-causal. TANS is an adaptive process which learns from the signal through the taken samples, since the sampling function depends on local characteristics of the signal. Finding an appropriate sampling function depends on different applications with various requirements such as the sampling rate, the distortion requirement, the computational complexity, etc. Here, to maintain focus on sampling rate and adaptation of sampling increments, we do not explicitly include quantization effects.

4.3 TANS with Finite Sampling Rates

In [79], two TANS schemes are proposed; one based on polynomial extrapolation (TPE), which assumes the third derivative of the signal is bounded, and a TANS method by incremental variation (TIV). In this section, we introduce a TANS scheme where sampling rates cannot be arbitrary as in the ones of TPE, but should be chosen from a finite set $\{R_1, R_2, \ldots, R_k\}$, created according to a specific signal model. In other words:

$$T_i = \frac{1}{R_{s_i}}, \tag{4.1}$$

where s_i is the sampling index which belongs to $\{1, 2, \ldots, k\}$. This scheme is called TANS with finite sampling rates (TFR). Similarly to a general TANS framework, the sampling index at time t_i (s_i) should only depend on previously taken samples so that storing/transmitting sampling time-stamps would be unnecessary. Computing this sampling index function depends on the signal model and sampling characteristics. For instance, consider a signal $X(t)$ with k states which are repeated periodically with a known order. The expected length of state j is denoted by l_j. We use TFR with k rates $\{R_1, \ldots, R_k\}$ to take measurements from this signal. Suppose N_i is the number of taken samples until time t_i from the current period of the signal. Then, the following is a TFR sampling scheme based on a mean-field approximation:

$$\begin{aligned} s_i = \underset{1 \le r \le k}{\arg\min} \quad & r \\ \text{s.t.} \quad & \sum_{s=1}^{r} (l_s R_s - N_i) \ge 0. \end{aligned} \tag{4.2}$$

This sampling function uses N_i to estimate the state of the signal at time t_i, and then takes samples with the corresponding rate of that state. There are some points to be noted about this sampling function:

- The TFR sampling function of Equation (4.2) assumes that the beginning of

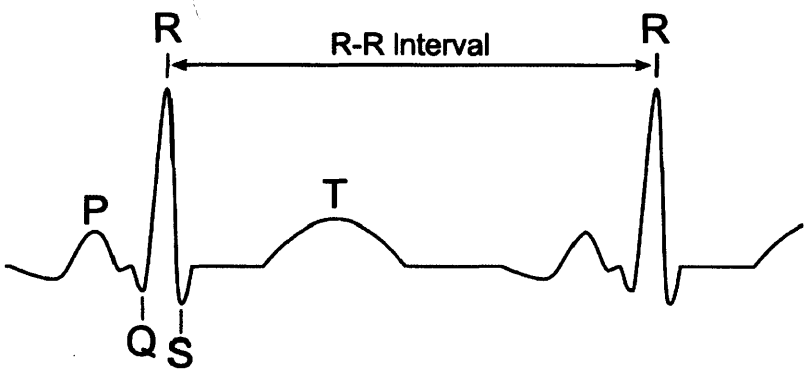

Figure 4-2: An ECG signal modeled as a P-QRS-T complex.

each signal period is known or can be detected using the taken samples. This assumption can be satisfied for some signal models. For example, ECG signals have a distinguished peak in each of their periods that can be used to detect the index of the signal period. We will discuss this in more detail below.

- Several parameters of this sampling function should be learned from the signal during a training period. Specifically, the number of states of the signal, their expected lengths and their rates should be learned if they are not given.

- Suppose $D_i(R)$ is the expected distortion of the state i of the signal given the sampling rate is R. If $D_i(R) > D_j(R)$ for all R, then $R_i > R_j$. In other words, a higher sampling rate is used if the signal is more variable in a state.

One practical example of such a signal model is an ECG signal model depicted in Fig. 4-2. We call the peak region around the point R, state 1, while state 2 covers the area close to the peak between points Q and S, and state 3 covers the rest of the ECG signal period. We learn TFR sampling parameters of Equation (4.2) using a training dataset once, where $R_1 = 180$, $R_2 = 360$, and $R_3 = 36$ samples/sec and $l_1 = 6$, $l_2 = 23$ and $l_3 = 33$, on average. Note that, state 2 has the highest sampling rate among others since detecting a transition from state 2 to 1 at the end of each signal period is crucial. Specifically, if $X(t_i) > th$ (in our example, $th = 50$), we say

a transition occurs from state 2 to 1 and a new signal cycle has been started. State 3 is assigned to the lowest sampling rate since there is not much information in this region of the signal.

4.4 Performance Evaluation on Real Datasets

In this section, we examine the performance of TFR against the other TANS methods and state-of-the-art sampling schemes in a real application. Although the comparison is performed in the context of a health monitoring application, the proposed approach and results are generally applicable to a wide range of signals and applications. Fig. 4-3(a) shows an ECG signal from the MIT-BIH database[1] [78], which has been sampled with a frequency of 360Hz and quantized to 10 bits. Using this signal, the performance of different sampling and compression schemes are examined and compared based on their rate-distortion curves generated through simulations. The best scheme would have the lowest rate (*i.e.* highest compression ratio) for the same distortion level, or equivalently, the lowest distortion for the same rate.

Since the energy consumption of the sampling process is approximately proportional to its sampling frequency, it is desirable from an energy perspective to take as few samples as possible. However, the limit on the sampling rate imposed by the Nyquist theorem guarantees that distortion will be introduced if a signal is sampled below that limit. Fig. 4-3(b) shows the ECG signal after having been downsampled by a factor of 6 and reconstructed with linear interpolation. As can be seen in this figure, many of the features of the initial signal are missing. Thus, although this simplistic technique lowers the energy consumption of sampling and transmission processes by approximately a factor of 6, it does not provide satisfactory results in terms of the distortion.

Other techniques have been proposed in the literature which have better rate-

[1]The DC component of the signal has been removed.

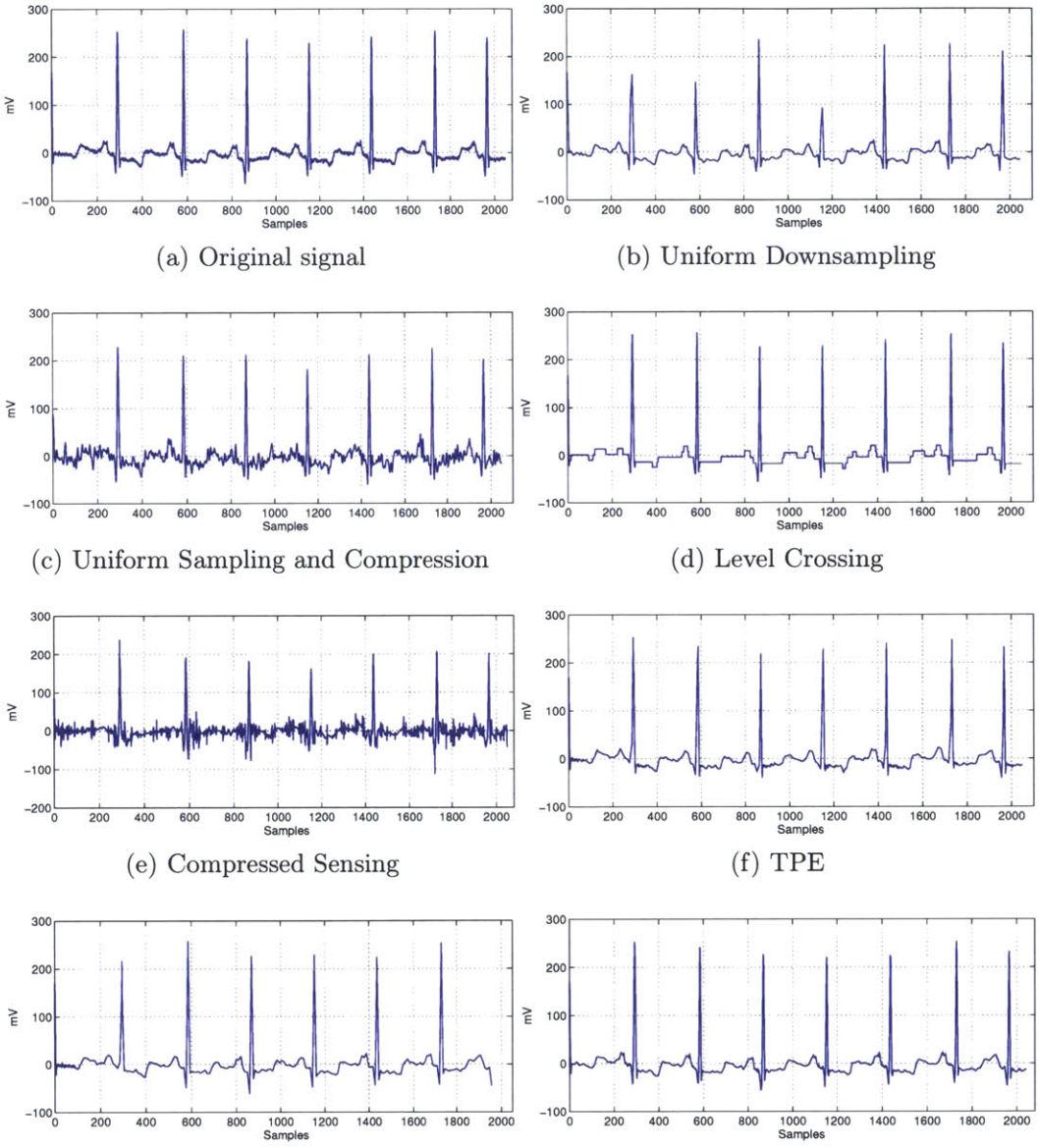

(a) Original signal

(b) Uniform Downsampling

(c) Uniform Sampling and Compression

(d) Level Crossing

(e) Compressed Sensing

(f) TPE

(g) TIV

(h) TFR

Figure 4-3: (a) A 6-sec ECG signal from MIT-BIH database, with the DC component removed. (b-h) Reconstructed ECG signals with an effective compression ratio of 6, using different sampling-compression schemes: (b) Uniform Downsampling, (c) Uniform Sampling followed by a DCT-based compression scheme. (d) Level-crossing Nonuniform Sampling. (e) Compressed sensing. (f) TANS by polynomial extrapolation (TPE). (g) TANS by incremental variations (TIV). (h) TANS with finite sampling rates (TFR).

distortion performance at the expense of higher complexity. In our analysis, we compare the performance of a few widely used schemes against the proposed TANS schemes. Fig. 4-3 (c)-(h) show the reconstructed signals of the original ECG signal after having been compressed by a factor of 6 using different schemes. In more details, the compared approaches are:

(i) **Uniform sampling and compression:** One widely used technique to minimize the amount of captured data sampled uniformly at Nyquist rate is to use compression algorithms, either lossless or lossy, where data is mapped to a more efficient representation before transmission. The majority of lossy compression algorithms proposed in the literature are transformation-based methods, such as wavelet- and DCT-based algorithms. These methods project signals to a certain domain with a more compact representation and, exploiting signal energy concentration, discard the smallest coefficients through thresholding.

Depending on the application, different transformations may be preferable. In our comparisons, we use a DCT-based compression algorithm where DCT coefficients with magnitude smaller than a threshold are discarded. We choose this method mainly because it exhibits a better rate-distortion trade-off than using a wavelet transformation [80] and has practical implementation benefits as well [81]. Fig. 4-3(c) shows the reconstructed ECG signal after having been compressed with a DCT based algorithm with block size of 2048 samples, resulting in a compression ratio of 6. Adjusting the threshold of the encoding process balances between the required number of transmitted signal samples and the reconstruction distortion.

The main energy inefficiency of this approach is that samples are taken at the acquisition stage at a relatively high frequency and then, some of these samples are discarded during the compression stage, resulting in extra energy consumption. For this reason, several nonuniform schemes have been proposed in the literature, in which the sampling moments are triggered only when the signal crosses some predefined thresholds and consecutive samples close to the same value are not taken.

(ii) **Level crossing sampling:** A common nonuniform sampling technique is level-crossing sampling, where the signal is compared with its previously taken value continuously and a new sample is taken when the difference exceeds a threshold [82]. However, apart from the samples themselves, time-stamps have to be transmitted since they are required in the reconstruction process. The reconstructed ECG signal using level-crossing sampling is shown in Fig. 4-3(d).

(iii) **Compressed Sensing (CS):** CS is an efficient signal-agnostic acquisition method for sparse signals [74]. The encoding process of a signal $X \in \mathbb{R}^N$, being k-sparse in some domain, is:

$$Y = \mathbf{\Phi} X, \tag{4.3}$$

where $\mathbf{\Phi} \in \mathbb{R}^{M \times N}$ and is called measurement matrix. If $M \sim O(k \log(N/k))$ measurements are taken from a signal X, CS exactly recovers the initial signal with high probability [83] if $\mathbf{\Phi}$ satisfies the RIP condition:

$$(1 - \delta_k)\|s\|_2 \leq \|\Phi s\| \leq (1 + \delta_k)\|s\|_2, \tag{4.4}$$

for all $k-$sparse signals s, where δ_k is a constant $\in (0, 1)$. Signal reconstruction may be performed through an optimization problem which can be formulated as:

$$\min_{\hat{\boldsymbol{s}} \in \mathbb{R}^n} \| \hat{\boldsymbol{s}} \|_{l_1}, \text{ s.t. } Y = \mathbf{\Phi}\mathbf{\Psi}\hat{S}, \tag{4.5}$$

where $\mathbf{\Psi} \in \mathbb{R}^{N \times N}$ is a matrix representing the synthesis operator of an orthonormal basis where the signal X has a sparse representation. The initial signal is recovered by multiplying the solution of the optimization problem with the inverse basis matrix:

$$\hat{X} = \mathbf{\Psi}\hat{S}. \tag{4.6}$$

Alternatives to this basis pursuit (BP) formulation [84] include lasso [85], the Dantzig selector [86], greedy methods [87, 88] and iterative methods related to belief

propagation [89]. Exact asymptotic performance under Bayesian formulations can be computed using the methods of [90]. In our simulations, a BP reconstruction algorithm is used, implemented with the CVX optimization package [91]. A Gaussian matrix is used as the measurement matrix with entries from $\mathcal{N}(0, 1/N)$, and a wavelet basis (*coiflet 4*) is used as the sparsifying domain. The result of the reconstruction process is shown in Fig. 4-3(e) for a compression ratio of 6.

(iv) **TPE, TIV and TFR:** These TANS schemes are adaptive sampling schemes and their sampling moments are calculated based only on previously taken samples through their sampling functions, without the need for tracking the current value of the signal continuously and for transmitting time-stamps. The sampling function of TFR used in the experiments is described in Section 4.3. Fig. 4-3(f-h) shows the reconstructed signals using these three adaptive schemes where most of the original signal features are preserved.

Although subjective distortion metrics have been proposed in the literature specifically designed for ECG signals, here we use two distortion metrics, MSE and PRD, defined as follows:

$$MSE = \frac{1}{N}\sqrt{\sum_{n=1}^{N}\left(X(n) - \hat{X}(n)\right)^2},$$

$$PRD(\%) = \sqrt{\frac{\sum_{n=1}^{N}\left(X(n) - \hat{X}(n)\right)^2}{\sum_{n=1}^{N} X^2(n)}} \times 100\%.$$

Different distortion levels for uniform sampling and DCT-based compression is performed by adjusting the threshold of the encoding process, resulting in a variable number of DCT coefficients, while for the nonuniform scheme, the rate distortion curve is derived by using different numbers of quantization levels. For TFR, the curve is derived by modifying the rates of each sampling region while for TPE and TIV, D and $(th1, th2)$ parameters are tuned respectively. For the rate-distortion comparison of these schemes, several ECG signals were used, each of approximately an hour

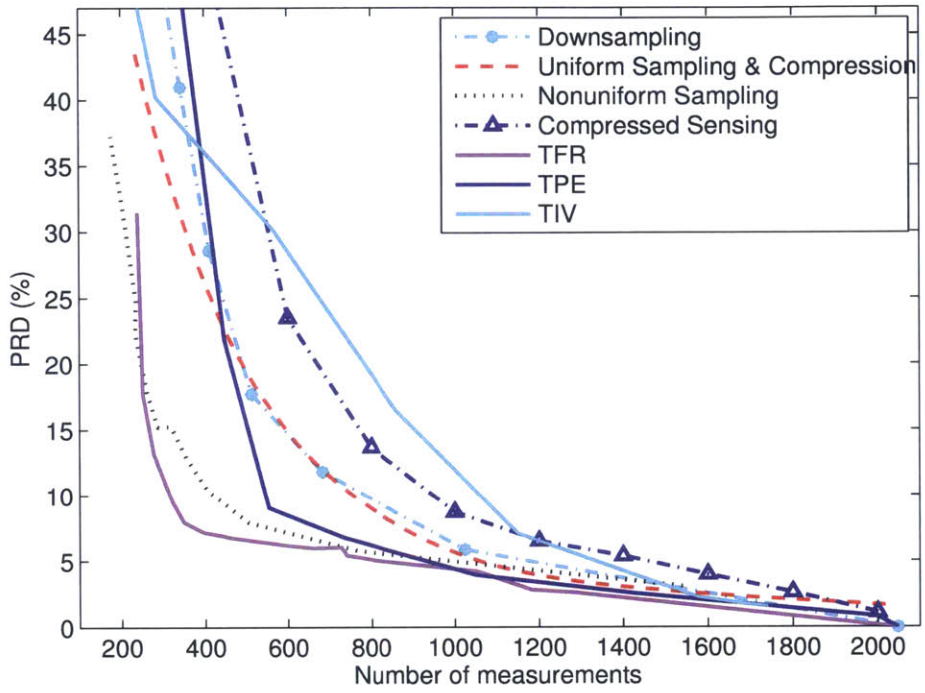

Figure 4-4: PRD in terms of the transmitted number of samples for each technique.

long duration. As illustrated in Fig. 4-4 and 4-5, TFR consistently outperforms the other techniques in terms of distortion across all rate regimes. For instance, at a PRD of 10%, the approximate rate improvement of TFR is a factor of 1.2, 2.5, 2.5 and 3 compared to a uniform downsampling, a DCT-based compression scheme, a level-crossing nonuniform sampling scheme and compressed sensing, respectively.

4.5 Energy Analysis of TFR

4.5.1 Implementation Considerations of TFR

A high-level block diagram of a system implementing TANS is shown in Fig. 4-6. It is composed of a nonuniform ADC and a block implementing the sampling function, called timing control logic (TCL). The nonuniform ADC shown in the block diagram is a standard ADC with the only difference that the sample spacing is not even but rather is dynamically adapted. Thus, triggering the ADC to capture a sample is

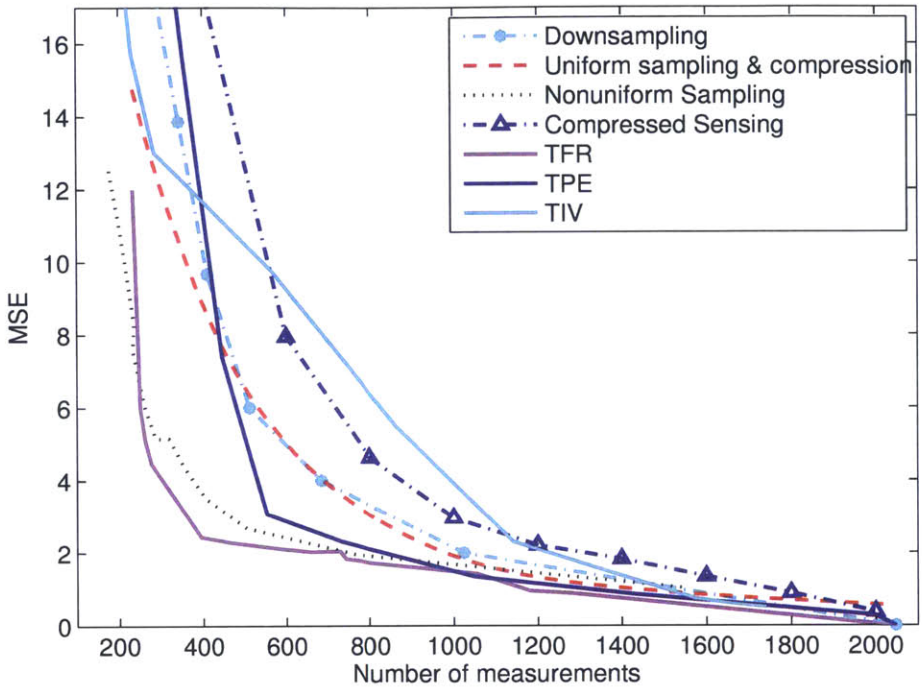

Figure 4-5: MSE in terms of transmitted number of samples for each technique.

not performed by an oscillating clock, as in a uniform ADC, but by the TCL block. This means that at the acquisition stage, TFR does not need extra circuitry, such as input voltage comparators, integrators and time-to-voltage converters which are used in nonuniform sampling schemes such as level crossing. Thus, no additional energy dissipation is consumed at the acquisition stage.

Depending on the memory (m) of the sampling function, the TCL block stores the m most recently taken samples and determines the next sampling time. The block diagram of Fig. 4-6 represents the general case of implementing the proposed adaptive sampling framework where different variations of the TCL block are used for different TANS schemes. For instance, the TCL block in the case of TIV calculates $w(t_i)$ using an adder and a divider, compares T_i with two predefined thresholds and adjusts its value accordingly. In the case of TFR, the TCL block implements a finite state machine using $log_2(k)$ registers, indicating the current sampling rate (R_i). Three accumulators and two comparators are used to calculate/store the current values of

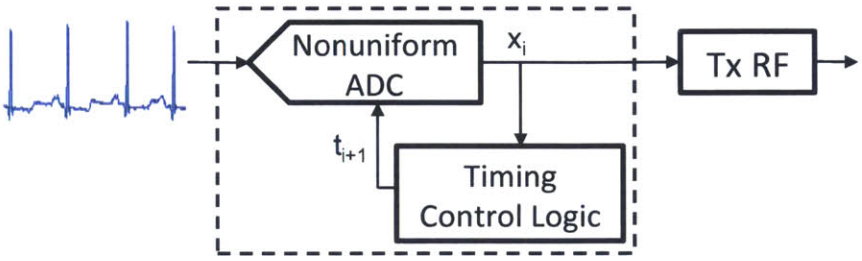

Figure 4-6: High-level block diagram of a system implementing TFR. A nonuniform ADC is controlled by a timing control logic, implementing the sampling function depending on the signal and sampling model.

the length of each state (l_i) and to trigger a state transition, respectively.

4.5.2 Energy Comparison and Evaluation

In this section, we use a detailed system-level analysis in order to examine and compare the energy efficiency of different sampling and compression schemes. In our comparisons, state-of-the-art published results are used for each individual component of these schemes, such as ADC, compression algorithms, etc. Although our analysis is not an exhaustive comparison of all sampling schemes that have been proposed so far in the literature, it illustrates the advantages of TFR in terms of its rate and energy efficiency. In more detail, TFR is compared against the following methods:

- **Uniform sampling and DCT-based compression**: A high-level block diagram of this scheme is shown in Fig. 4-7(a), where uniformly sampled data at fixed sampling frequency F_s are compressed by a DSP block implementing the DCT transform and the thresholding process, described in Section 4.5.1.

- **Level-crossing nonuniform sampling**: Fig. 4-7(b) shows the block diagram of a level-crossing sampling system using a nonuniform ADC, which can be viewed as a joint sampling and compression stage. When the local bandwidth or activity of the signal is low, automatically less samples are taken. To achieve this, the voltage difference of the input signal with the previously taken sample

is compared continuously by an analog-front-end (AFE) circuit. When the difference exceeds a threshold value, the ADC is triggered and a sample (x_i) is taken, along with its time-stamp (t_i). This extra circuitry which tracks the input signal continuously, needs to be powered on all the time which consumes power constantly. Implementation challenges as well as simulation results are described in detail in [92], where a low power, low sampling frequency level crossing ADC is designed and optimized.

- **Compressed Sensing (CS)**: Two main approaches exist for the implementation of the CS block shown in Fig. 4-7(c). According to the first, a signal is sampled with a rate above the Nyquist limit by a standard uniform ADC and then multiplied by the CS measurement matrix, as explained in Section 4.4, resulting in the transmission of a number of samples ($M \ll N$) corresponding to sub-Nyquist sampling. This approach uses CS as a signal-agnostic compression technique and, because of its low complexity requirements, has been used in the design of low power systems [76, 93].

  The second approach targets directly capturing signals at sub-Nyquist rates. Examples of this approach include the analog-to-information converters (AIC) and random modulators [94, 95]. As explained in [96], for low sampling frequency applications, similar to the one considered in our case, these schemes consume higher power mainly because of their implementation requirements of multiple parallel branches with mixers and amplifiers, which makes them more suitable for high-speed applications. Demonstration of a low power implementation of these schemes, competitive to the original CS approaches, is still an ongoing effort. Thus, relying on the arguments of references [93] and [96], although the sampling rate is lower compared to the previously described CS method, the overall energy consumption tends to be higher and therefore it is not included in our comparisons.

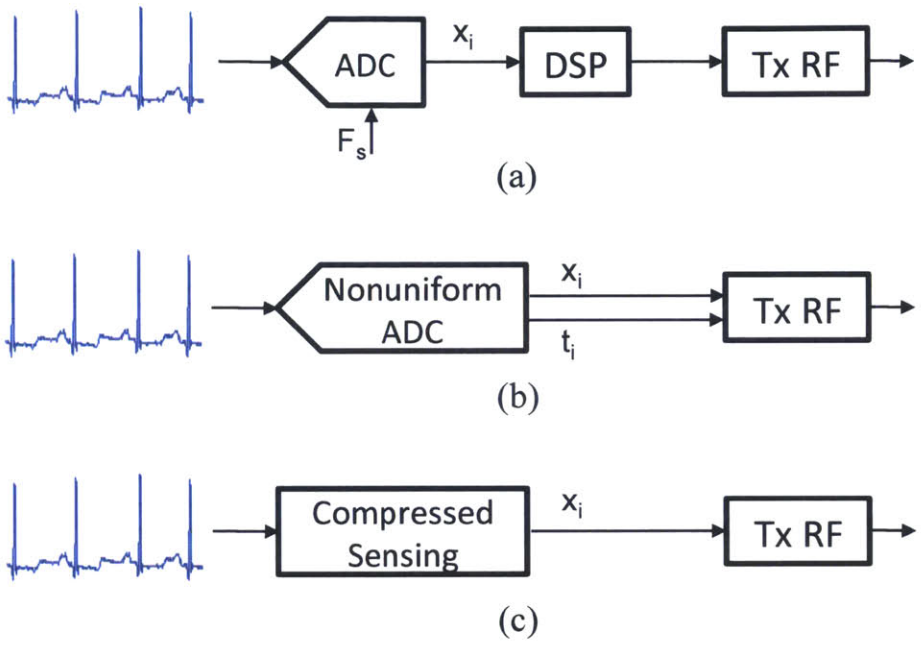

Figure 4-7: (a) A system using uniform sampling followed by transformation-based compression. (b) A level-crossing nonuniform sampling system. (c) A compressed sensing system.

In our analysis, we assume that all schemes sample the same ECG signal, use a compression ration (CR) which results in a target PRD value of 10%, and use the same transmission block[2]. The total energy consumption for each scheme is:

$$E_{tot} = E_{samp} + E_{compr} + E_{TX}, \tag{4.7}$$

where E_{samp}, E_{compr} and E_{TX} are the energy consumption of the sampling, compression and transmission stages, respectively. In addition, we assume that the energy consumption at the acquisition stage is approximately proportional to the sampling frequency, ignoring any leakage component. So, E_{samp} can be written as:

$$E_{samp} = R \cdot E_{samp}^{ref} = R \cdot P_{samp}^{ref} \cdot t, \tag{4.8}$$

[2]As a reference, we assume that transmitting a bit of information consumes: $E_{bit} = 10pJ/bit$ in the transmission block [97] and each transmitted sample is quantized using: B_{quant} =10 bits.

where R is the sampling rate and $E^{ref}_{samp}/P^{ref}_{samp}$ is a reference energy/power consumption. Based on an ultra low power ADC optimized for low sampling rate applications [98], we assume that a reference ADC power consumption is 1.6uW for 1kHz sampling frequency. For the purpose of this comparison, we assume that the time period (t) equals 6 seconds, which corresponds to the signal duration of Fig. 4-3.

The uniform sampling followed by DCT-based compression and CS schemes sample the signal at 360 samples/sec, thus their energy consumption is:

$$E^{unif}_{samp} = E^{CS}_{samp} = (0.36 \cdot 1.6 \cdot 6)\mu J = 3.45\mu J. \tag{4.9}$$

Using reported results from [92], the power consumed at the acquisition stage of a low-power level-crossing nonuniform scheme is approximately $23uW$, therefore its consumed energy at the acquisition stage is:

$$E^{lev}_{samp} = (23 \cdot 6)\mu J = 138\mu J. \tag{4.10}$$

TFR achieves the same PRD by taking fewer samples. According to Fig. 4-4, its sampling rate for the target PRD is approximately 50 samples/sec, since a compression ratio (CR) of approximately 7 is achieved, thus its consumed sampling energy is:

$$E^{TFR}_{samp} = (0.05 \cdot 1.6 \cdot 6)\mu J = 0.48\mu J. \tag{4.11}$$

The data compression blocks of the considered schemes have different computational requirements and, therefore, different energy consumptions (E_{compr}). Based on [99], a low-power implementation of a DCT-based compression algorithm consumes approximately $166uW$, while in [75] the power consumption of CS block is reported to be around $1.9uW$. Thus, their energy consumption for our ECG signal comparison would be:

$$E^{unif}_{compr} = 1mJ \text{ and } E^{CS}_{compr} = 11.4\mu J \tag{4.12}$$

Table 4.1: A energy comparison of 3 different schemes for sampling, compressing and transmitting a 6-sec ECG signal.

	Uniform Sampling and Compression	**Nonuniform Sampling**	**Compressed Sensing**	**TFR**
ADC	3.45μJ	138 μJ	3.45 μJ	0.48 μJ
Compression	1 mJ	0	11.4 μJ	6μJ
Transmission	80 μJ	44 μJ	80 μJ	30 μJ
Total	1083.45 μJ	182 μJ	102.45 μJ	36.48 μJ

Compression in TFR is performed by the sampling function which calculates the next sampling time. We use a hardware description language (HDL) to model the sampling function described in Section 4.3 and, using the standard hardware design flow[3], we measure the energy consumption of the TCL block of TFR to be:

$$E_{compr}^{TFR} = 6\mu J. \tag{4.13}$$

Finally, the transmission energy is given by:

$$E_{TX} = E_{bit} \cdot (\frac{R}{CR} \cdot B_{quant} \cdot t + H), \tag{4.14}$$

where E_{bit} is the energy per bit, B_{quant} is the number of quantization bits and H is the overhead information in bits used in the DCT thresholding process indicating the indexes of non-zero coefficients, and in the level-crossing scheme representing the time-stamps required for the reconstruction process. For the CS and TFR schemes, H equals zero.

[3]We model the sampling function using Verilog and then we proceed with synthesis, place-and-route, extraction and post-layout simulation. CAD tools from Cadence and Synopsys are used, as well as libraries from a 65nm TSMC process.

Table 4.1 shows the energy components for each sampling scheme as well as their total energy consumption. It can be seen that, TFR outperforms all approaches considered in the analysis. Specifically, TFR provides a benefit of at least an order of 3 in terms of the total energy consumption compared to state-of-the-art sampling approaches. This energy efficiency benefit is achieved by adapting the sampling rate without requiring extra circuitry at the acquisition stage and by avoiding the transmission of the time-stamps. In addition, the energy overhead of the TCL block, which controls the ADC, is significantly lower when compared to standard block-based compression algorithms.

4.6 Summary

In this chapter, we proposed TANS with finite sampling rates (TFR) and analyzed its rate and energy efficiencies.We demonstrated that TFR reduces the sampling rate and therefore the energy consumption of the acquisition process. In this framework, time intervals between samples can be computed by using a function of previously taken samples, called the sampling function. After creating a detailed implementation model, we compared the performance of TFR against uniform sampling, level-crossing nonuniform sampling and compressed sensing. We showed that TFR outperforms all the compared approaches and significantly improves the rate and energy consumption of the acquisition process of WSNs [100, 101, 102].

Chapter 5

AdaptCast: Efficient and reliable acquisition, transmission and reconstruction of sparse signals

This chapter studies the problem of efficient acquisition and reliable transmission of sparse sources over wireless channels with additive noise. The considered setup is of major importance for several WSNs since they usually have strict reliability and power consumption constraints, and the majority of physical signals encountered in them are inherently sparse. We propose AdaptCast, a PHY integrated signal representation-to-transmission scheme which parsimoniously describes the collected sparse data and ensures increased robustness against channel errors across a wide range of signal to noise (SNR) values in a rateless fashion. AdaptCast's performance doesn't suffer from the sudden degradation in the tradeoff between distortion and SNR of rated channel coding schemes owing to its direct, relative bit importance preserving modulation mapping and denoising reconstruction algorithm. Through rate-distortion analysis, we prove that AdaptCast is asymptotically optimal in terms of distortion in the high SNR regime in point-to-point links. Our simulation results validate our analysis and demonstrate that AdaptCast is applicable to a wide range of

applications and performs close to an idealized layered transmission scheme in terms of reliability and end-to-end distortion.

5.1 Motivation

5.1.1 Related Work

A common layered approach for transmission of information in WSNs, justified by Nyquist's sampling [68] and Shannon's separation theorem [39], is to decouple signal acquisition, compression of sources (source coding) and reliable information transmission (channel coding), as shown in Fig. 5-1(a). Source coding techniques compress acquired data by transforming them to other domains and/or exploiting statistical source properties [103, 104]. Channel coding techniques insert redundancy in transmitted data for increased communications reliability in the presence of channel noise and their incorporation in WSNs is considered in numerous works [5, 6, 7]. Most practical PHY FEC schemes operate without knowledge of the source, treating equally every bit; unequal error protection (UEP) schemes weight the assignment of additional resources, e.g. power, frequency or rate redundancy, to each bit depending on its relative importance [105, 106], but their adoption in WSNs is limited mainly due to their high computational complexity and application specific nature. Rateless coding schemes are proposed as an alternative approach without requiring feedback information [49, 107] while some cross-layer schemes provide a wider range of operational channel SNR [59, 66].

Joint source-channel coding (JSCC) schemes, as shown in Fig. 5-1(b), simultaneously compress and enhance the reliability of the acquired information against channel errors. In certain scenarios, these schemes might achieve superior performance compared to layered coding schemes, or the same but with significantly less delay and complexity. For instance, in the non-asymptotic regime, it has been shown that the error exponent of JSCC outperforms that of layered coding [108, 109] and

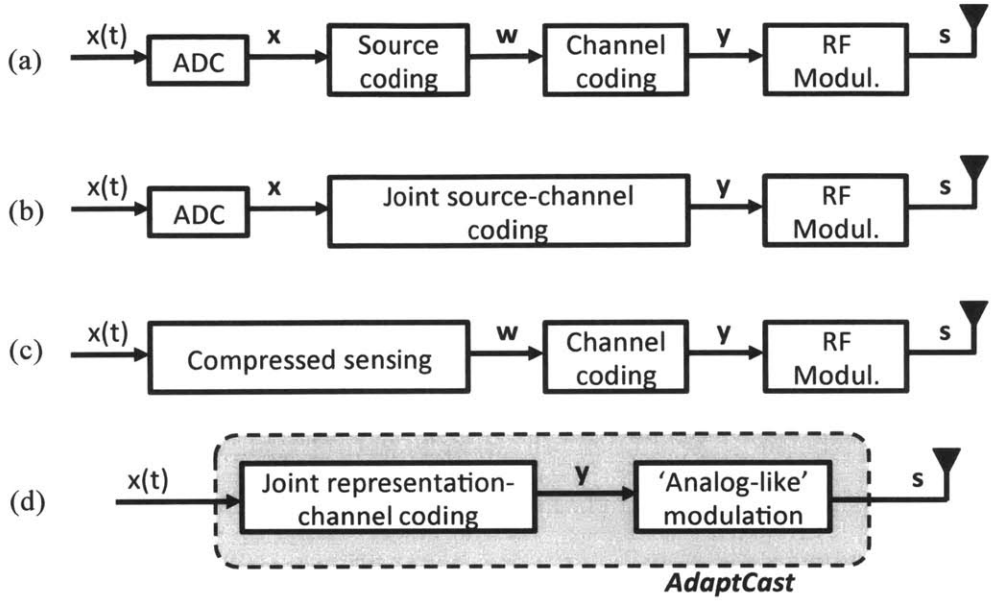

Figure 5-1: Block diagram of the typical approaches acquiring, compressing and transmitting analog sparse signals in WSNs. (a) Layered approach following Shannon's separation theorem, (b) Joint source-channel coding approach, (c) Compressed sensing with channel coding scheme, and (d) AdaptCast.

considerable advantages are associated with it in point-to-point [110] and multiuser scenarios [111, 112]. Although these schemes might guarantee gracefully degrading quality of received information and lower complexity than the layered approach, they are usually signal-specific approaches [113] and/or imply implementation unfriendly, fully analog or hybrid systems [114].

Because a plethora of naturally occurring signals exhibit high sparsity levels, e.g. images and human biosignals, as well as several signals in practical systems can be well approximated by sparse models, e.g. RF signals in radio receivers, researchers have proposed specific coding schemes to efficiently represent and process this family of signals. Compressed sensing (CS) is such a scheme for efficient acquisition of sparse signals based on random projections and incoherent sampling [74, 115]. Although systems with CS acquisition, as the one shown in Fig. 5-1(c), have several advantages over the aforementioned ones, e.g. signal independent operation and lower complexity, they inherit the typical limitations of PHY FEC schemes of requiring channel state

information (CSI) for appropriate rate selection and do not perform well in multiuser scenarios. Apart from signal acquisition, signal sparsity has been exploited in several works on designing robust channel coding schemes through efficient recovery methods [116, 117]. The trade-off between the number of measurements and detection errors is addressed in [118, 119] and the rate distortion behavior of sparse sources is studied in [120]. The sub-Nyquist sampling effects on the channel capacity and robust channel coding schemes through efficient sparse recovery methods are considered in [121].

In summary, the most prominent drawbacks and challenges associated with the prevailing acquisition, source and channel coding techniques in WSNs of Fig. 5-1(a)-(c) are the following:

- *Signal-specific assumptions*: The vast majority of compression techniques and JSCC schemes are tailored and customized to a specific signal model, preventing its use across multiple applications.

- *"Threshold effect"*: Practical PHY FEC schemes exhibit an all-or-nothing behavior, operating very well in a point-to-point channel of known SNR, but poorly in a more challenged environment.

- *Limited performance in multiuser scenarios*: Coding and transmitting information at a rate limited to the worst receiver, which is the prevailing approach for multiuser transmission in WSNs, and not serving each node at a rate commensurate with its channel quality and processing capabilities, severely impacts the total network performance.

- *Feedback and CSI requirements*: Instantaneous and perfect feedback increases the system requirements in terms of transmitted information and available resources, making its incorporation and implementation in WSNs a challenging and sometimes impractical task.

5.1.2 Overview of AdaptCast

This thesis proposes an integrated signal representation-to-transmission PHY design architecture, called AdaptCast, which not only combines the main advantages of the aforementioned approaches but also addresses their limitations. AdaptCast, initially presented in [122], is composed of a joint representation-channel coding scheme followed by an "analog-like" modulation block, as shown in Fig. 5-1(d). The first block uses concepts from CS in order to take advantage of the inherent sparsity in physical signals and efficiently represent the captured information without assuming a detailed signal model. The second block uses dense constellations coupled with a relative bit importance and distance preserving modulation mapping. Based on the synergistic operation of these two blocks, AdaptCast exhibits the following characteristics:

- it is application and signal model independent,
- it provides graceful degradation in signal distortion as channel quality degrades,
- it can simultaneously serve multiple receivers at their highest possible information rate, and
- it operates in a rateless fashion without requiring channel estimation and feedback for rate selection.

We investigate AdaptCast's performance through both a rate distortion analysis, providing asymptotic bounds on its achieved distortion, and simulations with signals captured in typical sensor applications, demonstrating its signal model independent operation. In more detail, considering strictly sparse signals with nonzero coefficients from a Gaussian distribution, we prove the optimality of the proposed method in terms of distortion asymptotically in the high SNR regime. In addition, we compare through simulations AdaptCast's performance against an idealized, layered transmission scheme with instantaneous and perfect CSI, and a more realistic one with outdated CSI in a slow fading environment. Our results show that AdaptCast can

efficiently transmit information in WSNs across a wide range of channel conditions, performing close to the idealized scheme in a unicast scenario, while providing significant advantages in a multiuser setting.

5.2 Notation and System Architecture

This section introduces the notation used across the rest of the chapter and describes AdaptCast's fundamental ideas and main building blocks.

5.2.1 Notation and Source Model

Consider a memoryless source $\mathcal{X}$ which emits an i.i.d. sequence of random variables $X_1, X_2, \cdots$. Let $\boldsymbol{x} \in \mathbb{R}^n$ represent a vector of n source realizations, where $\boldsymbol{x} = \{x_1, x_2, \cdots, x_n\}$. We will refer to $\boldsymbol{x}$ as the source signal and x_i as its i^{th} component or coefficient. In our analysis, we consider a high dimensional setting in which $n \to \infty$ and examine the asymptotic performance of the various coding schemes, while, in our simulations, n is finite. We define signal sparsity density (p) as the ratio

$$p = \frac{k}{n}, \tag{5.1}$$

and based on its value, we identify two regimes: *(i)* linear regime, where $p \xrightarrow{n\to\infty} (0, 1)$, and *(ii)* sublinear regime, where $p \xrightarrow{n\to\infty} 0$.

Definition 1 A source signal $\boldsymbol{x} \in \mathbb{R}^n$ is a strictly k-sparse signal ($\boldsymbol{x} \in \Sigma_k(p)$) if it has at most k non-zero coefficients in a transformation domain defined by an orthogonal matrix $\Psi \in \mathbb{R}^{n\times n}$

$$\boldsymbol{x} \in \Sigma_k(p) \coloneqq \{\boldsymbol{x} = \Psi\boldsymbol{\theta} : \theta \in \mathbb{R}^n \text{ and } \|\boldsymbol{\theta}\|_0 \leq k\}, \tag{5.2}$$

where $\|\cdot\|_0$ is the ℓ_0-norm and denotes the number of nonzero components of a signal.

Several models for the amplitude of non-zero coefficients have been proposed in the literature, e.g. power laws and Laplacian models. In this chapter, we assume that they are realizations of i.i.d. Gaussian random variables, mainly because it provides a worst-case analysis in terms of minimum square error, but also for practical and tractability purposes.

Definition 2 A source signal $\boldsymbol{x} \in \mathbb{R}^n$ is a Gaussian k-sparse signal ($\boldsymbol{x} \in G_k(p, \sigma_x^2)$) if *(i)* $\boldsymbol{x}$ is strictly k-sparse, *(ii)* the position of the k non-zero coefficients is uniformly selected out of the $\binom{n}{k}$ possibilities and *(iii)* their magnitude is an i.i.d. random variable, drawn from the normal distribution

$$\begin{aligned} \boldsymbol{x} \in G_k(p, \sigma_x^2) :=& \{\boldsymbol{x} \in \mathbb{R}^n : \boldsymbol{x} \in \Sigma_k, \Omega \sim \mathcal{U}(1, \binom{n}{k}) \\ & \text{and } x_i \sim \mathcal{N}(0, \sigma_x^2)\}, \end{aligned} \tag{5.3}$$

where $\Omega = \mathbf{supp}(\boldsymbol{x}) := \{i \in [n] : x_i \neq 0\}$.

We assume the signal is transmitted through an AWGN channel of capacity $C(\sigma_z^2)$ and we measure the end-to-end distortion (D) between the initial ($\boldsymbol{x}$) and recovered source signal ($\hat{\boldsymbol{x}}$) by the mean squared error (MSE)

$$MSE(\boldsymbol{x}, \hat{\boldsymbol{x}}) := \mathbb{E}\Big[\frac{1}{n}\|\boldsymbol{x} - \hat{\boldsymbol{x}}\|_2^2\Big]. \tag{5.4}$$

and the percentage root-mean-square difference (PRD)

$$PRD(\boldsymbol{x}, \hat{\boldsymbol{x}}) := \mathbb{E}\Big[\frac{\| \boldsymbol{x} - \hat{\boldsymbol{x}} \|_2}{\| \boldsymbol{x} \|_2}\Big] 100\%. \tag{5.5}$$

5.2.2 Signal Acquisition

AdaptCast follows the random projections and incoherent bases principles to achieve a parsimonious signal representation, similarly to CS. In more detail, assume signal $\boldsymbol{x}$ needs to be transmitted to an intended receiver and let $\boldsymbol{\Phi} \in \mathbb{R}^{M \times N}$

be a measurement matrix. According to [74], if the measurement matrix satisfies the R.I.P. condition [123] for all $\boldsymbol{x} \in \Sigma_k(p)$, where δ_k is a constant $\in (0, 1)$, then only $M = O(k \log N)$ coefficients suffice to reconstruct the initial signal with very high probability. These coefficients are given by the linear operation of

$$\boldsymbol{y} = \boldsymbol{\Phi} \cdot \boldsymbol{x}. \tag{5.6}$$

Each element of $\boldsymbol{y}$ is called a measurement of $\boldsymbol{x}$. Thus, by only acquiring and communicating M measurements of $\boldsymbol{x}$, the receiver can decode the initial signal within some desired distortion limits.

Although random projections and CS form an information theoretic suboptimal compression method in terms of rate [124], it has been widely considered as a candidate method for signal-independent acquisition in resource constrained systems mainly because of its low computational implementation requirements and the fact that several signals typically encountered in WSNs naturally exhibit high sparsity levels [125, 126]. Section 5.3 and 5.5.1 provide some fundamental bounds and simulation results on the rate distortion performance of AdaptCast, respectively.

5.2.3 Signal Transmission

After the sparse signal has been efficiently represented by the measurements vector ($\boldsymbol{y}$) and quantized to the appropriate level, a dense constellation of a digital modulation scheme is used to transmit the information across the channel. Standard PHY randomization techniques, such as scrambling and interleaving, and typical PHY FEC schemes usually result in obliviously created modulated symbols. However, AdaptCast does not use any of these techniques, ensuring that measurements' relative amplitude information is preserved across their entire transmission. In particular, the proposed design preserves the relative importance of transmitted bits by using a direct, distance-based mapping rule and a dense constellation of order matching the

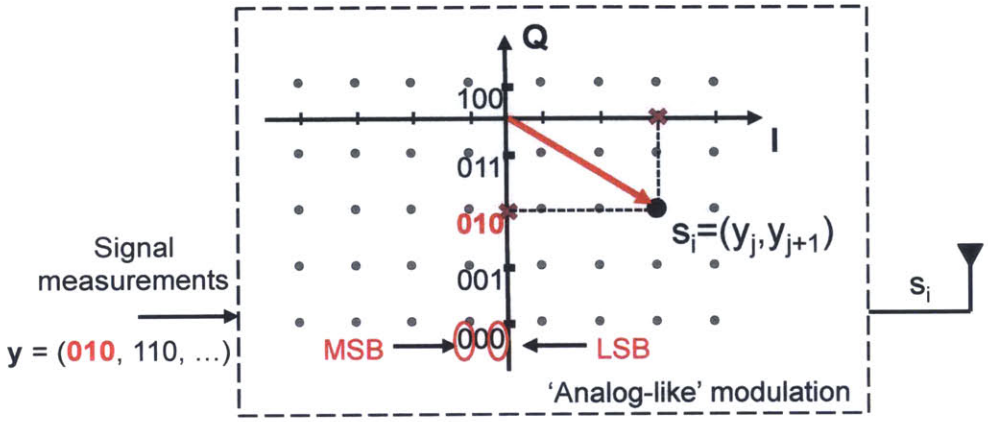

Figure 5-2: AdaptCast uses dense modulation schemes in which signal measurements (y_i) are mapped to modulated symbols (s_i) for transmission through a direct mapping.

precision of the transmitted measurements.

An example of such a transmission approach is shown in Fig. 5-2. A QAM modulation scheme is used with a constellation order that enables direct mapping of quantized measurements y_i's to constellation symbols s_i's. This property guarantees that additive channel noise and its local perturbations to the transmitted symbols will have minimum effect in terms of distortion which will directly depend on the experienced channel quality, similarly to analog modulation schemes. For instance, if the '011' symbol is transmitted on the Q-axis and noise causes its demodulation as a neighboring symbol, e.g. '100', the absolute value of the error is minimum although three error bits, defined by the conventional BER analysis approach, have occurred. Thus, unlike Gray coding that ensures one bit error between neighboring symbols in the constellation diagram, AdaptCast's direct mapping maintains relative bit significance and provides inherent unequal error protection. This concept is further explained and its performance benefits are explored in Section 5.4.1.

5.2.4 Signal Reconstruction

At the receiver side, a noise-corrupted signal ($\hat{\boldsymbol{s}}$) is received, demodulated and mapped to an incomplete and noisy set of measurements ($\hat{\boldsymbol{y}}$). The recovery of the

reconstructed signal ($\hat{\boldsymbol{x}}$) follows the reverse order of the encoding process and is based on principles of CS reconstruction [74]. An optimization problem, formulated as

$$\min_{\hat{\boldsymbol{\theta}} \in \mathbb{R}^n} \| \hat{\boldsymbol{\theta}} \|_1, \text{ subject to } \hat{\boldsymbol{y}} = \boldsymbol{\Phi} \cdot \boldsymbol{\Psi} \cdot \hat{\boldsymbol{\theta}}, \tag{5.7}$$

where $\hat{\boldsymbol{x}} = \boldsymbol{\Psi} \cdot \hat{\boldsymbol{\theta}}$, provides the sparsest solution that corresponds to the received signal. Numerous convex relaxations, such as basis pursuit (BP) [74] and Dantzig selector [127], and greedy algorithms, such as matching pursuit (MP) [128] and iterative thresholding methods [129, 88], have been proposed in the literature with close to optimal performance and strong analytical guarantees. AdaptCast approximates the reconstruction problem of Eq. 5.7 using an optimized orthogonal matching pursuit (OMP) [130] algorithm, providing a good tradeoff between reconstruction quality and computational complexity. Section 5.4.2 presents the detailed description and performance results of the reconstruction algorithm.

5.3 Performance Bounds of AdaptCast

In this section, we examine AdaptCast's rate distortion performance and compare its performance bounds with the ones of a layered coding scheme. Our analysis considers only strictly-sparse sources but results can be extended to approximately-sparse sources as well.

5.3.1 Rate-distortion Performance

The rate distortion function of a source provides a fundamental lower bound on the rate (R) required to achieve on average a description of the source with certain reconstruction distortion (D). Closed form expressions of the $R(D)$ function are known for only a limited number of cases with simple source distributions [103]. A Gaussian k-sparse source has a mixed distribution and can be written as the product

of a discrete Bernoulli r.v., which determines the positions of the non-zero coefficients, and a continuous normal r.v. representing the amplitude [131]. Thus, we can write

$$\mathcal{X} = \mathcal{V} \cdot \mathcal{G} \tag{5.8}$$

where $\mathcal{V} \sim B(p)$ with $p = \Pr\{\mathcal{V} = 1\} \ll 1$ and $\mathcal{G} \sim \mathcal{N}(0, \sigma_x^2)$. An asymptotic approximation of the $R(D)$ function of $\boldsymbol{x} \in G_k(p, \sigma_x^2)$ is given by Eq. 5.9 and it can be proved that it is tight in the low distortion regime.

Lemma 1 The rate distortion function of $\boldsymbol{x} \in G_k(p, \sigma_x^2)$ can be approximated by

$$R(D) \approx h(p) + \frac{p}{2}\log(\frac{p\sigma_x^2}{D}), \tag{5.9}$$

where $h(p)$ is the binary entropy function.

Eq. 5.9 can be derived by considering a two-step coding approach for source $\boldsymbol{x} \in G_k(p, \sigma_x^2)$. First, the positions of the non-zero coefficients are sequentially encoded followed by encoding of their magnitude information. This requires $h(p)$ and $\frac{1}{2}\log(\frac{p\sigma_x^2}{D})$ bits, respectively. In the low distortion regime, this process is shown to be asymptotically optimal [120].

5.3.2 Performance of Layered Coding Schemes

According to Shannon's separation theorem, a rate-distortion achieving source code followed by a capacity achieving channel code does not incur any performance penalty on the channel cost-distortion trade-off in point-to-point channels, asymptotically [39]. Thus, in layered coding schemes, as shown in Fig. 5-1(a), a source signal $\boldsymbol{x} \in \mathbb{R}^n$ is processed by two independent encoders, sequentially mapping the n-symbol source sequence to an intermediate compressed sequence $\boldsymbol{w} \in \mathbb{R}^l$ $(l \leq n)$ and then to a channel coded sequence $\boldsymbol{y} \in \mathbb{R}^m$ $(m \geq l)$ before being mapped to modulated

symbols $\boldsymbol{s}$ for channel transmission. This optimal performance in terms of the rate distortion trade off is usually known as optimal performance theoretically attainable (OPTA).

Lemma 2 The optimal performance theoretically attainable (OPTA) by layered coding schemes in terms of distortion (D_{opta}) for communicating $\boldsymbol{x} \in G_k(p, \sigma_x^2)$ over an AWGN channel with capacity $C(\sigma_z^2)$ is

$$D_{opta} = \frac{p\sigma_x^2 2^{2h(p)/p}}{(1+SNR)^{2/p}}. \tag{5.10}$$

Eq. 5.10 can be easily derived by considering the requirement that any coding scheme should satisfy in order to achieve reliable transmission

$$R(D) \leq C(\sigma_z^2), \tag{5.11}$$

where $C(\sigma_z^2) = \frac{1}{2}\log(1+SNR)$ and $SNR = \frac{\sigma_x^2}{\sigma_z^2}$. Thus, the lowest achieved distortion by layered coding schemes (D_{opta}), assuming infinite delay and complexity, can be derived by equating $R(D)$ in Eq. 5.11 with the channel capacity

$$R(D_{opta}) = C(\sigma_z^2). \tag{5.12}$$

Using Lemma 1 and the capacity formula of an AWGN channel, D_{opta} can be achieved.

5.3.3 Performance of Sparse Recovery

AdaptCast does not make the distinction between source and channel coding, as shown in Fig. 5-1(d). It uses a linear encoding function to map the initial source signal to a set of measurements and then an analog-like modulation scheme to preserve the relative importance of transmitted data. Thus, assuming an AWGN channel of

capacity $C(\sigma_z^2)$, the received signal $\hat{\boldsymbol{y}} \in \mathbb{R}^m$ is

$$\hat{\boldsymbol{y}} = \boldsymbol{y} + \boldsymbol{z} = \Phi \boldsymbol{x} + \boldsymbol{z}, \tag{5.13}$$

where $\Phi \in \mathbb{R}^{n \times m}$ with $n \geq m$ and $z_i \sim \mathcal{N}(0, \sigma_z^2)$.

The reverse process of the encoder is followed at the decoder, recovering $\hat{\boldsymbol{x}}$ through a demodulation and reconstruction process exploiting the signal's structure $\hat{\boldsymbol{x}} = \mathcal{D}(\hat{\boldsymbol{y}})$ where $\mathcal{D}(\cdot) : \mathbb{R}^m \rightarrow \mathbb{R}^n$. Estimating the initial sparse signal $\boldsymbol{x}$ based on the noisy received signal $(\hat{\boldsymbol{y}})$ is a foremost problem in signal processing and statistics. Considering the linear encoding process given by Eq. (5.13), fundamental results from estimation theory suggest that multivariate linear regression via least squares can recover the transmitted signal and no other linear reconstruction process can achieve lower average distortion [132]. Since this approach assumes knowledge of the signal support (Ω), it will be called an oracle-assisted reconstruction process, recovering $\hat{\boldsymbol{x}}$. In more detail, the recovered signal is given by

$$\hat{\boldsymbol{x}}_{|\Omega} = A_{\Omega}^{\dagger} \boldsymbol{y}, \text{ and } \hat{\boldsymbol{x}}_{|\Omega^c} = 0, \tag{5.14}$$

where Ω^c denotes the complement of the support set and $\dagger$ the Moore-Penrose pseudo-inverse operator. Even in the absence of knowledge of the signal support, it has been shown that the distortion of the recoverred signal can be approached within a logarithmic factor [86] and many practical reconstruction algorithms have been proposed with remarkable performance and robustness [88, 129]. Thus, a bound on the distortion achieved by AdaptCast can be derived and is presented in the following Lemma.

Lemma 3 Considering the communication of a source signal $\boldsymbol{x} \in G_k(p, \sigma_x^2)$ over an AWGN channel of capacity $C(\sigma_z^2)$, the minimum achieved distortion by AdaptCast is

$$D_{AC} = c \frac{p^2 \sigma_x^2}{SNR}, \tag{5.15}$$

where c is a constant.

Proof sketch: Assuming knowledge of the signal support and appropriate construction of the encoding matrix A so that only the non-zero components are taken into account, the minimum reconstruction distortion would be

$$D_{AC} = \frac{1}{n}\frac{\sigma_z^2 k}{\frac{m}{k}}. \tag{5.16}$$

Substituting $k = pn$ and $m = \Theta(n)$ required for successful recovery, we get Eq. 5.15.

Lemma 3 enables us to prove the main result of this chapter, which is the asymptotic optimality of the considered coding approach in the high SNR regime. In the finite SNR regime, it becomes obvious that the distortion of layered coding schemes reduces faster than the distortion of the proposed sparsity-exploiting scheme, based on Eq. 5.10 and 5.15.

Theorem 1 In the high SNR regime, the asymptotic performance of AdaptCast in terms of distortion approaches the distortion achieved by capacity achieving layered coding schemes

$$\lim_{SNR\to\infty}(D_{opta} - D_{AC}) = 0 \tag{5.17}$$

Proof sketch: In the linear sparsity regime ($\frac{k}{n} = p \xrightarrow{n\to\infty} (0,1)$), Eq. 5.17 can be derived by combining Eq. 5.10 and 5.15, and applying basic calculus techniques. In the sublinear regime ($\frac{k}{n} = p \xrightarrow{n\to\infty} 0$), we substitute $p = c_1 t$ and $SNR = \frac{c_2}{t}$, and by letting $t \to 0$ we validate Eq. 5.17.

5.4 Signal Reception and Reconstruction

This section describes AdaptCast's demodulation and signal reconstruction process. Simulation results on the relative bit importance preservation and smooth degradation of signal distortion as channel noise increases are also presented.

5.4.1 "Analog-like" Modulation/Demodulation

At the receiver, AdaptCast first demodulates the received symbols ($\hat{\boldsymbol{s}}$) using a standard minimum-distance demodulation rule. The modulation properties, i.e. modulation type and constellation order, are agreed with the transmitter once and remain fixed during the signal transmission. The demodulated symbols are parsed and directly mapped to received signal coefficients ($\hat{\boldsymbol{y}}$), following the reverse process described in Section 5.2.3. The described pipeline is a linear system which ensures channel noise is strictly additive and relative bit-importance is preserved, as opposed to typical modulation pipelines used in state-of-the-art WSNs, in which oblivious creation of modulated symbols destroys the relative bit-importance information.

Contrary to many applications, such as transmission of big digital files over wireless backhaul links, which have strict distortion requirements usually expressed by specific BER thresholds, several WSNs applications can tolerate some end-to-end distortion. This implies that BER is not always the most efficient and representative metric to quantify and optimize for the performance of any communication system, especially when there are soft distortion constraints. AdaptCast's transmission paradigm, including the modulation/demodulation step, is specifically designed to efficiently support the soft transmission of signals in WSNs and achieve a smoothly degrading performance with respect to the channel noise. This is demonstrated by an experiment in which a signal is randomly generated, quantized in five bits and transmitted through an AWGN channel. Two different constellation mapping approaches are compared: a Gray mapping and AdaptCast's direct mapping. Fig. 5-3 shows the performance of the two approaches measured by $\mathrm{PRD}(\boldsymbol{y}, \hat{\boldsymbol{y}})$. AdaptCast's direct mapping ensures a significantly smoother increase in the distortion as the SNR decreases due to the relative bit-importance preservation.

The same result can be better visualized by examining not only the frequency of errors but also their magnitude. Fig. 5-4 plots the error magnitude between

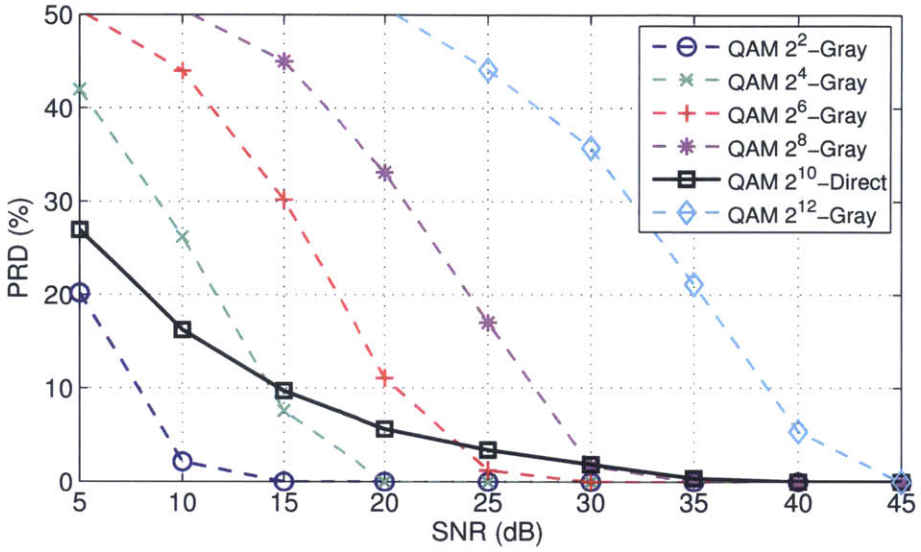

Figure 5-3: Effect of the constellation order and mapping approach on the received signal distortion. Gray coding is used for all constellations with dashed lines while direct mapping is used for the constellation corresponding to the solid one.

transmitted and demodulated samples:

$$\delta_i = y_i - \hat{y}_i. \tag{5.18}$$

This corresponds to two lines of Fig. 5-3 for a specific SNR value. It can be seen that, although the frequency of erroneous symbols is higher in the denser (second) constellation because of the decreased distance of neighboring symbols, the error magnitude takes significantly smaller values compared to the first constellation. This happens because of the inherent unequal error protection of AdaptCast's "analog-like" modulation/demodulation and direct mapping. The distribution of the normalized error probability with respect to bit location and importance is shown in Fig. 5-5, in which bit-1 and bit-5 correspond to MSB and LSB, respectively.

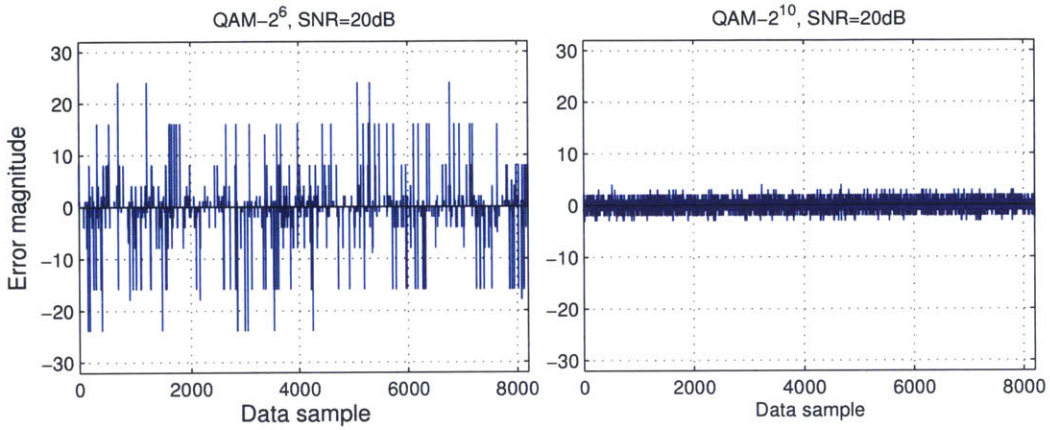

Figure 5-4: Magnitude of error in the received 5-bit samples transmitted over the channel.

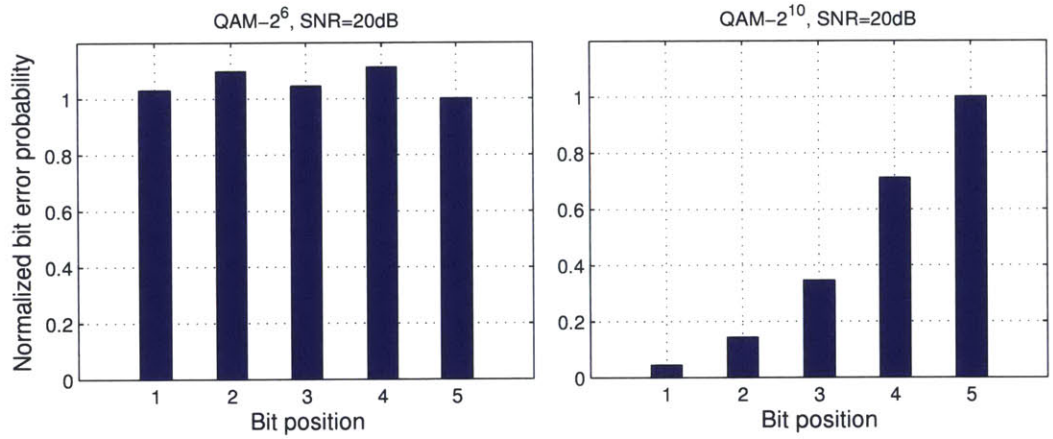

Figure 5-5: Normalized distribution of errors in each bit position. Bit 1 corresponds to MSB and bit 5 to LSB.

5.4.2 Signal Reconstruction

AdaptCast uses a dense constellation with symbols having small distances from their neighboring ones but channel noise affects mainly their LSBs, as shown above. Numerous signal denoising methods have been proposed in the literature, successfully suppressing unwanted noise in captured or received signals. The vast majority of these techniques are application specific [133, 134], making use of precise signal features to identify and separate noise. However, since AdaptCast targets a wide range of

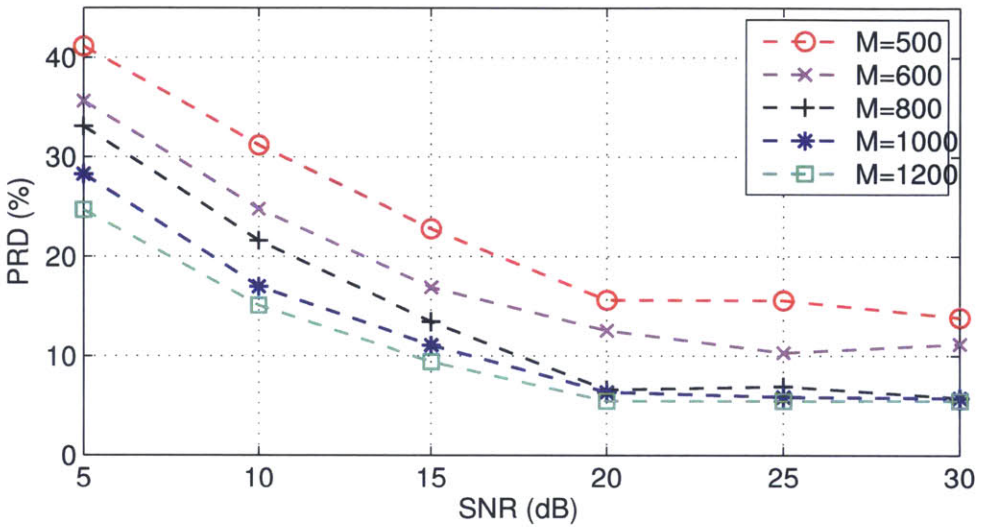

Figure 5-6: Distortion of a reconstructed ECG signal transmitted through an AWGN channel in terms of its SNR. A block size of 2048 samples ($N = 2048$) is used.

WSNs applications, a signal-agnostic method is used based on sparse signal recovery principles. BP [74], OMP [130], ROMP [135] and CoSaMP [88] are some widely used reconstruction methods, each of them with different reconstruction quality and computational complexity.

AdaptCast uses an OMP-based algorithm, mainly because of its robustness in the presence of noise and relatively low computational requirements. Fig. 5-6 shows the reconstruction distortion of the algorithm for an ECG signal [136] transmitted through an AWGN channel, parameterized by the number of measurements (M), or equivalently, the compression ratio. It can be seen that the reconstruction algorithm performs well across a wide range of SNR values and efficiently increases robustness of transmitted data. AdaptCast's acquisition process not only results in a parsimonious signal representation but also in increased data reliability by enabling the reconstruction algorithm to leverage the signal structure and suppress the added channel noise.

5.5 Performance Evaluation

This section demonstrates AdaptCast's applicability in a wide range of typical WSNs applications. In addition, it evaluates its performance in the context of a health monitoring application against two layered coding schemes.

5.5.1 Signal Independent Operation

AdaptCast's acquisition, transmission and reconstruction process is signal agnostic without requiring knowledge or being tailored to a detailed signal model. This is in contrast with the majority of WSN protocols and systems which employ signal dependent acquisition, compression and decompression techniques. AdaptCast supports interoperability among different applications and could potentially contribute to a universal scheme for WSNs.

The end-to-end distortion achieved by AdaptCast depends on the signal sparsity and the experienced channel quality, which do not need to be known in advance. Fig. 5-7 shows AdaptCast's representation and reconstruction performance using signals typically encountered in WSNs. In more detail, an ECG signal from MIT-BIH arrhythmia database [136], images from a thermal camera [137], seismic data [138] and a hydraulic pressure signal from underwater pipe leak detection systems [139] are used. As expected, every signal has its own information rate and as the compression ratio increases, representing the signal with fewer coefficients, the distortion increases as well. However, the figure shows that AdaptCast follows the rate distortion trade off for all signals in a universal manner, regardless of their signal model and sparsity levels.

5.5.2 Compared Approaches

We compare AdaptCast against two layered coding schemes following Shannon's separation theorem, a "genie-aided" and a baseline scheme, in the context of a health

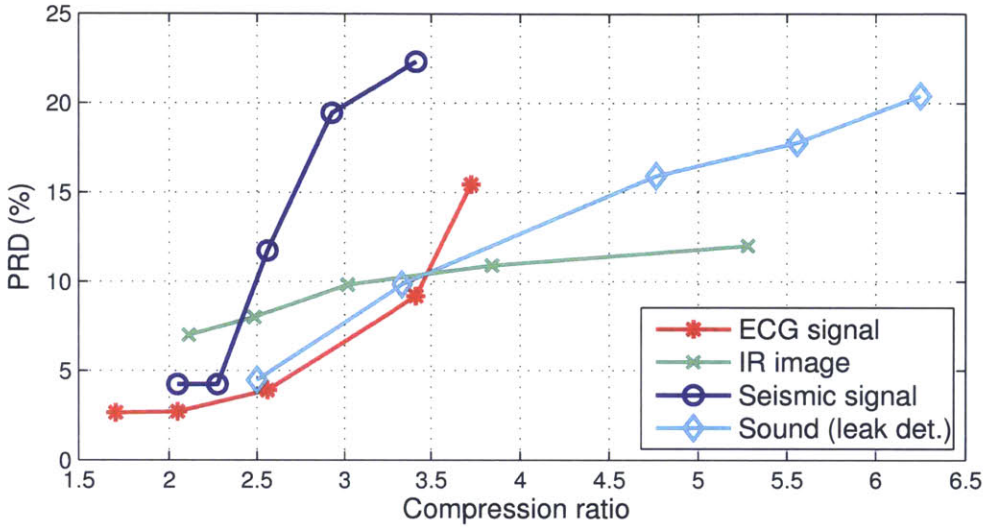

Figure 5-7: AdaptCast's representation performance for four different signals encountered in typical WSN applications: ECG signal, IR image from thermal camera, seismic signal and sound (hydraulic pressure) signal from underwater leak detection.

monitoring application. We assume that a captured biosignal is transmitted from a sensor node to a receiving hub and we are interested in the achieved reliability and distortion performance. In more detail, we use an ECG signal from [136], which is sampled at 360Hz, quantized in 8 bits and processed in blocks of 2048 samples.

The two layered schemes use a lossy ECG compression scheme of a wavelet transformation with adaptive coefficients thresholding, similar to [140]. A BCH code supporting two coding rates of (63,30) and (63,51) is used as the channel coding method, and QAM schemes of three constellation orders (QAM-2^2, QAM-2^4 and QAM-2^6) are used for signal modulation. The rate selection in the genie-aided scheme is performed by an ideal genie providing perfect and instantaneous CSI at the transmitter, always making the optimal rate selection. The baseline uses feedback information transmitted from the receiving node with the acknowledgment frames every fifth packet in order to adjust the transmission rate. Finally, we assume a slow fading channel model with coherence time greater than the packet transmission.

AdaptCast operates in a rateless fashion without relying on feedback informa-

tion. Its system parameters are optimized once for the specific application, providing the best balance between compression performance, resilience against channel noise and reconstruction distortion, and are fixed during the entire experiment. In our experiments, the number of measurements (M) is 800 and a QAM-2^{12} modulation scheme is used. Unlike the genie-aided and baseline scheme, AdaptCast does not require CSI. Although the reduced feedback information is a crucial design property of AdaptCast that can lead to significant performance gains, it is not quantified in the comparison results of this work since we want to decouple any advantage associated with improved feedback mechanisms from benefits related to the proposed novel transmission method.

5.5.3 Performance Comparison

The performance of AdaptCast and genie-aided scheme is shown in Fig. 5-8. The six different rate configurations of the genie-aided scheme correspond to the dashed lines of the graph and all exhibit similar "threshold effect" behavior; they perform well above a given SNR value but have a rapid performance degradation below that. As expected, lower coding rates and smaller constellations correspond to smaller threshold SNR values. Assuming the existence of the genie and the selection of the highest possible transmission rate which results in the lowest distortion, the performance of the genie-aided scheme is the lower envelope of all coding rates. For instance, at a SNR of $20dB$ the idealized scheme uses QAM-2^6 and BCH (63,30) since a choice of the higher coding rate would result in excessive distortion and the lower rate would lead to unnecessary use of resources, e.g. power and bandwidth.

AdaptCast performs very close to the genie-aided scheme, without access to any CSI. In the high SNR regime, the additional distortion is due to the sparse reconstruction algorithm. As the SNR decreases, AdaptCast's distortion is smoothly increasing resulting in a graceful degradation of the reconstruction quality as the channel noise increases. This is achieved by the preservation of the relative bit importance and the

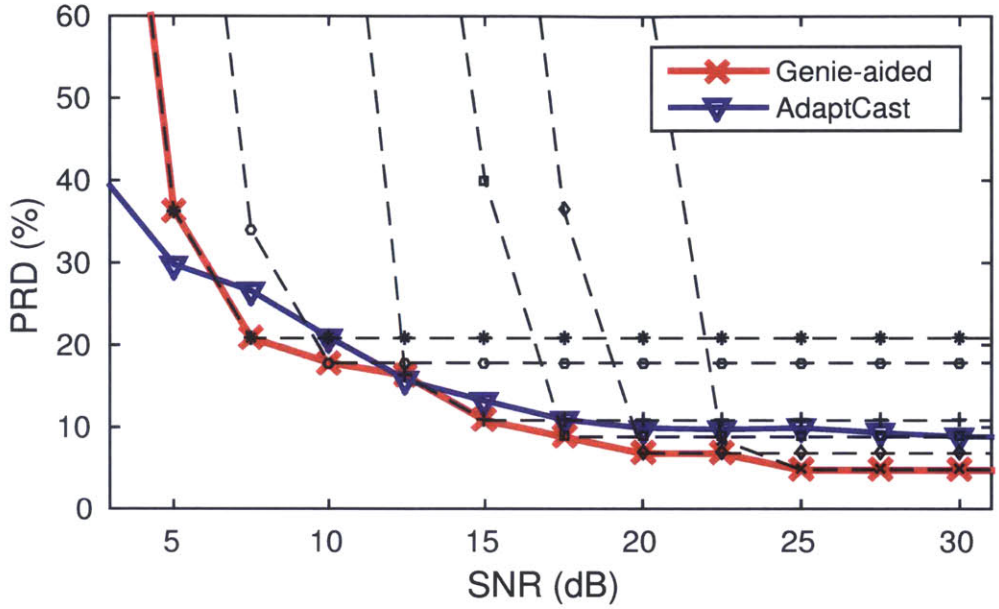

Figure 5-8: Reconstruction distortion in terms of channel SNR for the genie-aided and AdaptCast scheme.

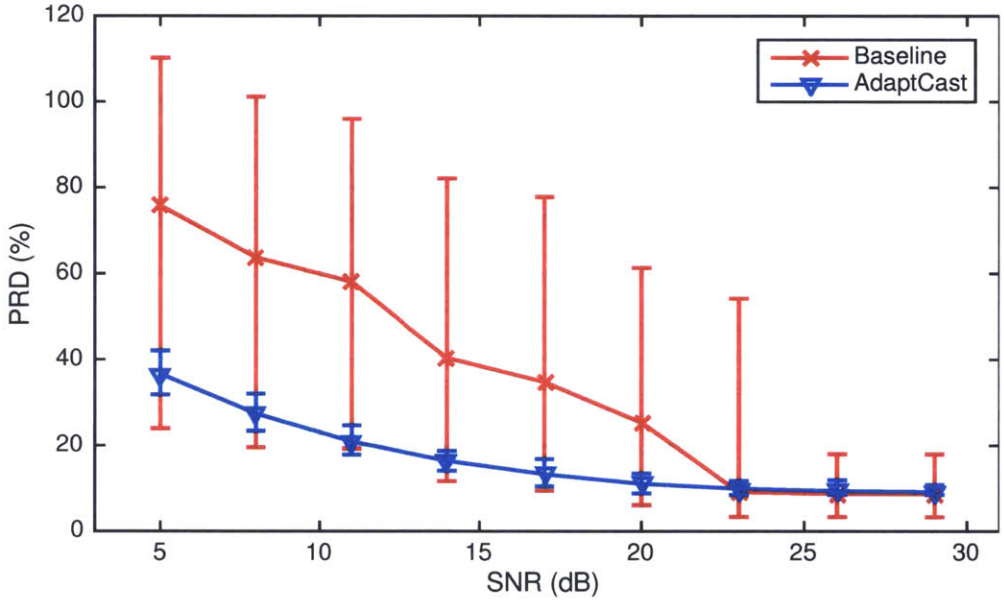

Figure 5-9: Reconstruction distortion in terms of channel SNR for the baseline and AdaptCast scheme. Error bars represent the performance deviation caused by channel fluctuations and the outdated CSI of the baseline scheme.

direct mapping of signal amplitude information to modulated symbols. Fig. 5-9 captures the deleterious effect of SNR fluctuations on the performance of layered schemes

in the absence of instantaneous CSI. In more detail, the fading channel causes significant performance degradation of the baseline scheme with a considerable standard deviation, as shown by the error bars. In contrast, AdaptCast exhibits a smooth distortion increase with the channel SNR and small deviations around the mean PRD values. Compared to the baseline scheme, for a target PRD of 30%, AdaptCast performs better by approximately $10dB$.

Apart from the good performance in point-to-point scenarios, AdaptCast can offer significant advantages in multiuser settings in WSNs. For instance, considering a broadcasting scenario, a sensor node using the predominant layered schemes for WSNs would transmit in the lowest rate corresponding to the receiver with the worst channel. This could significantly limit the overall performance. However, because of its analog-like modulation and rateless coding method, AdaptCast can achieve transmission information rate to each node commensurate with their individual channel quality and without requiring feedback information.

5.6 Summary

In this chapter, we present an application-independent integrated source representation to transmission scheme, called AdaptCast, for efficient communication of captured sparse signals in WSNs [122]. AdaptCast leverages sparsity existing in many physical signals to parsimoniously represent them and, by preserving their relative bit importance during transmission, it achieves a graceful degradation of the signal distortion as the channel SNR decreases. According to our simulations results, it performs close to an idealized layered scheme with perfect CSI in a point-to-point scenario and provides several performance benefits in multiuser settings. AdaptCast does not introduce any computational intense algorithm in the transmitting sensor nodes, limiting its encoding process to a linear operation and pushing most of the system's complexity to the receiver's side. This property makes it very appealing in

asymmetric networks, such as the majority of WSNs [67].

Chapter 6

Conclusion and Future Directions

6.1 Summary of Contributions

WSNs is an emerging technology with enormous potential to transform human lives, improve the operations in several industries and assist in protection of the environment, just to mention a few compelling uses of this technology. The list of applications is lengthly and is constantly growing. Their importance has been highlighted by several governmental, academic and industrial parties, and WSNs are expected to be a crucial component of the connected and data-driven future world.

Although there are several engineering challenges associated with the widespread deployment and operation of WSNs, ensuring efficient methods for information acquisition and reliable transmission within the stringent energy constraints of typical sensor nodes is of utmost importance. This thesis proposes new acquisition schemes and communication algorithms in order improve the transmitted reliability and overall energy efficiency of WSNs. Benefits of the proposed techniques are captured through theoretical analyses, simulations, as well as experiments with off-the-shelf or custom built systems under realistic conditions. The unique approach of the thesis is to examine system optimizations, not only across layers of the protocol stack, but also across different blocks of the sensor node, such as the acquisition and communication

blocks. In addition, it presents co-optimizations of the proposed algorithms and the underlying hardware platforms, and the design of custom circuit architectures when necessary.

The main contribution of the thesis are summarized in Table 6.1, organized per chapter. Interested readers can also read the corresponding references for more details on the work beyond what was presented in this thesis.

6.2 Future Directions

Numerous research and engineering challenges need to be addressed in order for WSNs to realize their full potential. As explained in the previous chapters, signal acquisition and information transmission are two crucial blocks of any WSN, and optimizing their performance could have a significant impact on the overall system. This thesis covered some topics on these two areas, however there are several opportunities for future work.

Chapter 2 considers the performance of FEC schemes typically used at the PHY of WSNs, such as convolutional codes. More powerful coding schemes have been proposed but they are not currently practical in WSNs because of their high computational complexity. Low complexity coding schemes or codes performing very well with short packet lengths are currently investigated in the literature [107, 141]. In addition, technological advances might allow the efficient implementation of complex algorithms in low power systems in the near future. Thus, a careful examination and design of appropriate FEC schemes should be considered.

RLNC is considered in star topology WSNs and its interplay with FEC schemes is explored through analytical and experimental results. In order to fully exploit the benefits of RLNC, more complex topologies have to be considered. In addition, performance benefits of RLNC have to be examined with the whole communication stack of a sensor node, including the MAC, TCP and application layers, in order to

Table 6.1: Main contributions of the thesis, organized per chapter.

	Thesis Contributions
Chapter 2	• Identifies performance benefits of RLNC in star topology WSNs and explores its interaction with FEC schemes • Presents the co-optimization of code performance and computational complexity • Proposes the first custom hardware design of a low power transmitter with variable rate FEC and RLNC accelerators
Chapter 3	• Proposes a PHY-independent PPR scheme, called PRAC, which harnesses information from partial packets and reduces the number of required retransmissions in WSNs • Experimental validation of PRAC and assessment of its throughput and energy efficiency
Chapter 4	• Investigates the rate and energy efficiency of a nonuniform sampling scheme, called TANS, and propose a new sampling method, called TANS with finite set of sampling rates (TFR) • Demonstrates the efficiency benefits of TFR against state-of-the-art sampling methods through simulations in the context of a health monitoring application
Chapter 5	• Proposes a joint signal representation-to-transmission scheme for WSNs, called AdaptCast, leveraging the inherent signal sparsity • Proves AdaptCast's asymptotic optimality in terms of end-to-end distortion through a rate-distortion analysis • Validates AdaptCast's signal-model independent operation and performance in several WSNs scenarios through simulations and comparisons with other schemes

precisely characterize the benefits. Experimental results presented in Chapter 2 assess performance of FEC and RLNC schemes assuming no higher layers exist, measuring the raw performance at the link layer.

Chapter 3 presents a PHY independent PPR scheme, harnessing information from partial packets captured in WSNs. Currently, no wireless sensor or card, including the ones in WLAN systems, exposes PHY soft information to higher layers. However, because of the advances in the software defined radio (SDR) platforms, that might be the case in the near future. Thus, extending PRAC to exploit PHY soft information would significantly reduce the number of retransmitted packets, increasing throughput and energy efficiency.

A novel integrated representation-to-transmission scheme is proposed in Chapter 5 and its performance is investigated through simulations. The hardware implementation analysis and practical energy efficiency examination based on detailed energy models of the underlying circuit architectures is the next logical step for the analysis of the proposed scheme. Technological advances are rapidly changing the design of different circuit components and the relationship among their main performance metrics. For instance, micro-electromechanical devices have been proposed in specific use cases as more efficient compared to traditional RF blocks with better power consumption and noise behaviors. Even if, based on current designs, AdaptCast is viewed as less attractive for an efficient implementation targeting WSNs, a detailed hardware analysis would indicate the break points in the technological roadmap in which the proposed scheme would be practical and more energy efficient.

Last but not least, considering modern WSN applications, security has emerged as a crucial feature. As WSNs are serving more and more use cases, sometimes associated with high monetary values or life critical applications for the general public, protecting the transmitted information and ensuring resiliency against different attacks becomes necessary. A holistic consideration of signal acquisition, transmission and encryption could lead to new insights and practical schemes, which would unleash the potential of WSNs.

Bibliography

[1] "Cisco visual networking index: Global mobile data traffic forecast update," in *Cisco*, 2014.

[2] D. Evans, "How the next evolution of the internet is changing everything," in *Cisco IBSG*, 2011.

[3] T. Ho, M. Médard, R. Koetter, D. Karger, M. Effros, J. Shi, and B. Leong, "A random linear network coding approach to multicast," *Information Theory, IEEE Transactions on*, vol. 52, no. 10, pp. 4413–4430, Oct. 2006.

[4] S. Lin and D. J. Costello, *Error Control Coding: Fundamentals and Applications*, 2nd ed. Prentice Hall: Englewood Cliffs, NJ, 2004.

[5] S. L. Howard, C. Schlegel, and K. Iniewski, "Error control coding in low-power wireless sensor networks: When is ECC energy-efficient?" *EURASIP J. Wirel. Commun. Netw.*, vol. 2006, no. 2, pp. 1687–1472, Apr. 2006.

[6] G. Balakrishnan, M. Yang, Y. Jiang, and Y. Kim, "Performance analysis of error control codes for wireless sensor networks," in *Information Technology, Fourth International Conference on*, April 2007, pp. 876–879.

[7] M. Holland, T. Wang, B. Tavli, A. Seyedi, and W. Heinzelman, "Optimizing physical-layer parameters for wireless sensor networks," *ACM Trans. Sen. Netw.*, vol. 7, no. 4, pp. 28:1–28:20, Feb. 2011.

[8] M. Luby, M. Mitzenmacher, M. Shokrollahi, and D. Spielman, "Efficient erasure correcting codes," *Information Theory, IEEE Transactions on*, vol. 47, no. 2, pp. 569–584, Feb. 2001.

[9] M. Vehkapera and M. Médard, "A throughput-delay trade-off in packetized systems with erasures," in *Information Theory, Proceedings. International Symposium on*, Sept 2005, pp. 1858–1862.

[10] T. Courtade and R. Wesel, "Optimal allocation of redundancy between packet-level erasure coding and physical-layer channel coding in fading channels," *Communications, IEEE Transactions on*, vol. 59, no. 8, pp. 2101–2109, 2011.

[11] G. Angelopoulos, A. Paidimarri, A. Chandrakasan, and M. Médard, "Experimental study of the interplay of channel and network coding in low power sensor applications," in *Communications (ICC), 2013 IEEE International Conference on*, June 2013, pp. 5126–5130.

[12] C. Fragouli and E. Soljanin, "Network coding fundamentals," *Found. Trends Netw.*, vol. 2, pp. 1–133, January 2007.

[13] L. Keller, E. Atsan, K. Argyraki, and C. Fragouli, "SenseCode: Network coding for reliable sensor networks," *ACM Transactions on Sensor Networks*, vol. 9, no. 2, 2013.

[14] A. Antonopoulos, C. Verikoukis, C. Skianis, and O. B. Akan, "Energy efficient network coding-based MAC for cooperative ARQ wireless networks," *Ad Hoc Netw.*, vol. 11, no. 1, pp. 190–200, Jan. 2013.

[15] A. Paidimarri, P. Nadeau, P. Mercier, and A. Chandrakasan, "A 2.4 GHz multi-channel FBAR-based transmitter with an integrated pulse-shaping power amplifier," *Solid-State Circuits, IEEE Journal of*, vol. 48, no. 4, pp. 1042–1054, April 2013.

[16] R. Ahlswede, N. Cai, S.-Y. Li, and R. Yeung, "Network information flow," *Information Theory, IEEE Transactions on*, vol. 46, no. 4, pp. 1204 –1216, Jul. 2000.

[17] C. Fragouli, J.-Y. Le Boudec, and J. Widmer, "Network coding: An instant primer," *SIGCOMM Comput. Commun. Rev.*, vol. 36, no. 1, pp. 63–68, Jan. 2006.

[18] D. MacKay, "Fountain codes," *Communications, IEEE Proceedings*, vol. 152, no. 6, pp. 1062–1068, Dec. 2005.

[19] D. Lucani, M. Stojanovic, and M. Médard, "Random linear network coding for time division duplexing: When to stop talking and start listening," in *INFOCOM 2009, IEEE*, April 2009, pp. 1800–1808.

[20] X. Shi, M. Médard, and D. Lucani, "When both transmitting and receiving energies matter: An application of network coding in wireless body area networks," in *NETWORKING 2011 Workshops*, ser. Lecture Notes in Computer Science. Springer Berlin Heidelberg, 2011, vol. 6827, pp. 119–128.

[21] J. P. Vilela, L. Lima, and J. Barros, "Lightweight security for network coding," *CoRR*, vol. abs/0807.0610, 2008. [Online]. Available: http://arxiv.org/abs/0807.0610

[22] I.-H. Hou, Y.-E. Tsai, T. Abdelzaher, and I. Gupta, "AdapCode: Adaptive network coding for code updates in wireless sensor networks," in *INFOCOM 2008. The 27th Conference on Computer Communications. IEEE*, April 2008.

[23] R. Rout and S. Ghosh, "Enhancement of lifetime using duty cycle and network coding in wireless sensor networks," *Wireless Communications, IEEE Transactions on*, vol. 12, no. 2, pp. 656–667, February 2013.

[24] H. Li and Q. Huan-yan, "Parallelized network coding with SIMD instruction sets," in *Computer Science and Computational Technology, 2008. ISCSCT '08. International Symposium on*, vol. 1, Dec 2008, pp. 364–369.

[25] H. Shojania, B. Li, and X. Wang, "Nuclei: GPU-accelerated many-core network coding," in *INFOCOM 2009, IEEE*, april 2009, pp. 459 –467.

[26] P. Vingelmann, P. Zanaty, F. Fitzek, and H. Charaf, "Implementation of random linear network coding on OpenGL-enabled graphics cards," in *Wireless Conference, 2009. EW 2009. European*, May 2009, pp. 118 –123.

[27] S. Kim, W. S. Jeong, W. W. Ro, and J.-L. Gaudiot, "Design and evaluation of random linear network coding accelerators on FPGAs," *ACM Trans. Embed. Comput. Syst.*, vol. 13, no. 1, pp. 13:1–13:24, Sep. 2013.

[28] A. Paramanathan, M. Pedersen, D. Lucani, F. Fitzek, and M. Katz, "Lean and mean: network coding for commercial devices," *Wireless Communications, IEEE*, vol. 20, no. 5, pp. 54–61, October 2013.

[29] K.-s. Koo and M. Govindarasu, "Design and experiment of testbed using network coding for power management," *SIGBED Rev.*, vol. 12, no. 3, pp. 40–44, Aug. 2015.

[30] M. Qazi, M. Sinangil, and A. Chandrakasan, "Challenges and directions for low-voltage SRAM," *Design Test of Computers, IEEE*, vol. 28, no. 1, pp. 32–43, Jan 2011.

[31] I. Hsu, T. Truong, L. Deutsch, and I. Reed, "A comparison of VLSI architecture of finite field multipliers using dual, normal, or standard bases," *Computers, IEEE Transactions on*, vol. 37, no. 6, pp. 735 –739, Jun. 1988.

[32] R. Azarderakhsh, K. Jarvinen, and M. Mozaffari-Kermani, "Efficient algorithm and architecture for elliptic curve cryptography for extremely constrained secure

applications," *Circuits and Systems I: Regular Papers, IEEE Transactions on*, vol. 61, no. 4, pp. 1144–1155, April 2014.

[33] S. Mathew, S. Satpathy, V. Suresh, M. Anders, H. Kaul, A. Agarwal, S. Hsu, G. Chen, and R. Krishnamurthy, "340mV-1.1V, 289Gbps/W, 2090-gate NanoAES hardware accelerator with area-optimized encrypt/decrypt $GF(2^4)^2$ polynomials in 22 nm tri-gate CMOS," *Solid-State Circuits, IEEE Journal of*, vol. 50, no. 4, pp. 1048–1058, April 2015.

[34] "CC2511 data sheet," Texas Instruments, Dallas, TX. [Online]. Available: http://www.ti.com/lit/gpn/cc2511f32

[35] "ZX76-31-PP-S+ data sheet," Mini Circuits, Brooklyn, NY. [Online]. Available: http://www.minicircuits.com/pdfs/ZX76-31-PP+.pdf

[36] G. Angelopoulos, M. Médard, and A. P. Chandrakasan, "Energy-aware hardware implementation of network coding," in *Network Coding Applications and Protocols Workshop, NC-Pro*, May 2011.

[37] J. Costello, D.J., J. Hagenauer, H. Imai, and S. Wicker, "Applications of error-control coding," *Information Theory, IEEE Transactions on*, vol. 44, no. 6, pp. 2531 –2560, Oct. 1998.

[38] R. T. Morris, J. C. Bicket, and J. C. Bicket, "Bit-rate selection in wireless networks," Master's thesis, MIT, Tech. Rep., 2005.

[39] C. E. Shannon, "A mathematical theory of communication," *The Bell System Technical Journal*, vol. 27, pp. 379–423, 623–656, 1948.

[40] D. Chase, "Code combining–a maximum-likelihood decoding approach for combining an arbitrary number of noisy packets," *Communications, IEEE Transactions on*, vol. 33, no. 5, pp. 385–393, May 1985.

[41] K. Jamieson and H. Balakrishnan, "PPR: partial packet recovery for wireless networks," in *SIGCOMM*, 2007, pp. 409–420.

[42] K. C.-J. Lin, N. Kushman, and D. Katabi, "ZipTx: Harnessing partial packets in 802.11 networks," in *MobiCom*, 2008, pp. 351–362.

[43] "TI products, CC2500/CC2550DK Development kit." [Online]. Available: http://focus.ti.com/docs/toolsw/folders/print/cc2500-cc2550dk.html

[44] Z. Kashani and M. Shiva, "Power optimised channel coding in wireless sensor networks using low-density parity-check codes," *Communications, IET*, vol. 1, no. 6, pp. 1256 –1262, Dec. 2007.

[45] M. Vutukuru, H. Balakrishnan, and K. Jamieson, "Cross-layer wireless bit rate adaptation," in *SIGCOMM*, Aug. 2009.

[46] J. Camp and E. Knightly, "Modulation rate adaptation in urban and vehicular environments: cross-layer implementation and experimental evaluation," in *MobiCom*, 2008.

[47] M. Luby, "LT codes," in *Proc. of the 43rd Symp. on Foundations of Computer Science*, ser. FOCS '02, 2002.

[48] A. Shokrollahi, "Raptor codes," *IEEE/ACM Trans. Networking*, vol. 14, Jun. 2006.

[49] U. Erez, M. Trott, and G. W. Wornell, "Rateless coding for Gaussian channels," *Information Theory, IEEE Transactions on*, vol. 58, no. 2, pp. 530–547, 2012.

[50] A. Gudipati and S. Katti, "Strider: automatic rate adaptation and collision handling," in *SIGCOMM*, Aug. 2011.

[51] E. Soljanin, N. Varnica, and P. Whiting, "Incremental redundancy hybrid ARQ with LDPC and Raptor codes," *IEEE Transactions on Information Theory*, 2005.

[52] "IEEE standard for local and metropolitan area networks part 16: Air interface for broadband wireless access systems," *IEEE Std 802.16-2009 (Revision of IEEE Std 802.16-2004)*, pp. C1 –2004, 29 2009.

[53] 3GPP, *Evolved Universal Terrestrial Radio Access (E-UTRA) Multiplexing and Channel Coding, TS 36.212 v9.2.0.* Prentice Hall: Englewood Cliffs, NJ, June 2010.

[54] G. R. Woo, P. Kheradpour, D. Shen, and D. Katabi, "Beyond the bits: cooperative packet recovery using physical layer information," in *MobiCom*, 2007, pp. 147–158.

[55] S. Katti, D. Katabi, H. Balakrishnan, and M. Médard, "Symbol-level network coding for wireless mesh networks," in *SIGCOMM*, 2008.

[56] R. K. Ganti, P. Jayachandran, H. Luo, and T. F. Abdelzaher, "Datalink streaming in wireless sensor networks," in *SenSys*, 2006, pp. 209–222.

[57] J. Xie, W. Hu, and Z. Zhang, "Revisiting partial packet recovery in 802.11 wireless LANs," in *MobiSys*, 2011, pp. 281–292.

[58] B. Han, A. Schulman, F. Gringoli, N. Spring, B. Bhattacharjee, L. Nava, L. Ji, S. Lee, and R. Miller, "Maranello: practical partial packet recovery for 802.11," in *NSDI*, 2010, pp. 14–14.

[59] H. Dubois-Ferrière, D. Estrin, and M. Vetterli, "Packet combining in sensor networks," in *SenSys*, 2005.

[60] D. S. Lun, M. Médard, R. Koetter, and M. Effros, "On coding for reliable communication over packet networks," *CoRR*, vol. abs/cs/0510070, 2005.

[61] P. Wu and N. Jindal, "Coding versus ARQ in fading channels: How reliable should the PHY be?" *Communications, IEEE Transactions on*, vol. 59, no. 12, pp. 3363–3374, 2011.

[62] D. Lucani, M. Stojanovic, and M. Médard, "Random linear network coding for time division duplexing: When to stop talking and start listening," in *INFOCOM*, 2009.

[63] P. A. Iannucci, J. Perry, H. Balakrishnan, and D. Shah, "No symbol left behind: a link-layer protocol for rateless codes," in *MobiCom*, 2012.

[64] R. Cavallari, F. Martelli, R. Rosini, C. Buratti, and R. Verdone, "A survey on wireless body area networks: Technologies and design challenges," *Communications Surveys Tutorials, IEEE*, vol. PP, no. 99, pp. 1–23, 2014.

[65] "TI products, CC2511." [Online]. Available: http://www.ti.com/lit/gpn/cc2511f32

[66] G. Angelopoulos, A. Chandrakasan, and M. Médard, "PRAC: Exploiting partial packets without cross-layer or feedback information," in *Communications (ICC), IEEE International Conference on*, June 2014, pp. 5802–5807.

[67] G. Angelopoulos, A. Chandrakasan, and M. Médard, "Energy savings via harnessing partial packets in body area networks," in *Proceedings of the 9th International Conference on Body Area Networks*, ser. BodyNets '14, 2014, pp. 320–325.

[68] H. Nyquist, "Certain topics in telegraph transmission theory," *American Institute of Electrical Engineers, Transactions of the*, vol. 47, no. 2, pp. 617–644, April 1928.

[69] D. Wei, "Sampling based on local bandwidth," Master's thesis, MIT, Tech. Rep., 2007.

[70] F. Marvasti, *Nonuniform sampling: Theory and Practice*, 1st ed. Kluwer Academic, New York, NY, 2001.

[71] S. Mian Qaisar, L. Fesquet, and M. Renaudin, "Adaptive rate sampling and filtering based on level crossing sampling," *EURASIP Journal on Advances in Signal Processing*, vol. 2009, no. 1, p. 971656, 2009.

[72] T. A. Claasen and W. Mecklenbrauker, "On stationary linear time-varying systems," *Circuits and Systems, IEEE Transactions on*, vol. 29, no. 3, pp. 169–184, 1982.

[73] K. Horiuchi, "Sampling principle for continuous signals with time-varying bands," *Information and Control*, vol. 13, no. 1, pp. 53 – 61, 1968.

[74] D. Donoho, "Compressed sensing," *Information Theory, IEEE Transactions on*, vol. 52, no. 4, pp. 1289 –1306, 2006.

[75] F. Chen, A. Chandrakasan, and V. Stojanovic, "A signal-agnostic compressed sensing acquisition system for wireless and implantable sensors," in *Custom Integrated Circuits Conference (CICC), 2010 IEEE*, Sept 2010, pp. 1–4.

[76] A. Dixon, E. Allstot, D. Gangopadhyay, and D. Allstot, "Compressed sensing system considerations for ECG and EMG wireless biosensors," *Biomedical Circuits and Systems, IEEE Transactions on*, vol. 6, no. 2, pp. 156–166, April 2012.

[77] S. Feizi, V. Goyal, and M. Médard, "Time-stampless adaptive nonuniform sampling for stochastic signals," in *Acoustics, Speech and Signal Processing (ICASSP), 2012 IEEE International Conference on*, March 2012, pp. 3809–3812.

[78] A. L. Goldberger, L. A. N. Amaral, L. Glass, J. M. Hausdorff, P. C. Ivanov, R. G. Mark, J. E. Mietus, G. B. Moody, C.-K. Peng, and H. E. Stanley, "Phys-

ioBank, PhysioToolkit, and PhysioNet: Components of a new research resource for complex physiologic signals," *Circulation*, vol. 101, no. 23, pp. e215–e220, 2000 (June 13).

[79] S. Feizi, V. Goyal, and M. Médard, "Locally adaptive sampling," in *Communication, Control, and Computing (Allerton), 2010 48th Annual Allerton Conference on*, Sept 2010, pp. 152–159.

[80] R. Benzid, A. Messaoudi, and A. Boussaad, "Constrained ECG compression algorithm using the block-based discrete cosine transform," *Digital Signal Processing*, vol. 18, no. 1, pp. 56 – 64, 2008.

[81] B. Yu, L. Yang, and C.-C. Chong, "ECG monitoring over bluetooth: Data compression and transmission," in *Wireless Communications and Networking Conference (WCNC), 2010 IEEE*, April 2010, pp. 1–5.

[82] K. Kozmin, J. Johansson, and J. Delsing, "Level-crossing ADC performance evaluation toward ultrasound application," *Circuits and Systems I: Regular Papers, IEEE Transactions on*, vol. 56, no. 8, pp. 1708–1719, Aug 2009.

[83] E. Candes and T. Tao, "Near-optimal signal recovery from random projections: Universal encoding strategies?" *Information Theory, IEEE Transactions on*, vol. 52, no. 12, pp. 5406–5425, Dec 2006.

[84] S. S. Chen, D. L. Donoho, and M. A. Saunders, "Atomic decomposition by basis pursuit," *SIAM Journal on Scientific Computing*, vol. 20, no. 1, pp. 33–61, 1998.

[85] R. Tibshirani, "Regression shrinkage and selection via the lasso," *Journal of the Royal Statistical Society, Series B*, vol. 58, pp. 267–288, 1994.

[86] T. T. Emmanuel Candes, "The Dantzig selector: Statistical estimation when p is much larger than n," *The Annals of Statistics*, vol. 35, no. 6, pp. 2313–2351, 2007.

[87] J. Tropp and A. Gilbert, "Signal recovery from random measurements via orthogonal matching pursuit," *Information Theory, IEEE Transactions on*, vol. 53, no. 12, pp. 4655–4666, Dec 2007.

[88] D. Needell and J. Tropp, "CoSaMP: Iterative signal recovery from incomplete and inaccurate samples," *Applied and Computational Harmonic Analysis*, vol. 26, no. 3, pp. 301 – 321, 2009.

[89] D. Donoho, A. Maleki, and A. Montanari, "Message passing algorithms for compressed sensing: I. motivation and construction," in *Information Theory (ITW 2010, Cairo), 2010 IEEE Information Theory Workshop on*, Jan 2010, pp. 1–5.

[90] S. Rangan, A. Fletcher, and V. Goyal, "Asymptotic analysis of MAP estimation via the replica method and applications to compressed sensing," *Information Theory, IEEE Transactions on*, vol. 58, no. 3, pp. 1902–1923, March 2012.

[91] M. Grant and S. Boyd, "CVX: Matlab software for disciplined convex programming, version 2.1," http://cvxr.com/cvx, Mar. 2014.

[92] R. Grimaldi, S. Rodriguez, and A. Rusu, "A 10-bit 5kHz level-crossing ADC," in *Circuit Theory and Design (ECCTD), 2011 20th European Conference on*, Aug 2011, pp. 564–567.

[93] F. Chen, A. Chandrakasan, and V. Stojanovic, "Design and analysis of a hardware-efficient compressed sensing architecture for data compression in wireless sensors," *Solid-State Circuits, IEEE Journal of*, vol. 47, no. 3, pp. 744–756, March 2012.

[94] M. Mishali and Y. Eldar, "From theory to practice: Sub-Nyquist sampling of sparse wideband analog signals," *Selected Topics in Signal Processing, IEEE Journal of*, vol. 4, no. 2, pp. 375–391, April 2010.

[95] S. Kirolos, J. Laska, M. Wakin, M. Duarte, D. Baron, T. Ragheb, Y. Massoud, and R. Baraniuk, "Analog-to-information conversion via random demodulation," in *Design, Applications, Integration and Software, 2006 IEEE Dallas/CAS Workshop on*, Oct 2006, pp. 71–74.

[96] O. Abari, F. Chen, F. Lim, and V. Stojanovic, "Performance trade-offs and design limitations of analog-to-information converter front-ends," in *Acoustics, Speech and Signal Processing (ICASSP), 2012 IEEE International Conference on*, March 2012, pp. 5309–5312.

[97] P. Mercier, D. Daly, and A. Chandrakasan, "An energy-efficient all-digital UWB transmitter employing dual capacitively-coupled pulse-shaping drivers," *Solid-State Circuits, IEEE Journal of*, vol. 44, no. 6, pp. 1679–1688, June 2009.

[98] S. Jocke, J. Bolus, S. Wooters, A. Jurik, A. Weaver, T. Blalock, and B. Calhoun, "A 2.6-μw sub-threshold mixed-signal ECG SoC," in *VLSI Circuits, 2009 Symposium on*, June 2009, pp. 60–61.

[99] E. Chua and W.-C. Fang, "Mixed bio-signal lossless data compressor for portable brain-heart monitoring systems," *Consumer Electronics, IEEE Transactions on*, vol. 57, no. 1, pp. 267–273, February 2011.

[100] S. Feizi, G. Angelopoulos, V. Goyal, and M. Médard, "Energy-efficient time-stampless adaptive nonuniform sampling," in *Sensors, 2011 IEEE*, oct. 2011, pp. 912 –915.

[101] M. Rambeloarison, S. Feizi, G. Angelopoulos, and M. Médard, "Empirical rate-distortion study of compressive sensing-based joint source-channel coding," in *Signals, Systems and Computers (ASILOMAR), 2012 Conference Record of the Forty Sixth Asilomar Conference on*, Nov 2012, pp. 1224–1228.

[102] S. Feizi, G. Angelopoulos, V. Goyal, and M. Médard, "Backward adaptation for power efficient sampling," *Signal Processing, IEEE Transactions on*, vol. 62, no. 16, pp. 4327–4338, Aug 2014.

[103] T. M. Cover and J. A. Thomas, *Elements of Information Theory.* USA: Wiley, 2006.

[104] V. Goyal, "Theoretical foundations of transform coding," *Signal Processing Magazine, IEEE*, vol. 18, no. 5, pp. 9–21, Sep 2001.

[105] S. Borade, B. Nakiboglu, and L. Zheng, "Unequal error protection: An information-theoretic perspective," *Information Theory, IEEE Transactions on*, vol. 55, no. 12, pp. 5511–5539, Dec 2009.

[106] R. Morelos-Zaragoza, M. Fossorier, S. Lin, and H. Imai, "Multilevel coded modulation for unequal error protection and multistage decoding-Part I: Symmetric constellations," *Communications, IEEE Transactions on*, vol. 48, no. 2, pp. 204–213, 2000.

[107] J. Perry, P. Iannucci, K. E. Fleming, H. Balakrishnan, and D. Shah, "Spinal Codes," in *SIGCOMM*, Aug 2012.

[108] I. Csiszar, "On the error exponent of source-channel transmission with a distortion threshold," *Information Theory, IEEE Transactions on*, vol. 28, no. 6, pp. 823–828, Nov 1982.

[109] Y. Zhong, F. Alajaji, and L. Campbell, "On the joint source-channel coding error exponent for discrete memoryless systems," *Information Theory, IEEE Transactions on*, vol. 52, no. 4, pp. 1450–1468, April 2006.

[110] V. Kostina and S. Verdu, "Lossy joint source-channel coding in the finite blocklength regime," *Information Theory, IEEE Transactions on*, vol. 59, no. 5, pp. 2545–2575, May 2013.

[111] R. Soundararajan and S. Vishwanath, "Hybrid coding for Gaussian broadcast channels with Gaussian sources," in *Information Theory, 2009. ISIT 2009. IEEE International Symposium on*, June 2009, pp. 2790–2794.

[112] A. Jain, D. Gunduz, S. Kulkarni, H. Poor, and S. Verdu, "Energy-distortion tradeoffs in Gaussian joint source-channel coding problems," *Information Theory, IEEE Transactions on*, vol. 58, no. 5, pp. 3153–3168, May 2012.

[113] J. Hagenauer, "Source-controlled channel decoding," *Communications, IEEE Transactions on*, vol. 43, no. 9, pp. 2449–2457, Sep 1995.

[114] V. Prabhakaran, R. Puri, and K. Ramchandran, "Hybrid digital-analog codes for source-channel broadcast of Gaussian sources over Gaussian channels," *Information Theory, IEEE Transactions on*, vol. 57, no. 7, pp. 4573–4588, July 2011.

[115] E. Candes and T. Tao, "Near-optimal signal recovery from random projections: Universal encoding strategies?" *Information Theory, IEEE Transactions on*, vol. 52, no. 12, pp. 5406–5425, Dec 2006.

[116] ——, "Decoding by linear programming," *Information Theory, IEEE Transactions on*, vol. 51, no. 12, p. 4203âĂŞ4215, Dec 2005.

[117] E. Candes and M. Wakin, "An introduction to compressive sampling," *Signal Processing Magazine, IEEE*, vol. 25, no. 2, pp. 21–30, 2008.

[118] S. Aeron, V. Saligrama, and M. Zhao, "Information theoretic bounds for compressed sensing," *Information Theory, IEEE Transactions on*, vol. 56, no. 10, pp. 5111–5130, Oct 2010.

[119] G. Reeves and M. Gastpar, "Approximate sparsity pattern recovery: Information-theoretic lower bounds," *Information Theory, IEEE Transactions on*, vol. 59, no. 6, pp. 3451–3465, June 2013.

[120] C. Weidmann and M. Vetterli, "Rate distortion behavior of sparse sources," *Information Theory, IEEE Transactions on*, vol. 58, no. 8, pp. 4969–4992, Aug 2012.

[121] Y. Chen, A. Goldsmith, and Y. Eldar, "Channel capacity under sub-Nyquist nonuniform sampling," *Information Theory, IEEE Transactions on*, vol. 60, no. 8, pp. 4739–4756, Aug 2014.

[122] G. Angelopoulos, M. Médard, and A. Chandrakasan, "AdaptCast: An integrated source to transmission scheme for wireless sensor networks," in *Communications (ICC), 2015 IEEE International Conference on*, June 2015, pp. 2894–2899.

[123] E. Candes and T. Tao, "Decoding by linear programming," *Information Theory, IEEE Transactions on*, vol. 51, no. 12, pp. 4203–4215, 2005.

[124] V. Goyal, A. Fletcher, and S. Rangan, "Compressive sampling and lossy compression," *Signal Processing Magazine, IEEE*, vol. 25, no. 2, pp. 48–56, 2008.

[125] F. Chen, F. Lim, O. Abari, A. Chandrakasan, and V. Stojanovic, "Energy-aware design of compressed sensing systems for wireless sensors under performance and reliability constraints," *Circuits and Systems I: Regular Papers, IEEE Transactions on*, vol. 60, no. 3, pp. 650–661, 2013.

[126] J. Prades-Nebot, Y. Ma, and T. Huang, "Distributed video coding using compressive sampling," in *Picture Coding Symposium*, 2009, pp. 1–4.

[127] E. Candes and T. Tao, "The dantzig selector: Statistical estimation when p is much larger than n," *The Annals of Statistics*, vol. 35, no. 6, pp. 2313–2351, 12 2007.

[128] S. Mallat and Z. Zhang, "Matching pursuits with time-frequency dictionaries," *Signal Processing, IEEE Transactions on*, vol. 41, no. 12, pp. 3397–3415, Dec 1993.

[129] T. Blumensath and M. E. Davies, "Iterative hard thresholding for compressed sensing," *CoRR*, vol. abs/0805.0510, 2008.

[130] D. Donoho, Y. Tsaig, I. Drori, and J.-L. Starck, "Sparse solution of underdetermined systems of linear equations by stagewise orthogonal matching pursuit," *Information Theory, IEEE Transactions on*, vol. 58, no. 2, pp. 1094–1121, Feb 2012.

[131] H. Rosenthal and J. Binia, "On the epsilon entropy of mixed random variables," *Information Theory, IEEE Transactions on*, vol. 34, no. 5, p. 1110âĂŞ1114, Sep 1988.

[132] E. J. CandÃĺs and M. A. Davenport, "How well can we estimate a sparse vector?" *Applied and Computational Harmonic Analysis*, vol. 34, no. 2, pp. 317 – 323, 2013.

[133] J.-L. Starck, E. Candes, and D. Donoho, "The curvelet transform for image denoising," *Image Processing, IEEE Transactions on*, vol. 11, no. 6, pp. 670–684, 2002.

[134] R. Sameni, M.-B. Shamsollahi, C. Jutten, and G. Clifford, "A nonlinear bayesian filtering framework for ECG denoising," *Biomedical Engineering, IEEE Transactions on*, vol. 54, no. 12, pp. 2172–2185, 2007.

[135] D. Needell and R. Vershynin, "Uniform uncertainty principle and signal recovery via regularized orthogonal matching pursuit," *Found. Comput. Math.*, vol. 9, no. 3, pp. 317–334, Apr. 2009.

[136] [Online]. Available: hhtp://physiobank.org/physiobank/database/

[137] J. Davis and M. Keck, "A two-stage template approach to person detection in thermal imagery," in *Application of Computer Vision, Seventh IEEE Workshops on*, vol. 1, 2005, pp. 364–369.

[138] [Online]. Available: http://www.iris.edu/dms/nodes/dmc/data/

[139] D. Chatzigeorgiou, R. Ben-Mansour, A. Khalifa, and K. Youcef-Toumi, "Design and evaluation of an in-pipe leak detection sensing technique based on force transduction," in *ASME International Mechanical Engineering Congress and Exposition*, vol. 1, 2012, pp. 364–369.

[140] B. Kim, S. Yoo, and M. Lee, "Wavelet-based low-delay ECG compression algorithm for continuous ECG transmission," *Information Technology in Biomedicine, IEEE Transactions on*, vol. 10, no. 1, pp. 77–83, 2006.

[141] P. Grover, K. Woyach, and A. Sahai, "Towards a communication-theoretic understanding of system-level power consumption," *Selected Areas in Communications, IEEE Journal on*, vol. 29, no. 8, pp. 1744–1755, September 2011.